Research supported by the National Science Foundation under grants ATM-0071371, ATM-0500061 and by a one-year AMS Graduate Fellowship

Observed Radar and Environmental Properties of United States Warm Season Bowing Convective Systems, 2003-2004

by

Paul Quelet

Richard H. Johnson, P.I.

Colorado State University

DEPARTMENT OF ATMOSPHERIC SCIENCE

PAPER NO. 781

Observed Radar and Environmental Properties of United States Warm Season Bowing Convective Systems, 2003-2004

by

Paul Quelet

Department of Atmospheric Science
Colorado State University
Fort Collins, CO 80523-1371

Fall 2006

Atmospheric Science Paper # 781

ABSTRACT

OBSERVED RADAR AND ENVIRONMENTAL PROPERTIES OF UNITED STATES WARM SEASON BOWING CONVECTIVE SYSTEMS, 2003-2004

This study examines radar-indicated structures and environments of bowing convective systems in the United States during the warm seasons of 2003 and 2004 (April-December). The bowing process is defined as local acceleration of a convective cell or cells on the convex leading edge of a convective system to form a "arch" or "bow"-shaped line. This study perused data for each day of the two-year time period and investigated the bowing process using 2-km national radar reflectivity composite data. This procedure yielded 381 bowing convective systems, the majority of which occurred from May to July. The locations of these systems show a distribution similar to past studies of warm season derechos with two primary corridors: one in the Upper Great Plains, and secondarily, a maximum toward the Central/Southern Great Plains.

The entire population of bowing convective systems is classified into five modes, based on their differences in initial convective cell structures, convection evolution processes, locations, diurnal beginning and ending times, severe weather reports, and kinematic/thermodynamic environments. These modes are termed bow echo/extensive stratiform, bow echo/minimal stratiform, bowing squall line, multiple bowing squall line, and bowing single cell. Bow echoes/extensive stratiform exhibited trailing stratiform precipitation and most commonly evolved from groups of cells. Bow

echoes/weak stratiform showed very limited trailing precipitation usually evolving from the merging of supercells with ordinary or multicells. Single and multiple bowing squall lines most often evolved from trailing stratiform mesoscale convective systems.

An assessment of bowing convective line lengths and movement speeds was performed. Bowing convective line lengths of bow echoes/extensive stratiform and bow echoes/weak stratiform ranged from 40-110 km. Bowing squall lines and multiple bowing squall lines had convective lines segments between 110-225 km while bowing single cells were observed between 20-40 km. The bowing convective systems observed in this study exhibit a preferred range of speeds between 10 and 24 m s^{-1}.

This study also examines the characteristics of trailing stratiform precipitation in bowing convective systems. Pre-existing or convectively generated trailing precipitation tends to enhance the longevity of a bowing convective system. In some cases an enhanced trailing stratiform precipitation region was arranged in a perpendicular fashion behind the bowing convective systems while in other cases the trailing precipitation sustained a wide stratiform precipitation transition zone with minimal precipitation separating a bowing convective line from moderate-to-heavy stratiform precipitation. The latter precipitation pattern showed a strong tendency to increase system longevity.

Examination of convection properties related to bowing convective systems demonstrates the importance of identifying supercells and multiple supercells evolving or interacting with exterior convection to initiate bowing convection. Convective cell mergers, which also usually aid in the initiation of bowing convection, are strongly preferred near the resultant apex. Observations of ensuing bowing convective lines display a preference toward strong convection that is nearly homogeneous (slabular as opposed to cellular) in the along-line direction.

It was further observed that warm season bowing convection is favored in hybrid synoptic boundary forcing environments (moving parallel to or initiating on a

synoptic boundary), while bowing convective systems forced by no synoptic boundary is of secondary importance. Also, bowing convective systems that moved parallel to synoptic boundaries exhibited enhanced longevities. No bowing convective system that traversed a synoptic boundary continued for longer than three hours.

Finally, this study classifies severe weather production from bowing convective systems into four spatial patterns based on their shape and the nature of their effects. These are termed narrow apex swath, widespread high winds, widening swath, and destructive rotation. These patterns were compared to past studies of detailed severe weather surveys. It was observed that severe hail production was favored early in the evolution of bowing convection while severe wind production could occur throughout a storm evolution. Although tornadoes were uncommon in bowing convective systems, they tended to appear in the early-to-mature stages of evolution.

ACKNOWLEDGEMENTS

I thank Almighty God for the atmosphere: vast and beautiful, awe-inspiring and grand. I am privileged to take part in the endeavors to study its inner workings.

I thank my advisor Dr. Richard H. Johnson for graciously allowing me the freedom to choose a topic of study that I could passionately pursue. I am also very grateful for him allowing me plenty of independence and time to develop as a individual scientist. His encouragement, motivation, and guidance have helped shape me as a new scientist; I am truly indebted to him.

I would like to thank, Dr. David W.J. Thompson, Dr. James W. Thomas, and Dr. Morris L. Weisman for their service in reviewing this work and providing valuable suggestions. Dr. Weisman was particularly helpful with his prior expertise on the subject of bow echoes and cold pool influence. Thank you all so much for your time; you are very much appreciated.

I would also like to thank Dr. Matthew D. Parker for help in understanding how to review lots of radar data. Thanks to Dr. Brian A. Klimowski of NWS Flagstaff, AZ and Mr. Patrick C. Burke of NWS Goodland, KS who were wonderfully generous to provide their warm season bow echo cases for comparison.

Many thanks to Sylvia Murphy, Mary Hailey, Adam Phillips, and Dennis Shea from the National Center for Atmospheric Research (NCAR) for help with the production of many figures using the NCAR Command Language (NCL).

Many thanks go to all the members of the Johnson research group—Rick Taft, Paul Ciesielski, Gail Cordova, Russ Schumacher, Steve Aves, Peter Rogers, Becky

Adams, Elinor Martin, and Brian McNoldy—for their assistance in multiple areas of completing this project.

Additionally, I would like to thank my family and friends for supporting me in this and all of my endeavors.

The Weather Services International (WSI) national composite radar data were provided by David Ahijevych at the National Center for Atmospheric Research (NCAR).

This research was supported by National Science Foundation (NSF) grants ATM–0071371, ATM–0500061, and by a one-year American Meteorological Society Graduate Fellowship sponsored by the National Aeronautics and Space Adminstration (NASA).

CONTENTS

FIGURES

TABLES

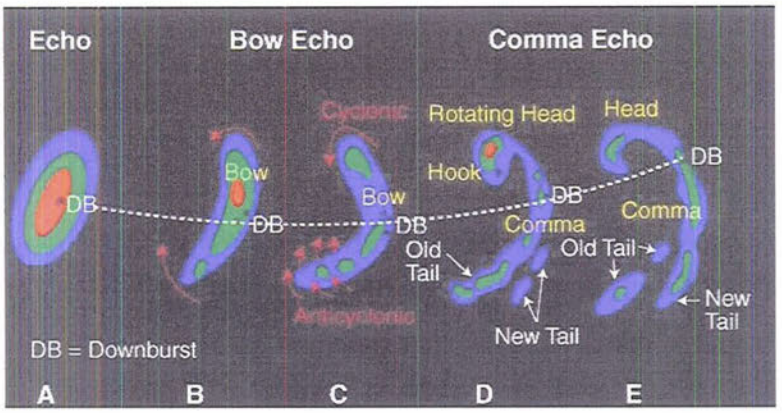

Figure 1.1: Fujita's conceptual model of the radar observed evolution of a single tall echo into a bow echo and subsequent dissipation to a comma echo. The colors blue-green-red indicate increasing radar reflectivity strength. Personal communication, Wakimoto (2005); adapted from Fujita (1978).

have added to the body of knowledge about the favorable conditions for these storms, the production of damaging winds, and the organizational properties of these severe weather producing systems.

This study will discuss many features of BCSs. Each of these facets are not separate entities; they are dynamically linked to one another. The strongest unifying feature is the system-generated surface **cold pool**. These areas of strongly cooled air are critical to the generation of a BCS.

1.2 Bow echo definitions

Since Fujita's original work, many attempts have been made to define the bow echo phenomenon. According to the Glossary of the American Meteorological Society (Glickman 2000), a bow echo is:

> A bow-shaped line of convective cells that is often associated with swaths of damaging straight-line winds and small tornadoes.
>
> Key structural features include an intense rear-inflow jet impinging on the core of the bow, with book-end or line-end vortices on both sides of the rear-inflow jet, behind the ends of the bowed convective segment. Bow echoes have been observed with scales between 20

> and 200 km and often have lifetimes between 3 and 6 hours. At early stages in their evolution, both cyclonic and anticyclonic bookend vortices tend to be similar strength, but later in the evolution, the northern cyclonic vortex often dominates, giving the convective system a comma-shaped appearance.

This definition includes much about the structural components often observed with bow echoes, but provides little discussion about the dynamical processes of bowing convection.

A study of U.S. bow echoes by Klimowski et al. (2004, hereafter KHB04) provided three necessary criteria for the identification of a bow echo. These are summarized as a bow-shaped convective echo, a tight reflectivity gradient on the leading edge, and an expanding radius with time. Furthermore, a study of U.S. cold season bow echoes from Burke and Schultz (2004, hereafter BS04) used a very similar definition. It identified bow echoes as storms that exhibit "outflow dominance" and strong rear inflow identified from vertical cross sections through bow echoes using single-Doppler radial velocity cross sections. In view of the above, the definition of a bow echo remains nebulous.

Consequently, the present study seeks to examine the nature of bowing convective systems to assist in refining current definitions. This work intends to emphasize the *convection evolution* and the *physical mechanisms* of these unique convective systems.

1.3 Initial motivation for this study

This study was initially motivated by the author's desire to examine storms that transition from one convective mode to another. A survey of past convection evolution studies revealed that one such evolution is a supercell to bow echo transition that has been documented in observational and numerical modeling studies (e.g. Moller et al. 1990; Moller et al. 1994; Finley et al. 2001; Klimowski et al. 2003;

BS04; KHB04). However, the dynamics of this transition have not been thoroughly documented. This led to further investigation of bow echoes through the consideration of Klimowski et al. (2003). These authors find that bow echoes were often associated with unexplained "convective mergers" and possessed highly variable kinematic/thermodynamic environmental properties. Furthermore, the authors noted a shorter longevity for their few non-severe-wind bow echoes as compared to their larger group that produced severe surface winds.

An initial survey of the radar data used in BS04 revealed large variability in the bow echoes. Using data from BS04, this author detected large variability in the trailing stratiform regions of their bow echoes studied. This variability appeared to be connected with bowing longevity and severity. Also, the study of many bow echoes by KHB04 contained a stated Northern High Plains bias. Thus, the incomplete nature of these previous studies prompted this study of *many* U.S. bowing convective systems for an in-depth analysis of bowing convection and climatological characteristics.

1.4 Goals of this study and implications for forecasting

The goals of this research are to:

- Document radar-observable and environmental characteristics of bowing convection that can provide insight into convection evolution and physical processes.
- Provide statistical and climatological information involving U.S. warm season bowing convection that has been previously unavailable.
- Document the variability of bowing convective lines and stratiform precipitation regions and their effects on the systems.

This study is important for the prediction of bowing convective systems because it will facilitate understanding of the observable properties associated with

bowing convective systems. The results should aid severe weather forecasters in understanding the variability of these properties. This study intends to provide information about the common convection evolution pathways of bowing convective systems so that their convective lines and stratiform regions can be monitored and better predicted for properties like longevity and severity. This study also connects past research on bow echoes and derechos; it provides insight into the differences between severe long-lived bow echoes and non-severe bow echoes.

Chapter 2

BACKGROUND AND MOTIVATION

2.1 The historical basis for bow echoes

Nolan (1959) is considered the first investigator to identify a bowing configuration in radar reflectivity fields associated with severe weather events. He termed this pattern a **line-echo-wave-pattern** (LEWP) depicting a line of radar echoes arranged in a quasi-sinusoidal fashion. A later study by Hamilton (1970) indicated that LEWPs were often associated with the occurrence of strong straight-line winds at the surface, particularly at the "bulge" point of the line.

It was Fujita (1978) who showed that the bulging echoes mentioned by Hamilton (1970) are radar signatures often associated with downbursts embedded or isolated from the larger system or LEWP. Consequently, Fujita renamed this radar signature the **bow echo**. He also proposed a conceptual model of the convection evolution into a bow echo (see Fig. 1.1, Chapter 1). Fujita's work was distinct from Nolan (1959) and Hamilton (1970) because the bowing systems proposed did *not* have to be part of a larger system of multiple bulging segments. Fujita was also able to make many assertions about the evolution, kinematics and severe weather associated with bow echoes, which current research has largely confirmed.

Fujita (1978) did not include a length scale on the conceptual model of Fig. 1.1. Also, he did not mention convective lines or stratiform rain regions variability among many bow echoes. The determination of exactly what type of convection was meant

by the tall echo remains difficult, but recent studies have shown that *many* initial modes can evolve into bow echoes (see section 2.3.1).

2.2 Definitions used in this study

Several important terms used in this study require definitions. Bowing convective systems, as mentioned in chapter 1, evolve into an "arch" or "bow"-shaped line through local acceleration of convective cell or cells on the convex leading edge as the convective system propagates. The term **bow echo** will be used throughout this chapter, retaining the definition from the AMS Glossary (Glickman 2000).

Also noted here is the common association of bow echoes with **derechos**, which are generally defined to be long-lived, convectively produced severe windstorms (originally defined by Hinrichs 1888, followed by many further studies including Johns and Hirt 1987, Evans and Doswell 2001, Coniglio et al. 2004a, and Coniglio and Stensrud 2004). Sometimes, bow echoes and derechos are spoken of equivalently; however, as noted by Coniglio and Stensrud (2004), *there is not a one-to-one correspondence between bow echoes and derechos.* In fact, the majority of bow echoes do not become derechos (at least, not according to the lifetime and distance specifications for derechos put forth by Johns and Hirt 1987) even though the radar signatures very often associated with derechos are often called bow echoes. Therefore, it is important to note not only the common occurrence of the two but also the distinction between the terms.

Spatial and temporal definitions used throughout this study closely follow definitions put forth by BS04 (except that the radar specifications in this study refer to a national radar 2-km composite):

- **First-echo time** is defined as the time of the first appearance of a 40-dBZ echo (a "convective" echo) within a squall line, group of cells/supercells, supercell, or single cell that eventually formed a bowing convective system.

- **Bow start time** is defined as the time of the first appearance of a bowing convective system on the 2-km radar composite.

- **Bow end time** is defined as the earliest time when a bowing convective system was no longer identifiable on the 2-km radar composite.

- **Development time** is defined as the time spanned by the developing convective cells from first-echo time to bow start time.

- **Development distance** is defined as the displacement of the centroid location of the developing convective cells from first-echo to the location of bow start.

- **Longevity** is defined as the lifetime of the bowing convective system from bow start time to bow end time.

- **Bowing convective system track length** is defined as the total displacement distance of the bowing convection from bow start time to bow end time.

2.3 Bow echo convective modes and structures

This section will describe the spectrum of findings about bowing and its related structures. As previously stated, the first conceptual model of the evolution of a bow echo was presented by Fujita (1978) in Fig. 1.1. This was a single conceptual model showing the evolution of convection into a bow echo. Since that study, further studies have documented additional initial and bowing convective modes besides the tall echo and bow echo. Other studies have revealed properties of convective storm mergers associated with bow echoes that will be discussed below. The descriptions of convective line regions, stratiform precipitation, and cold pool strengths are related to bow echoes later in this section.

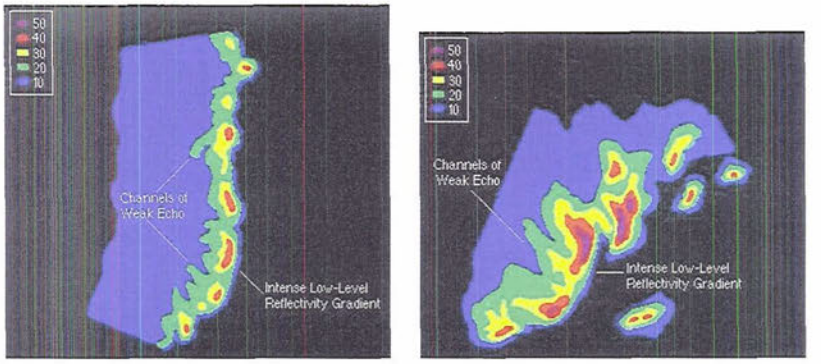

(a) Type I

(b) Type II

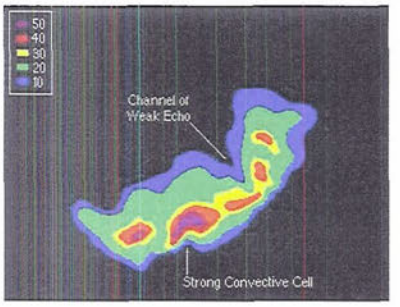

(c) Type III

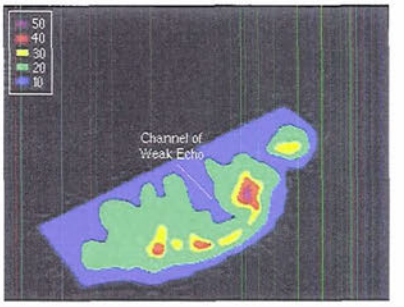

(d) Type IV

Figure 2.1: (a) Type I, (b) Type II, (c) Type III, and (d) Type IV conceptual radar reflectivity patterns for 20 observed derechos. The conceptualized radar reflectivity color scale is given in dBZ in the upper left of each panel. From http://meted.ucar.edu/convectn/mcs/mcsweb/mcsframe.htm; adapted from Przybylinski and DeCaire (1985).

2.3.1 Initial and bowing convective modes

After the study of Fujita (1978), a study of twenty derecho-producing bow echo-type MCSs associated with widespread areas of damaging winds in the north-central and eastern United States was completed by Przybylinski and DeCaire (1985). Their conceptual depictions of the radar echo distribution for each mode are displayed in Fig. 2.1.

Przybylinski and DeCaire (1985) stated that Type I was a narrow solid squall line up to 250 km in length with multiple bowing segments up to 100 km in length. Type II was a shorter system up to 150 km in length having a solid bow as the main convective line with convective cells ahead of the system that often merge

and intensify as the system interacts with them. Type III was somewhat shorter in length (usually in the 40 to 120 km range) with no convective cells observed in the system path with a very strong severe convective cell as part of the bow. Type IV was observed to evolve from an isolated **high-precipitation** (HP) **supercell** into a bow echo with new convective elements developing along the outflow boundary. Przybylinski and DeCaire (1985) noted that Type III was the most common bowing mode observed in their study. Additionally, most of the systems had an intense low-level reflectivity gradient on the convex leading edge where the bowing was occurring.

Later, Weisman (1993) performed a numerical modeling study to study idealized bow echoes. The resulting convective modes from his study are summarized as **weak cells**, **bow echoes**, and **supercells**. The mode that formed depended upon the **convective available potential energy** (CAPE) and the strength of the vertical wind shear. His study suggested a necessary parameter space of instability and vertical wind shear for the development of the bow echo structure, but these results are difficult to generalize because of the ideal nature of the numerical experiments and the simulated bow echoes being forced by symmetrical splitting supercells. Further studies indicate a broader parameter space for bow echo development as compared to Weisman (1993) (see appendix A).

As an extension of the studies of Przybylinski and DeCaire (1985) and Weisman (1993), the recent studies of KHB04 and BS04 have compiled observations of many bow echoes documenting details about the initial and bowing modes of convection. Thus, these studies provide some *additional* bow echo evolution conceptual models in addition to the original work of Fujita (1978).

BS04 studied cold season (October-April) bow echoes and noted six initial modes of convection before bow echo development. These are named as **squall line**, **groups of cells**, **supercell**, **pair**, **embedded**, and **squall line-cell merger** (Fig. 2.2). The results show that squall lines (49%), groups of cells (24%), and

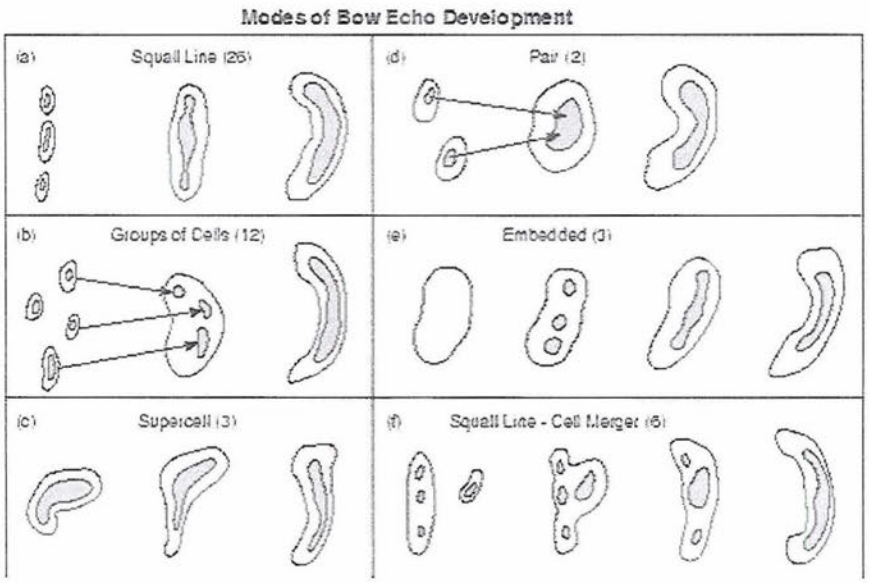

Figure 2.2: Conceptual models of initial convective modes and schematic evolutions of cold season bow echoes. The number of cases that developed from each mode for the study period is indicated in parentheses. Shaded areas represent higher radar reflectivity values. From Burke and Schultz (2004).

squall lines merging with cells (12%) were the most common modes to initiate the development of cold season bow echoes. The authors do not describe in any significant detail the slightly different appearance of the bowing convective modes (Fig. 2.2).

The study of KHB04 tabulated both the initial and bowing convective modes of bow echoes for 273 cases through various months of the year from 1996-2002 over the entire United States. There is, however, a stated Northern High Plains bias in their dataset, given that much of their data came from cases used in Klimowski et al. (2003). They proposed four primary modes of bow echoes with radar examples of each displayed in Fig. 2.3. These include a **Classic Bow Echo** (BE, 72%), **Bow Echo Complex** (BEC, 3%), **Cell Bow Echo** (CBE, 5%), and **Squall Line Bow Echo** (SLBE, 20%). Additionally, the frequency of bow echoes evolving from three initial convective modes (**weakly organized cells**, **squall lines**, **supercells**) into the four bowing modes is shown in Fig. 2.4, citing other previous studies with similar evolutions.

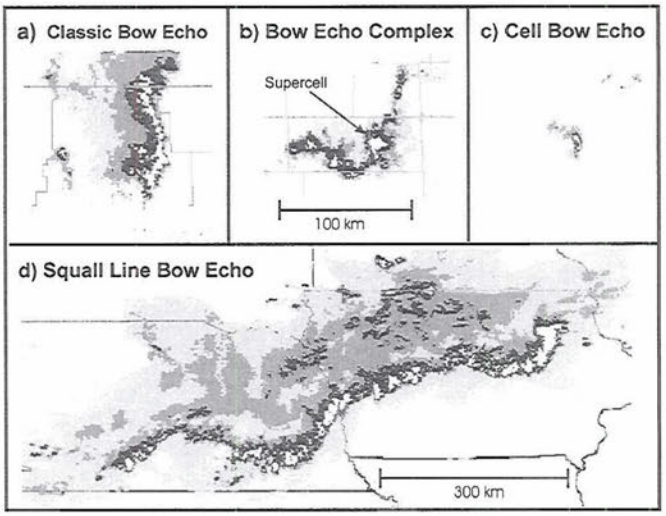

Figure 2.3: Radar examples of the four general types of bow echo modes found by Klimowski et al. (2004): (a) Classic Bow Echo (BE), (b) Bow Echo Complex (BEC), (c) Cell Bow Echo (CBE), and (d) Squall Line Bow Echo (SLBE). The BE, BEC, and CBE are all relative to the scale as given in (b) while the scale of (d) is shown. Reflectivity is shaded every 10 dBZ. From Klimowski et al. (2004).

The results of KHB04 show that the weakly organized cells were the preferred initial mode (45%) with nearly as many squall lines evolving into bow echoes (40%). These results demonstrate a different frequency than BS04 when comparing the groups of cells fraction to that of the weakly organized cells very closely (24% vs. 45%). Part of this disparity could be an indication of the differing forcing mechanisms among the data (e.g. strong, cold season baroclinic forcing versus weak, warm season convective forcing).

The final bowing modes of KHB04 show some parallels to Przybylinski and DeCaire (1985). The SLBE mode corresponds well to the Type I mode and the BEC compares somewhat with the Type III mode, while the BE mode could depict a similar mode to Type II, III, or IV. While the results are similar between the two studies, they do not agree on their classification system. KHB04 noted differences among the bow echo longevity and regional placement of the bowing convective modes, but they did not pursue the distinction further. Moreover, the previous studies mentioned

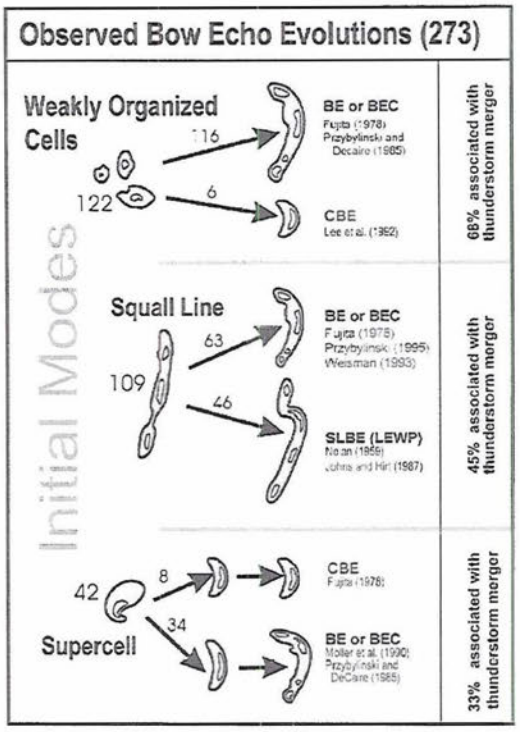

Figure 2.4: Illustration of the initial and bowing mode frequencies of bow echoes observed over the U.S. during multiple seasons for the years 1996 - 2002. The number of cases identified following each path is indicated above the arrows. References of similar observed radar evolutions from previous studies are given. The percentage of bow echoes preceded by merging cells for each initial mode is shown on the far right of the figure. From Klimowski et al. (2004).

do not precisely agree on the initial convective cell structures that produce bowing convection. This study will incorporate a classification system based on differing precipitation structures and evolutions which suggest differences in dynamics.

2.3.2 Convective cell mergers

The merging of convective cells prior to the development of bow echoes has been observed by Finley et al. (2001), Klimowski et al. (2003), KHB04, and BS04. In a numerical modeling study of an HP supercell transition to a bow echo, Finley et al. (2001) showed that the mergers of convective "daughter" cells caused an increase in vertical vorticity and stronger vertical velocity as well as falling pressures associated

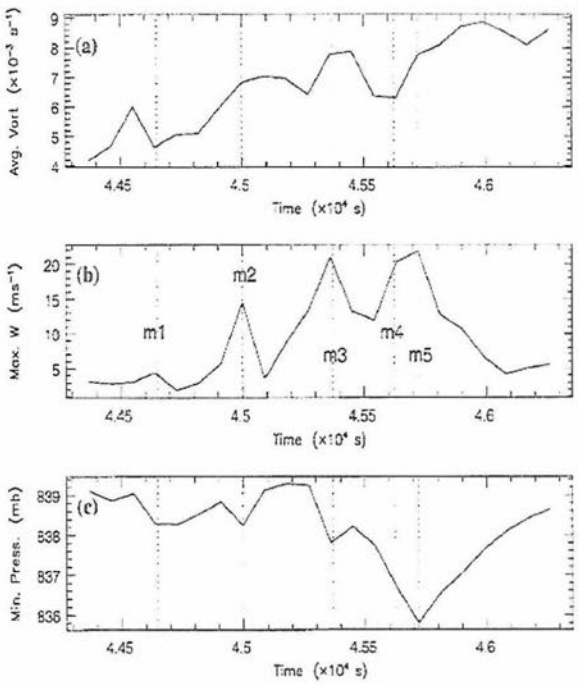

Figure 2.5: A time series of (a) area average vertical vorticity at height $z = 2$ km, (b) maximum vertical motion at height $z = 2$ km, and (c) minimum pressure at height $z = 1.3$ km in a simulated low-level mesocyclone that was evolving into a bow echo. Times of daughter cell merger events (m1-m5) are denoted with the dotted lines. From Finley et al. (2001).

at the time of each merger (Fig. 2.5) during the transition stage to a bow echo.

Klimowski et al. (2003), KHB04, and BS04 found 41%, 50-55% and 67% of their bow echoes studied to be associated with cell mergers, respectively. The KHB04 study further stratified the dependence of cell mergers by the initial convective mode, finding weakly organized cells most often associated with cell mergers prior to the initiation of bow echoes (Fig. 2.4).

Klimowski et al. (2003) and KHB04 have noted some characteristics of these merging cells and what processes tend to occur with these mergers. Klimowski et al. (2003) and KHB04 explain that cell mergers initiating bow echoes are often "aggressive" cells, tending to be fast-moving, differing in their motion to the mean wind, and dominating the change in convective structure to a bow echo, often very quickly.

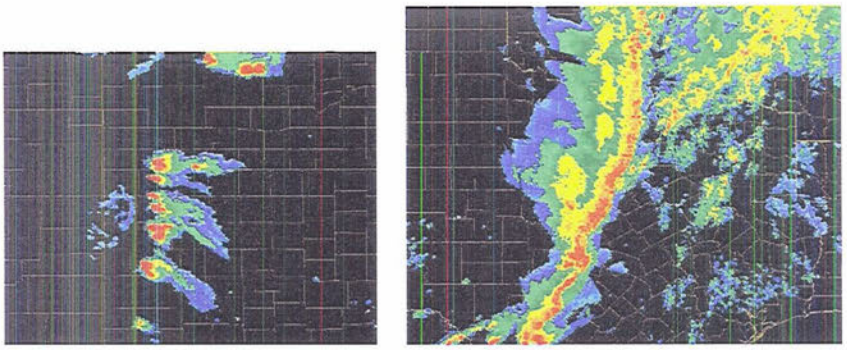

(a) Cellular convective line (b) Slabular convective line

Figure 2.6: (a) Radar reflectivity example of a cellular convective line. (b) Radar reflectivity example of a slabular convective line. Reflectivity is shown every 5 dBZ increasing blue-green-yellow-orange-red (as in a standard WSR-88D color scheme). From James et al. (2005).

They also appear to be associated with an increase in the breadth and magnitude of radar reflectivity through local precipitation rate increase and cell formation along an enhanced outflow.

The authors of the above studies did not note on which *flank* of preexisting convection the mergers tend to occur, but this information could be important for the prediction of these systems. The current study aims to more precisely describe the radar observed properties of aggressive cells.

2.3.3 Convective line evolution, stratiform rain distributions, and cold pool influences

This subsection discusses known properties of convective systems, including the convective line evolutions, stratiform rain distributions, and cold pool extents. The author of this study has not uncovered any research that examines these properties in depth for bowing convective systems. Instead, a brief review of these properties will be discussed with regard to squall lines.

The evolution and nature of the convective regions of squall lines has been

studied by James et al. (2005), who identified both **cellular** and **slabular** convective lines, having a linear structure but differing reflectivity properties. A radar example of a cellular convective line is given in Fig. 2.6a and a slabular convective line given in Fig. 2.6b; these convective lines differ in their spatial precipitation reflectivity continuity. Cellular convective lines have strong cells with nearly echo-free regions between the cells, while slabular convective lines are nearly homogeneous in the along-line direction.

James et al. (2005) noted environmental differences in convective lines between cellular and slabular convective lines. The authors demonstrate from their observations that slabular convective lines tend to have stronger low-level vertical wind shear, are nearly quasi-two dimensional with stronger low-level line-relative inflow, and have a lower vertical height to the lifting condensation level (LCL). When one compares these results with the sharp low-level reflectivity gradient requirement of bow echoes of Przybylinski and DeCaire (1985) and KHB04, it appears that a BCS could be related to a slabular convective line. However, some bow echoes (e.g. Przybylinski and DeCaire (1985) type III, KHB04 bow echo complex) have very strong convective cells as part of the convective line and could be related to cellular convective lines.

In a recent numerical modeling study, James et al. (2006) note that bowing convective lines could be an *intermediate* mode between cellular and slabular convective lines depending upon the low-level moisture content affecting the formation of cold pools. In response to these findings, the current study strives to categorize observed bowing convective lines into cellular or slabular convective lines and how this information relates to bowing convection longevity and severity.

This author has not discovered any research that documents the stratiform precipitation variability resulting from bow echoes. The work of Parker and Johnson (2000) and Parker and Johnson (2004,a,b,c) has shown important dynamical differences between **trailing stratiform** (TS), **leading stratiform** (LS), and **parallel**

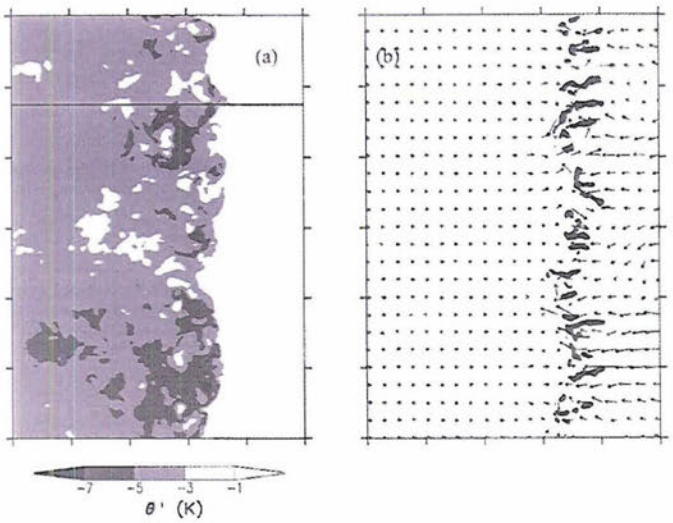

Figure 2.7: Cellular convective line simulation with 4 (g/kg) km^{-1} low-level mixing ratio lapse rate and thus moist low-levels. Tick marks indicate 20 km distances. (a) Potential temperature perturbation (K) at 100 m above ground. (b) Vertical velocity (shaded above 6 m s^{-1}) and approximate line-relative wind (arrows) at 3 km above ground. An arrow length of 10 km represents a wind speed of 25 m s^{-1}. From James et al. (2006).

stratiform (PS) MCSs, but questions remain regarding the typical evolution of the stratiform precipitation in bow echoes. How is trailing stratiform precipitation associated with the mode of development and the severity and longevity of bowing convective lines? The current study will strive to provide some insights into this question as it relates to previous studies of linear MCSs.

James et al. (2006) show differences in their resulting cold pools when comparing cellular (moist low-levels), slabular (dry low-levels), and bowing convective lines (intermediate moisture at low-levels) in numerical simulations using different low-level mixing ratio lapse rates while retaining the same CAPE (Figs. 2.7, 2.8, and 2.9; note the different temperature ranges in these figures). The authors argue that the low-level evaporation of intermediate strength for the simulation of 3 (g/kg) km^{-1} low-level mixing ratio lapse rate causes the bowing convective mode (Fig. 2.9). The cellular cold pool can be described as weak and inhomogeneous (Fig. 2.7) while the

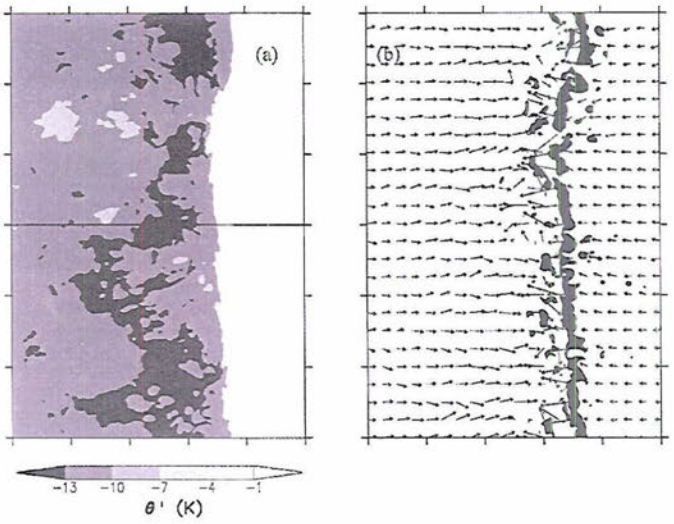

Figure 2.8: As in Fig. 2.7 but for the slabular simulation with 1 (g/kg) km^{-1} low-level mixing ratio lapse rate and thus dry low-levels. From James et al. (2006).

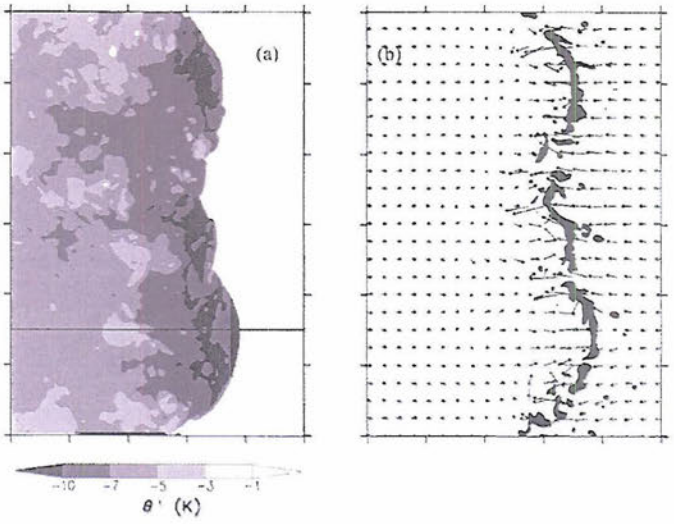

Figure 2.9: As in Fig. 2.7 but for the bowing simulation with 3 (g/kg) km^{-1} low-level mixing ratio lapse rate and thus intermediate moisture at low-levels. From James et al. (2006).

slabular cold pool can be described as everywhere strong and nearly homogeneous (Fig. 2.8) in the line-perpendicular and line-parallel directions with a nearly homogeneous lifting along the leading edge in the line-parallel direction. Simulations were tested with 2300 and 4600 J kg^{-1} of CAPE and with 0-2.5 km shear values of 16, 20, and 24 m s^{-1}. The resulting modes of convection were qualitatively similar when the mixing ratio lapse rate in the low levels is varied.

Furthermore, not mentioned in James et al. (2006), a comparison of the low-level potential temperature perturbations from Figs. 2.7 through Fig. 2.9 show that the *bowing mode simulation has pockets of cold air confined close to the convective line in the bowing segments* (Fig. 2.9). This could be important for the placement and anticipation of bowing segments in a convective line and the possible collocation with severe surface winds. In fact, the placement of the cold pool for observed systems could be a manifestation of the rearward extent of the heaviest precipitation as related to system evolution. This study looks to qualitatively assess this result for bowing convective systems by observational evidence of precipitation placement in observed bowing convection.

2.4 Bowing convection structural components

To further understand bowing convection, one must examine the structural components that influence its evolution. Since they were first defined by Fujita (1978) bow echoes have been well known to have a bowing convective line on the convex leading edge of the outflow. As argued by KHB04, the propagation speed of these systems suggests that strong outflow largely influences the system evolution. Additional components identifiable in bowing convection are discussed in the subsequent subsections.

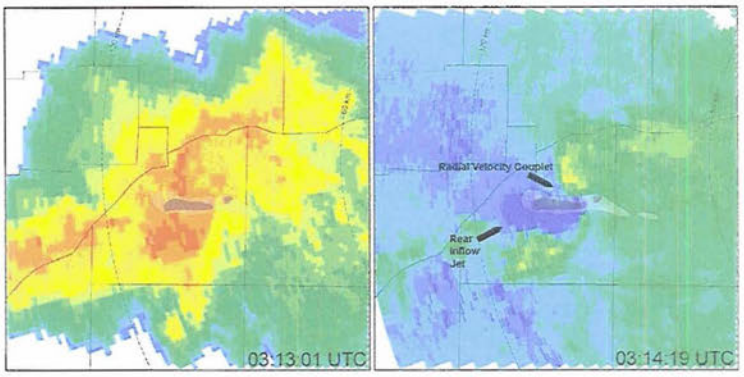

Figure 2.10: (left panel) Base reflectivity and (right panel) ground relative radial velocity (0.5-degree) at (left panel) 03:13:01 UTC and (right panel) 03:14:19 UTC 10 June 2003 (with F0 damaging wind swath overlaid in grey with F1 damage overlaid in blue). The maximum of rear-to-front flow behind the convective line is shown on the 2.4-degree elevation surface. Damage analysis is over east-central Nebraska. Radar is located to the east of the convective system in the images. From Wheatley and Trapp (2004).

2.4.1 Rear-inflow jet

Bow echoes have been well documented to possess a very strong **rear-inflow jet** (RIJ), which has been noted in many studies (e.g. Fujita 1978, Weisman 1993, Przybylinski 1995). This is similar to the **descending rear inflow** in a trailing stratiform MCS as noted by Houze et al. (1989).

The RIJs in bow echoes often produce damaging surface winds which can be noted from detailed damage surveys. Wheatley and Trapp (2004) examine a wind damage survey that shows that a strong RIJ (seen as blue "inbound" velocities on the radial velocity display) is collocated with the damaging surface wind swath path as noted from detailed damage surveys (see the overlayed grey damage survey in Fig. 2.10). However, personal communication with Dr. Roger Wakimoto (2005) has suggested that a vortex couplet (seen as the yellow to blue color couplet on the radial velocity display) exists for the above case so that a **mesovortex** is generated at the nose of the RIJ. Wakimoto argues that this is the more direct cause of the severe surface winds since it adds to the windspeed of the RIJ.

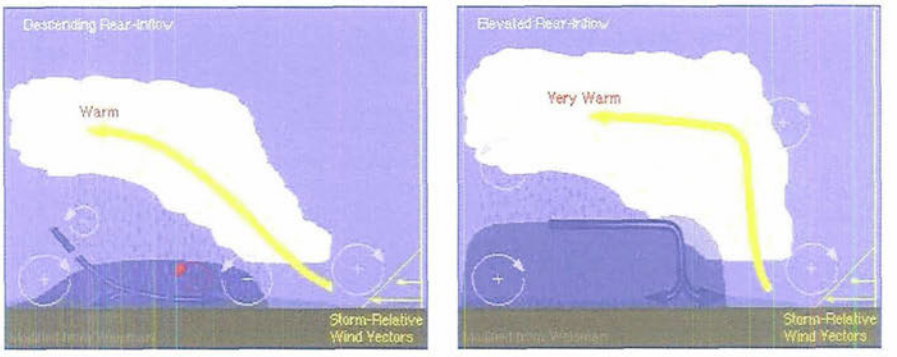

(a) descending rear-inflow (b) elevated rear-inflow

Figure 2.11: (a) Schematic of a gradually descending RIJ. The buoyancy gradients associated with warm air aloft are weaker than those associated with the rear flank of the cold pool, allowing for a more gradual descent of the RIJ. (b) Schematic of a RIJ that remains elevated. The buoyancy gradients aloft are strong relative to the cold pool below. This tends to make the RIJ remain more elevated and advance closer to the leading edge of the system, where its final descent can cause severe wind damage. From http://meted.ucar.edu/mesoprim/severe2/index.htm; adapted from Weisman (1992).

Weisman (1992) hypothesized from a numerical modeling study of RIJs that if a rear-inflow jet (in a squall line or bow echo) could remain elevated as it approached a strong convective line, then the propensity for strong, damaging surface winds was increased. This hypothesis states that the RIJ remains elevated if the buoyancy aloft is sufficiently large to enhance the rear-inflow with opposite sign vorticity as the low-level vorticity generated by the cold pool evaporative cooling (Fig. 2.11). Weisman (1992) mentions that an elevated RIJ is related to the strength and longevity of the leading line updrafts, and not necessarily to severe surface winds. Additional new information from the 9-10 June 2003 bow echo from BAMEX (Jorgensen et al. 2005) could provide evidence for severe winds not reaching the ground when an elevated RIJ, but as an elevated RIJ transitions to a descending RIJ.

Note that in the conceptual model of Weisman (1992) an RIJ develops as the trailing stratiform precipitation region develops. As a counterexample, an observational study by Klimowski (1994) of a very strong squall line in North Dakota noted

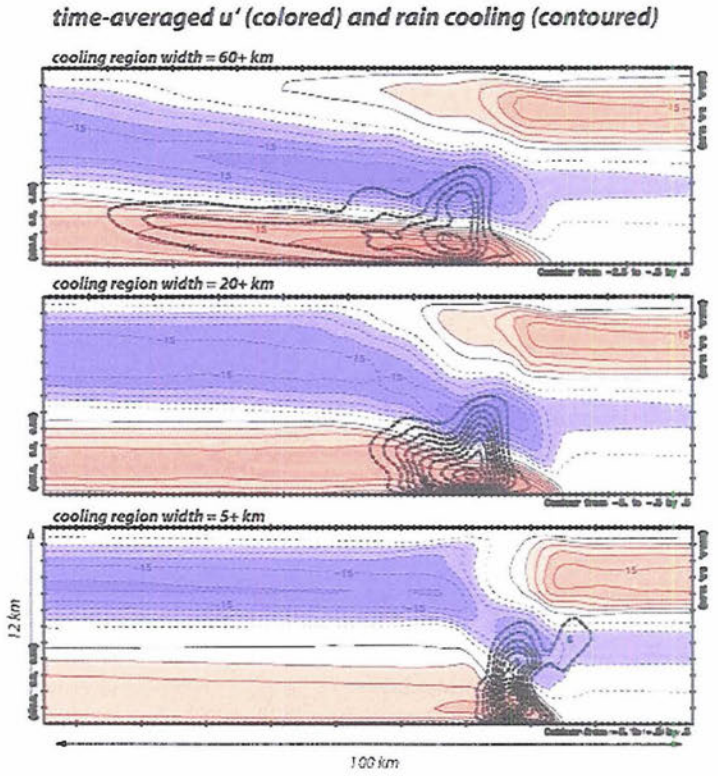

Figure 2.12: Time-averaged perturbation horizontal velocity (deviation from initial state, colored with thin contours) and thick contours of latent cooling for experiments with subcloud cooling regions that are roughly 60, 20 and 5 km wide (top to bottom). From Dr. Robert G. Fovell (personal communication).

rear inflow *without* a stratiform region initially. This study argued for the mid-level low pressure anomaly in the convective core of the squall line to accelerate the RIJ toward the convective line.

In another study of squall line rear-inflow (alternately called RIC, meaning "rear-inflow current"), Fovell (2003) says "how far back behind the leading edge of the RIC descends should be a function of the storm's evaporative cooling zone." Recent numerical simulations by Fovell (see Fig. 2.12, personal communication) have shown different surface wind strengths generated by varying the width of the subcloud cooling zone. Taken in tandem with the study of James et al. (2006), the results seem to demonstrate that the *width* of the subcloud cooling zone and its *proximity* to the convective line is very important to where the RIJ descends. The two studies suggest

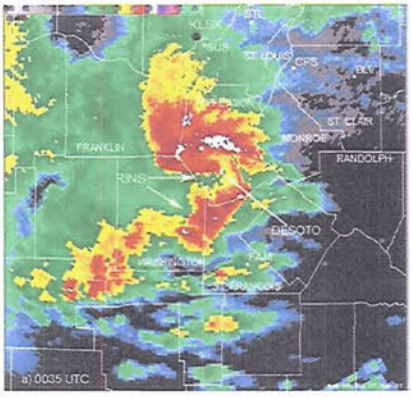

Figure 2.13: WSR-88D plan-view reflectivity from St. Louis (KLSX) radar at for 0035 UTC 07 May 2003 with the rear-inflow notches (RINs) labeled with white text and arrows. From Sieveking and Przybylinski (2004).

that an elevated RIJ is associated with a vertically erect system, but a longer fetch for the RIJ with potentially stronger surface winds can arise as a convective line leans against the vertical wind shear ("upshear"). The current study seeks to examine the effect of the stratiform regions for observed bowing convection, including how they relate to the bowing and the generation of the severe winds.

2.4.2 Rear-inflow notches

Bow echoes often exhibit **rear-inflow notches** (RINs) (e.g. Smull and Houze 1985b, Smull and Houze 1985a, Przybylinski 1995) which are small slits of low radar echo seen on a radar reflectivity display pinching behind the convective line (Fig. 2.13). RINs are argued to be a manifestation of drier air from the RIJ aloft descending to erode the precipitation field. These notches have been collocated with severe surface wind damage in previous studies (e.g. Przybylinski 1995, Weisman 2001, Sieveking and Przybylinski 2004). Previous observations have shown that multiple RINs can be observed behind a bowing line.

2.4.3 Line-end vortices

Fujita (1978) first noted the existence of circulations of opposite directions on the ends of a bow echo. Weisman (1993) further documented the existence of these vortices and termed them **line-end** or **bookend** vortices. He noted that these circulations could enhance the RIJ velocity field as much as 30-50%. These vortices tend to be on the scale of 20-50 km. Bowing convective systems of a larger dimension have been argued to become asymmetric with the cyclonic vortex dominating later in the life cycle through several processes (e.g. Skamarock et al. 1994, Loehrer and Johnson 1995, Hilgendorf and Johnson 1998, Weisman and Davis 1998).

2.4.4 Mesovortices in bowing convective systems

Recent studies have shown the importance of **mesovortices** often found along the convex leading edge of bow echoes with a preference for being located toward the cyclonic line-end vortex, usually 2-20 km in diameter. Mesovortices were anticipated early from observations of Przybylinski et al. (2000) and Schmocker et al. (2000). These vortices were observed to be associated with straight line wind damage and weak tornadoes *separate from* or sometimes *caused by* the RIJ (R.M. Wakimoto, personal communication, 2005, see section 2.4.1).

Weisman and Trapp (2003) and Trapp and Weisman (2003) investigated these structures with numerical modeling studies describing the genesis and how these vorticies could cause damaging surface winds aside from the RIJ. The authors propose that the downdraft tilting of cold pool vorticity in low-levels results in a mesovortex couplet with the cyclonic member being favored by the stretching of storm-scale plus planetary vorticity (f).

New observational evidence from the 5-6 July 2003 bow echo during the BAMEX field campaign (Wakimoto et al. 2006a,Wakimoto et al. 2006b) suggests that new cell development along the existing gust front caused a downdraft that was

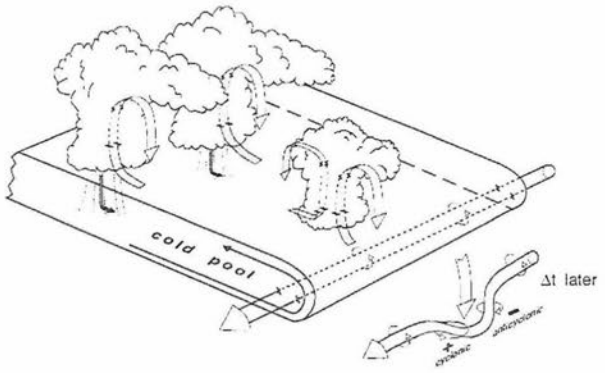

Figure 2.14: Schematic model illustrating the origin of vortex couplets along the outflow boundary of the Omaha bow echo. The diagram at the bottom right represents the distortion of the vortex tube with increasing time. From Wakimoto et al. (2006a).

mechanically forced because of compensating subsidence of a thermal cell rising along the gust front (not necessarily the precipitation downdraft, see Fig. 2.14). With regard to the severe winds caused by the mesovortex, Wakimoto et al. (2006a) and Wakimoto et al. (2006b) follow Trapp and Weisman (2003) to discuss the additive effects of bow echo motion and rotation on the rightward (usually southern) flank of the cyclonic vortex responsible for severe surface wind damage.

2.5 Bowing convective system and derecho climatologies

Climatologies of U.S. bow echoes are useful for understanding their spatial and temporal distributions, as well as typical dimensions and occurrence in tandem together or in groups. KHB04 and BS04 each gathered a large number of bow echo cases to communicate climatological characteristics. Coniglio and Stensrud (2004) compiled a derecho climatology from all seasons from 1986-2001 for a total of 244 derecho events extending the derecho climatologies of Johns and Hirt (1987) and Bentley and Mote (1998). These climatological distributions are useful to consider but pertain more to long-lived bow echoes and severe bow echoes since not every derecho can be classified as a bowing convective system.

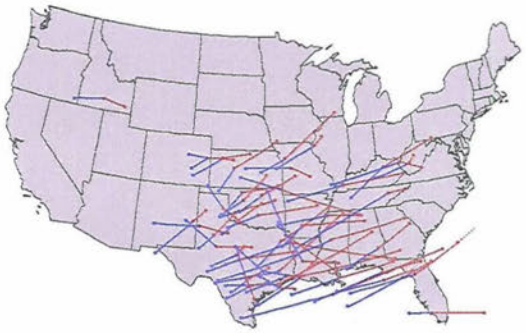

Figure 2.15: Track map for 51 bow echoes that occurred during the cold seasons from October to April for the years 1997-2001. Blue tracks are from first echo to bow echo start. Red tracks are from bow echo start to bow echo end. From http://www.nssl.noaa.gov/mag/bowecho/; adapted from Burke and Schultz (2004).

2.5.1 Spatial distributions of bow echoes and derechos

BS04 showed the spatial distribution of cold season bow echoes (Fig. 2.15). Their tracks show a preference toward the Southern Plains and Gulf Coast states, given that these storms were chosen for the cold season. The current study seeks to provide the spatial distribution for *warm season* bowing convective systems not previously published in past studies.

The spatial maps of derechos for the years of 1986-2001 of Coniglio and Stensrud (2004) are shown in Fig. 2.16 for the warm season, the cold season, and all months of the year, respectively. The results for derechos suggest a bimodal spatial distribution in activity with a broader maximum over the Upper Great Plains/Upper Mississippi Valley and a secondary maximum over the Southern/Central Plains. Both areas are active in the warm season, with the northern region dominating. The southern derecho corridor is most active in the cold season.

2.5.2 Temporal distributions of bow echoes and derechos

The frequency of bow echoes for each of the cold season months from the study of BS04 for 1997-2001 is shown in Fig. 2.17. The monthly distribution of the relative

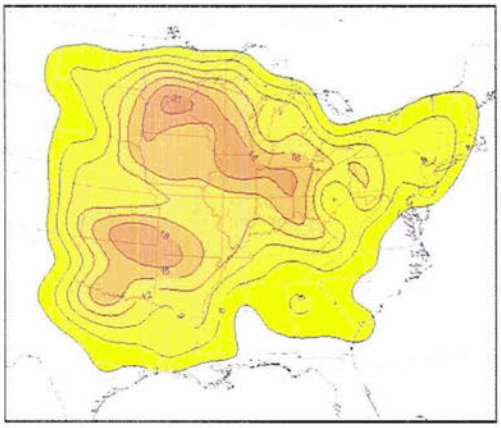

(a) Warm Season derechos, May-August

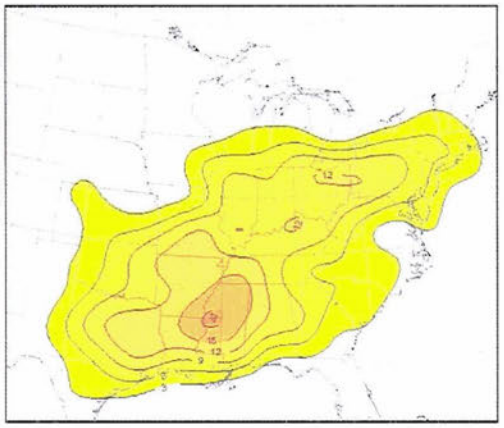

(b) Cold Season derechos, September-April

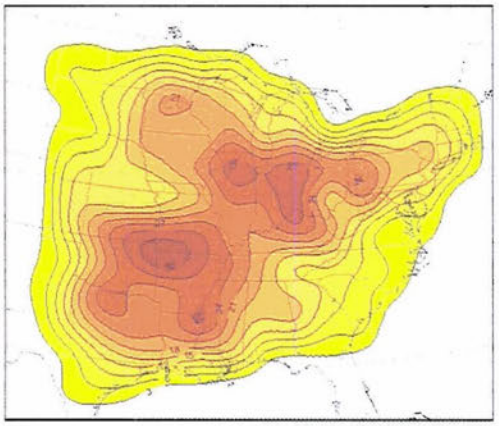

(c) All derechos, all months

Figure 2.16: Spatial distributions of areas affected by derechos contoured on 200 km grid cells from 1986-2001 with contours labeled for every 3 derechos. Warm season (May to August). Adapted from Coniglio and Stensrud (2004).

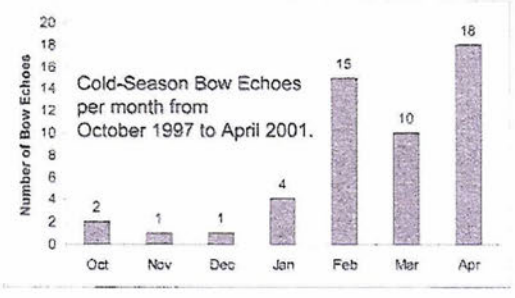

Figure 2.17: Monthly distribution of cold season bow echoes from 1997 to 2001. From Burke and Schultz (2004).

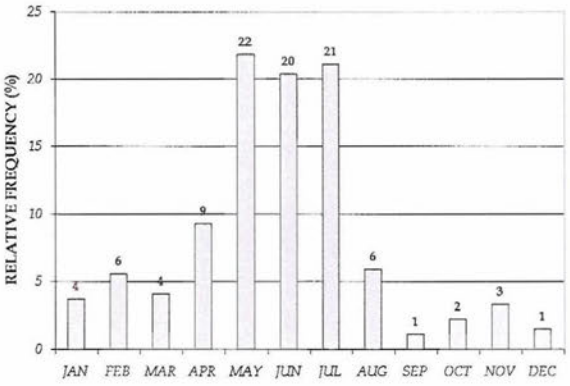

Figure 2.18: Relative frequency distribution for the month of occurrence for the 270 derecho events from 1983-2001. From Coniglio et al. (2004a).

frequency of 270 derechos from 1980-2001 from Coniglio et al. (2004a) is depicted in Fig. 2.18. These distributions show clearly that bow echoes (and particularly derechos) are *favored in the warm season*, with the highest number of events occurring between May and July. The distributions also suggest that the latter part of the cold season, namely the months January to April, are more favorable climatologically for bow echo and derecho development in comparison to the September to December months.

The diurnal distributions of cold season bow echoes from BS04 demonstrate that cold season bow echoes often have their first echoes in the early afternoon, are initiated in the evening, and end shortly after midnight on average (Fig. 2.19). However, the distributions show considerable variability so that the development times and longevities of the bow echoes are also highly variable (Fig. 2.20). The positively skewed distribution in the longevity demonstrates that most cold season bow echoes last 2 to 6 hours, while a smaller number of bow echoes last *much longer*, and are thus named **long-lived bow echoes** (LBEs) by BS04. Not all of the LBEs in BS04 met the criteria for derechos; however, the results imply that these long-lived bowing systems represent a distinct form of convective organization (Weisman 2001) with their continual regeneration of convection on their leading edge.

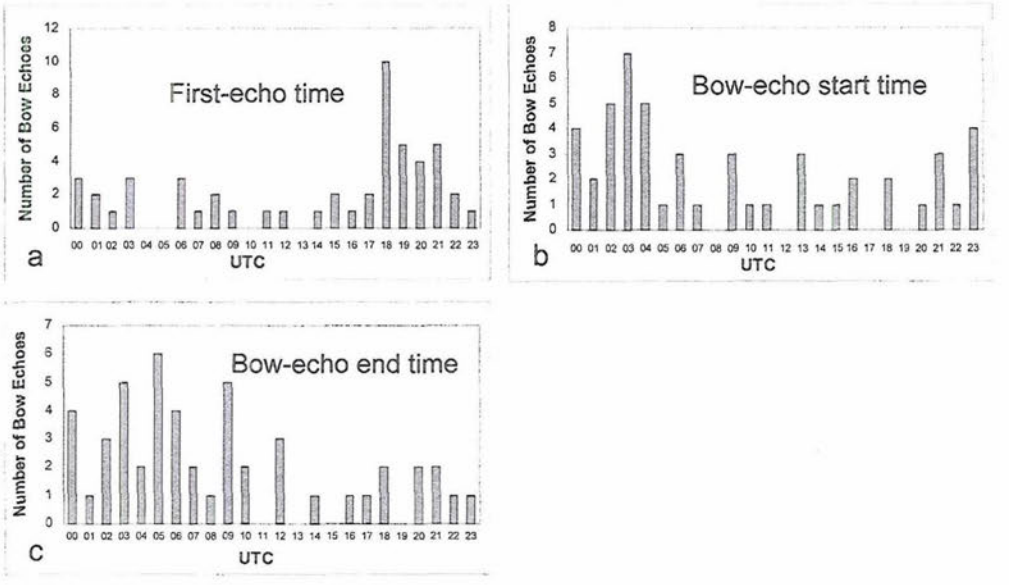

Figure 2.19: Frequency distributions for (a) first-echo time, (b) bow echo start time, and (c) bow-echo end time in UTC for bow echoes that occurred in the cold seasons from October 1997 to April 2001. The 1 hour bin labeled 01 represents times between 0000 and 0100 UTC, etc. From Burke and Schultz (2004).

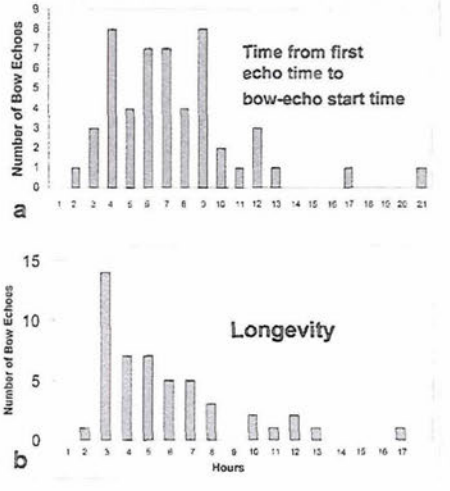

Figure 2.20: Frequency distributions for (a) development time and (b) longevity for bow echoes that occurred in the cold seasons from October 1997 to April 2001. The 1 hour bin labeled 1 represents longevity between 1 and 2 hours, etc. From Burke and Schultz (2004).

Table 2.1: Horizontal length scales assigned to bow echoes from past studies. The line lengths from Burke and Schultz (2004) were tabulated by the author of the present study.

Article	Bow echo horizontal length scales (km)
Johns (1993)	15 to 150
Glickman (2000) (AMS Glossary)	20 to 200
Weisman (2001)	40 to 120
Coniglio et al. (2004a)	10 to 300
Klimowski et al. (2004)	10 to 150
Burke and Schultz (2004)	20 to 200

One inconclusive property of bow echo diurnal variability is the possible decoupling of nocturnal atmospheric boundary layer (ABL), as discussed in Weisman (2001). Severe wind producing bow echoes have been documented to occur at night in the presence of a stable nocturnal boundary layer that does not as readily support the generation of a strong surface cold pool (e.g. Schmidt and Cotton 1989, Bernardet and Cotton 1998). Thus, Weisman (2001) poses the question, "are the mechanisms for bow-echo genesis and maintenance different for nocturnal versus daytime scenarios?" The current study attempts to document the diurnal variability of warm season bowing convection and severe weather.

2.5.3 Bow echo horizontal length scales

The horizontal length scales of bow echoes have been documented in many past studies with little conclusive evidence supporting a particular scale of the dynamics that are occurring (Table 2.1). KHB04 noted that the SLBEs were the longest lived bow echoes in their study, suggesting that a more linear mode of organization is favorable for longevity. They also noted that some squall lines did not always retain their initial scale once the bowing process occurred, which could be evidence for preferred convective line length to a certain group of bowing MCSs. Numerical

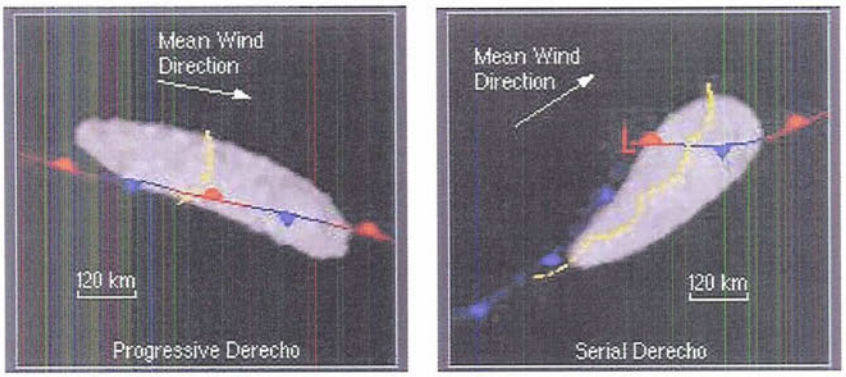

(a) progressive derecho (b) serial derecho

Figure 2.21: Schematic representation of features associated with (a) progressive and (b) serial derechos near the midpoint of their lifetimes. The total area affected by these derechos is shaded in grey. The frontal and squall line symbols are conventional. From http://meted.ucar.edu/convectn/mcs/mcsweb/mcsframe.htm; adapted from Johns and Hirt (1987).

simulations performed by Skamarock et al. (1994) found that the final scale of the resulting convective systems was largely independent of the initial size of the convective systems initiated. The numerical simulations of Weisman and Davis (1998) simulated bowing systems that tended to congeal into the 40-80 km range. Recently, James et al. (2006) found bowing segments in their bowing convective lines to manifest themselves between 15 and 40 km. These authors mention that the reasoning for the scales of cold pool spreading and upscale growth is not not well understood. In response, the present study seeks to thoroughly document the horizontal length scales of bow echoes to establish possible relationships between length, longevity, and severity.

2.6 Bowing convection and derecho synoptic scale boundaries

Johns and Hirt (1987) put forth synoptic conditions for derechos that they noted were most often bowing systems. These conditions show the importance of the influence of synoptic scale surface boundaries to the formation of derechos, as illustrated by the **progressive** and **serial** derecho schematics (Fig. 2.21). Progressive

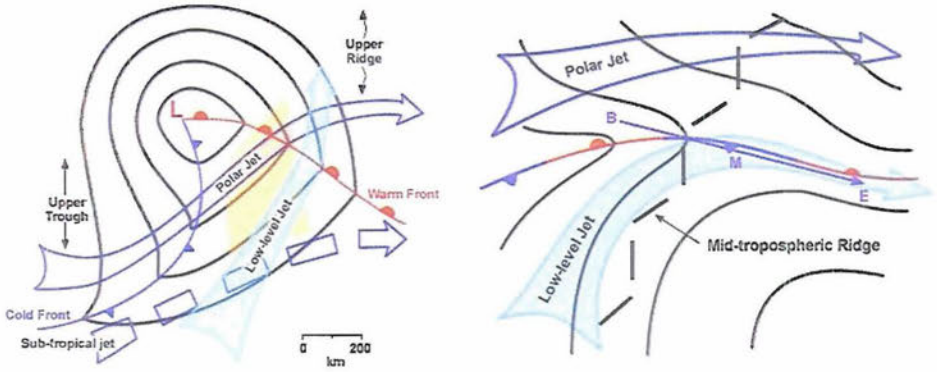

(a) dynamic pattern (b) warm season pattern

Figure 2.22: (a) Idealized sketch of favorable for the development of squall lines with extensive bow echo induced damaging winds (serial derechos). The thin lines denote sea level isobars in the vicinity of a quasi-stationary frontal boundary. Broad arrows represent the low-level jet stream (LJ), the polar jet (PJ), and the subtropical jet (SJ). (b) As in (a) except for situations with a midlatitude warm-season synoptic scale pattern favorable for the development of especially severe and long-lived progressive derechos. The line BME represents the track of the derecho. From http://meted.ucar.edu/mesoprim/severe2/index.htm; adapted from Johns (1993).

derechos form on the cool side of a quasi-stationary frontal boundary and propagate parallel to the boundary, usually east or southeastward. They can have multiple bowing systems in families or can display discrete propagation. This pattern is often favored in the warm season. Serial derechos occur in the warm sector of a strong midlatitude synoptic scale cyclone. They display a sinusoidal pattern of bowing segments so that the bowing system tends toward the LEWP of Nolan (1959), the Type I bowing system of Przybylinski and DeCaire (1985), or the SLBE of KHB04. These systems are more favored in the cold season or in a strong forcing regime as seen with the strong synoptic scale cyclone.

A later study by Johns (1993) composed conceptual conglomerated maps conducive for forecasting outbreaks of bowing systems responsible for severe surface wind damage. Two synoptic patterns were dominant, which are depicted in Fig. 2.22: the **dynamic** pattern and the **warm season** pattern, roughly corresponding to cold sea-

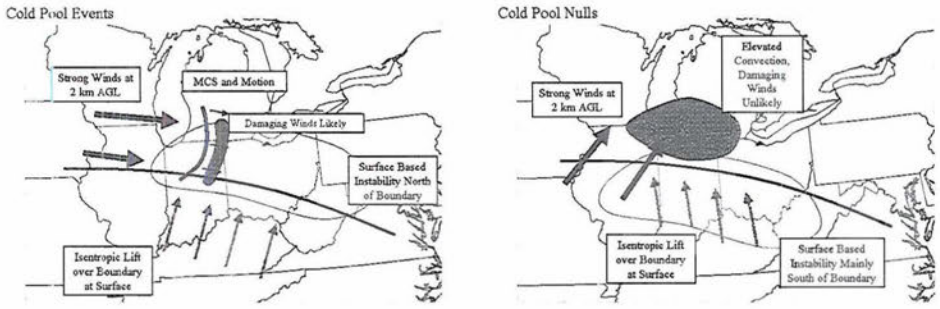

Figure 2.23: Conceptual models showing patterns that are (a) favorable and (b) unfavorable for damaging winds with systems forced by a cold pool gust front. From Kuchera and Parker (2004).

son strong forcing patterns (serial derechos) and warm season weak forcing patterns (progressive derechos), respectively.

Recently, studies of severe wind producing convective systems by Kuchera and Parker (2004) and Kuchera and Parker (2006) have revealed similar patterns to those of progressive and serial derechos of Johns and Hirt (1987) (Fig. 2.23 and Fig. 2.24). The authors emphasize in their study the importance of strong 2 km inflow into convective systems for severe wind production so that characteristic synoptic maps are formulated for favorable cases and null cases. These are called **cold pool** and **linear** events (likely closely corresponding to serial and progressive derechos, Johns 1993). To further validate the influences of synoptic boundaries, the present study will document the dependence of synoptic boundaries *specifically for bowing convective systems.*

2.7 Severe winds in bowing convective systems and derechos

In a study of 748 separate storm systems, Snook and Gallus (2004) showed that bow echoes account for the preponderance of severe wind reports in convective systems by almost a 2:1 ratio compared to any other convective system, with an average of 14.5 severe wind reports per storm (next closest was TS MCS with 7.35

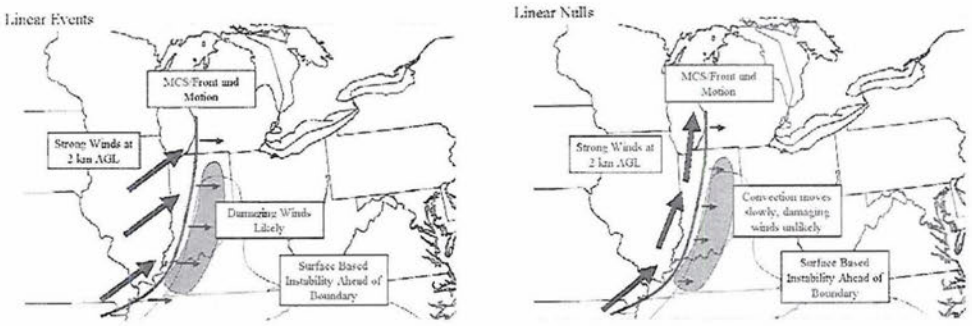

Figure 2.24: Conceptual models showing patterns that are (a) favorable and (b) unfavorable for damaging winds with systems forced by a strong linear mechanism. From Kuchera and Parker (2004).

reports per case). Bow echoes averaged approximately 0.8 extreme wind reports of 65 kts. wind or more per case (the most of any convective mode, with TS MCS the closest with 0.55 reports per case). The authors also showed that 1" diameter hail was also very common in bow echoes. However, bow echoes virtually never produced flooding and rarely ever produced 2" hail. This could be attributed to the large translational speeds of bow echoes. These findings along with many other previous studies (e.g. Fujita 1978, Przybylinski 1995, Weisman 2001) have shown the importance of understanding and forecasting bow echoes due to their common tendency to produce severe surface winds and severe weather.

A recent study by Kruk et al. (2005) has shown that the source of severe wind damage from bowing convection tends to change throughout the evolution of a convection system. There is a transition in severe wind production from macrobursts and tornadoes early to primarily straight-line winds later in a bow echo life cycle. Also, no mesovortex-induced severe surface winds were observed after rear-inflow was developed in their particular study. The present study will tabulate relative locations, magnitudes, and times of severe weather production from bowing convection.

Chapter 3

DATA AND METHODS

3.1 Selection of bowing cases

A major challenge in constructing a climatology of U.S. bowing convective systems (BCSs) includes selecting bowing cases subjectively and deciding upon an accepted definition. As previously discussed, problems arise in establishing definitions due to the complex nature of the phenomenon of "bowing".

There have been attempts to objectively identify MCSs from radar and satellite data (e.g. Steiner et al. 1995, Hodges and Thorncroft 1997, Machado et al. 1998, Baldwin et al. 2005). These methods are problematic in identifying bowing convection due to the large variability in their size, structure, and evolutionary behavior. Furthermore, the "bowing" process is difficult to capture in an algorithm due to the sporadic and complex motion of these systems.

Thus, cases for this study were subjectively selected by careful visual perusal of radar data throughout the United States. Despite the tedious nature of this task, this method yielded many BCS cases.

3.1.1 Spatial and temporal parameters for cases selected

The spatial area and time periods in this study were chosen to complement past studies of bowing convection. BS04 studied cold-season bow echoes (October to April, 1997-2001). To complement their work, warm season BCSs from April - September

for the years 2003-2004 were selected for study. The present study is regarded as important because cold season bowing convection could largely differ from convection in the warm season in properties such as location, longevity, and forcing mechanisms. Furthermore, KHB04 contained the Northern High Plains regional limitation. Taking these previous studies into consideration, a full examination for each day throughout the conterminous U.S. for 2003-2004 was performed to create an unbiased temporal and spatial documentation of U.S. BCSs.

3.1.2 Perusal and selection method

This study utilized three sources of online radar images to select cases:

(1) the Storm Prediction Center (SPC) Severe Thunderstorm Events Index (http://www.spc.noaa.gov/exper/archive/events/searchindex.html),

(2) the National Center for Atmospheric Research (NCAR) Image Archive (http://locust.mmm.ucar.edu/case-selection/), and

(3) the Plymouth State Weather Center Radar Control Message (RCM) Data Maps (http://vortex.plymouth.edu/rcm-u.html).

For each day from April 1 - September 30 for the years 2003 and 2004, the above archives of radar data images were examined in search of potential BCSs. While this search was guided by past studies of bowing convection events, the investigator kept an open mind with respect to the classification of bowing convection, with the anticipation that at the completion of two years of analysis, repeatable and classifiable patterns of bowing organization and behavior would emerge. The radar images were 2-km spatial resolution (except for the Plymouth State data source, which was 4-km) with 30 minute temporal resolution.

3.1.3 *Bowing convective system selection criteria*

Fujita (1978) went well beyond previous investigators (e.g. Nolan 1959, Hamilton 1970) in the study of bow echoes to propose a kinematic structure and a characteristic evolution for such systems. His methods included a thorough examination of radar evolutions of many case studies. Fujita emphasized that one of the distinct characteristics of bow echoes was their tendency to produce very long swaths of damaging straight-line winds, often collocated near the apex of the bow (see Chapter 1). He also recognized that these bow echoes could occur either individually or as part of a line-echo-wave-pattern (LEWP) (Weisman 2001).

The methodology of BS04 examined 1-h radar images with 4-km spatial resolution on the U.S. scale or drawing upon severe thunderstorm wind reports from the National Oceanic and Atmospheric Administration (NOAA) publication *Storm Data*. KHB04 stated that bow echoes were gathered in "an opportunistic fashion" so that their study was not a comprehensive climatology. In contrast, the search methods for BCSs in this study utilize a much more systematic approach.

The methodology in the present study mimics the methods of Fujita (1978) to examine *convection evolution* of bow echoes in radar reflectivity. It uses the methods of BS04 to initially identify bow echoes from online radar data while utilizing three sources instead of one with increased spatial and temporal resolution of images.

The criteria for a bowing convective system (BCS) case to be chosen in this study is as follows:

(1) A convective system (of cumulonimbus clouds) must arise that has at least 40-dBZ convective echoes.

(2) The convective system must evolve into an "arch" or "bow"-shaped line through *local acceleration* of the convective cell or cells on the convex leading edge as the system propagates.

(3) The bowing convection must demonstrate an expanding radius with time for at least 30 minutes, consistent with storms that propagate along a strong outflow (KHB04).

(4) Storm longevity must be at least 1 hour. This allows for at least two images of distinct "bowing" during the perusal process.

(5) The long-axis dimension of the bowing convective system must be at least 20 km. This permits sufficient image resolution using a 2-km radar pixel scale.

Of course, the possibility exists for bowing convection cases to be overlooked. However, with the trio of image sources, aside from extremely isolated or short-lived bowing convective systems, the author is confident that the sample sufficiently represents the warm-season bowing convective system population over the U.S. The above selection method yielded a total of 167 cases for 2003 and 214 cases for 2004, totaling 381 cases, a population size that has not been previously achieved in the examination of bowing convective systems.

3.2 National composite radar reflectivity data

The next step in this study was to closely examine each potential BCS with radar reflectivity data that was zoomed in to ascertain the development and movement of each case. The importance of the zoomed images is in the identification of mesoscale properties that BCSs exhibit (e.g. convective line region descriptions, differing stratiform precipitation regions, multiple bows). The images generated came from a national composite radar reflectivity dataset. Weather Services International (WSI) generates national composite radar reflectivity images from National Weather Service (NWS) WSR-88D radars for continuous images across the U.S. The data are divided into 16 bins of 5-dBZ intervals starting with 0-5 dBZ with a horizontal pixel resolution of 2-km x 2-km available in 15-min time intervals. The images display the

maximum instantaneous reflectivity found in a vertical column above each horizontal point in the display.

Once the cases were selected using the radar image sources detailed in section 3.1.2, radar data files were obtained from the NCAR WSI Radar Composite Archive (http://locust.mmm.ucar.edu/episodes/access_WSI_data.html). Using cases identified, the approximate times and grid sizes for each case were determined. The data were used to generate images and animations for each case. Multiple characteristics were noted from the animations including evolutionary properties, convective line characteristics, stratiform precipitation variability, recurring patterns related to the bowing convection, etc., that will be discussed further in Chapter 4.

3.2.1 Line-end rotation

Line-end vortices are perceived from rotation detectable in radar reflectivity animations, precipitation structure, and the terminal points of bowing curvature. Their frequency of occurrence is tabulated in this study. This method acknowledges that accurate assessment of line-end vortices from reflectivity data alone is difficult and likely creates a low bias in the vorticity; radial velocity data would aid the accuracy of tabulating rotation. Nevertheless, line-end vortex rotation is an important component of the evolution of bowing convective systems and is taken into account in this research.

3.2.2 Rate of bowing

The present study defines **slow bowing** convective systems as systems that bow slowly enough to never attain a "C shaped"[1] arched convective line on the leading edge. **Moderately bowing** convective systems bowed at a rate which achieves a

[1] A "C shaped" arch is defined as a curvature of approximately $\kappa = 0.014$ km^{-1}, or a radius of curvature of R $\approx$ 70 km.

"C shape" arch convective line on the leading edge in 4 h or more. **Fast bowing** convective systems attained a "C shape" arched convective line on the leading edge in 1 to 3 h. **Very fast bowing** convective systems accelerates to a "C shape" arched convective line on the leading edge in less than 1 h. These definitions will be important in the subjective assessment of bowing acceleration strength.

3.3 Synoptic surface charts

To further examine influences upon the bowing convective systems, surface pressure, satellite, radar, and surface boundary overlay images were obtained for study (Fig. 3.1). The satellite, radar, and surface pressure features were examined with hourly temporal resolution. Depictions of the synoptic features were available from the National Center for Environmental Prediction (NCEP) at 3-h intervals in relation to the known bowing convective systems. From the examination of the hourly maps throughout the evolution of the convective systems, the strength of the synoptic scale forcing was subjectively determined, following the methodology of Evans and Doswell (2001) to classify the forcing into Weak Forcing (WF), Hybrid Forcing (HF), or Strong Forcing (SF). Finally, the type of any synoptic scale boundary was noted along with the convective system location in relation to the sector of the midlatitude cyclone.

3.4 Severe weather reports

To further examine processes going on within the bowing convective systems, severe weather reports were examined. The SPC SeverePlot Software version 2.5 (http://www.spc.noaa.gov/software/svrplot2/) (e.g. Fig. 3.2) was obtained to tabulate the severe weather generated by the bowing systems. The software allowed for submitted queries from bow start to bow end. For each severe weather report, the times, type of report (severe hail, severe wind, or tornado), magnitudes (hail

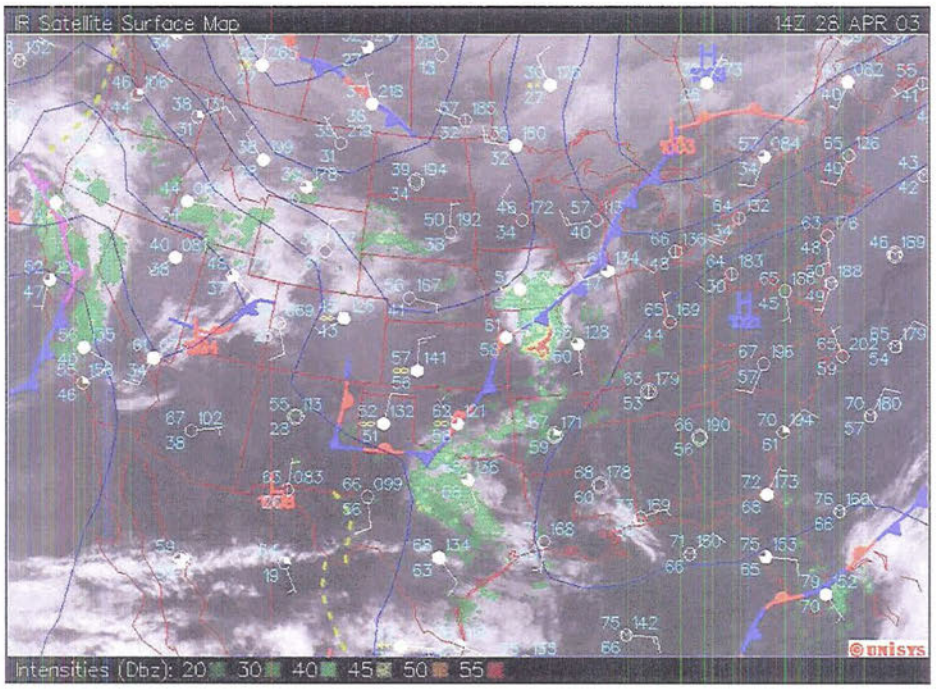

Figure 3.1: Example of surface pressure, satellite, radar, and surface boundary overlay image utilized in this study. Image is from 28 April 2003 with convective system located over central Missouri.

size, windspeed, or Fscale), relative locations, and distributions of severe weather throughout storm lifecycles were noted for study. Although the recent work of Trapp et al. (2006) cautions investigators in using severe wind reports to assess local surface wind damage, the present study focuses on the mesoscale aspects of BCS severe weather production, so there is greater confidence in the overall severe weather damage swaths.

The present study acknowledges the problems with severe weather reports. These could be underreported due to sparse populations (Weiss et al. 2002) or misrepresenting local damage surveys (Trapp et al. 2006). This study focuses primarily on the mesoscale aspects of severe weather production thus lending credibility to the results discussed.

The severe weather reports that make it into the SeverePlot software have been verified by local NWS offices. In most cases involving hail and wind damage, the local

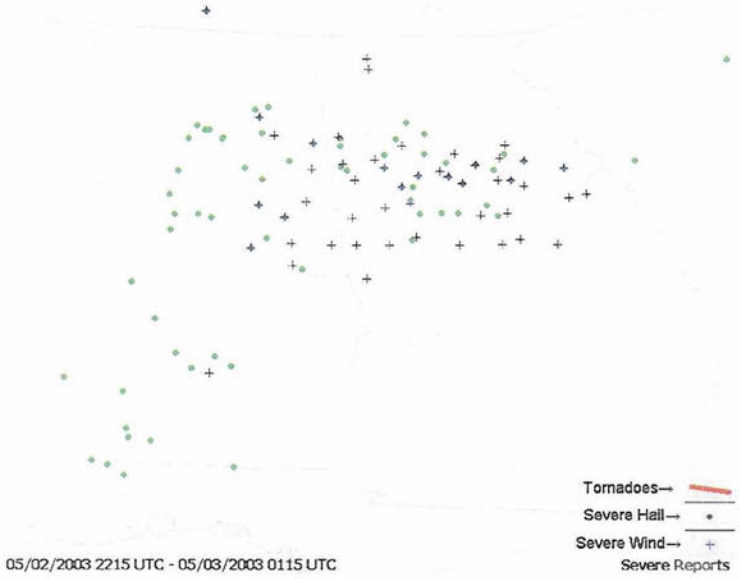

Figure 3.2: Example of hail, tornado, and severe wind reports generated by a bowing convective system. Image is from 2 to 3 May 2003 with convective system moving over Alabama and Georgia.

office relies on spotter reports of hail size and extent of damage. Possible tornadoes are commonly surveyed by NWS personnel to determine areal extent of damage and F-scale. Newspaper clippings and other sources may also provide input (John Hart, SPC, personal communication, 2006).

3.5 Proximity soundings

For a few cases selected, proximity soundings were obtained for additional study. The criteria for accepting a sounding was a distance of less than 200 km from the BCS centroid and a time difference from the bow centroid of less than 2 h from the bow start initiation point. The sounding had to be located downstream of the forming BCS. Each sounding was ensured to be in the same relative air mass (not across any synoptic scale fronts) as well as not influenced by precipitation which would modify the pre-convective environment.

of deviant cellular motions from surrounding convective cells. These observations were usually confirmable with observations of hook echoes and downstream precipitation anvils in the reflectivity data.

Six unique categories were assigned for classifying the initial convective modes which produce BCSs. The groups presented in this research that are similar to studies of KHB04 and BS04 include **group of cells**, **squall line**, **embedded**, and **supercell**. The additional groups proposed here are **mixed supercells and cells** and **multiple supercells**. In the terminology of this classification, "cells" refers to ordinary or multicellular convection not arranged in a squall line.

A **group of cells** involves the interaction and merging of ordinary or multicellular convection to produce a BCS. **Squall lines** produce bowing convection when either an entire squall line exhibits bowing acceleration or when a squall line displays acceleration of multiple bowing segments. **Embedded** precipitation produces bowing convection when a contiguous precipitation shield gives rise to a BCS nested within the precipitation region. The **supercell** mode describes the bowing of a single, isolated supercell. The **mixed supercells and cells** mode represents the evolution of one or more supercells in which the deviant motions instigate the interaction with ordinary or multicellular convection to produce a BCS. The **multiple supercells** group characterizes two or more supercells interacting with one another to form bowing convection. Composite radar reflectivity images illustrating each initial convective mode are shown in Fig. 4.1.

The categories of initial convective modes were chosen to distinguish between the convective characteristics unique to each mode. The processes on small scales cannot be robustly determined from the dataset utilized, so the following discussion is from the best assessment possible given the methodology used. A group of cells would tend to develop in a weak to moderate vertical wind shear environment with the evolution to a BCS involving convection merging along a common outflow. Bow-

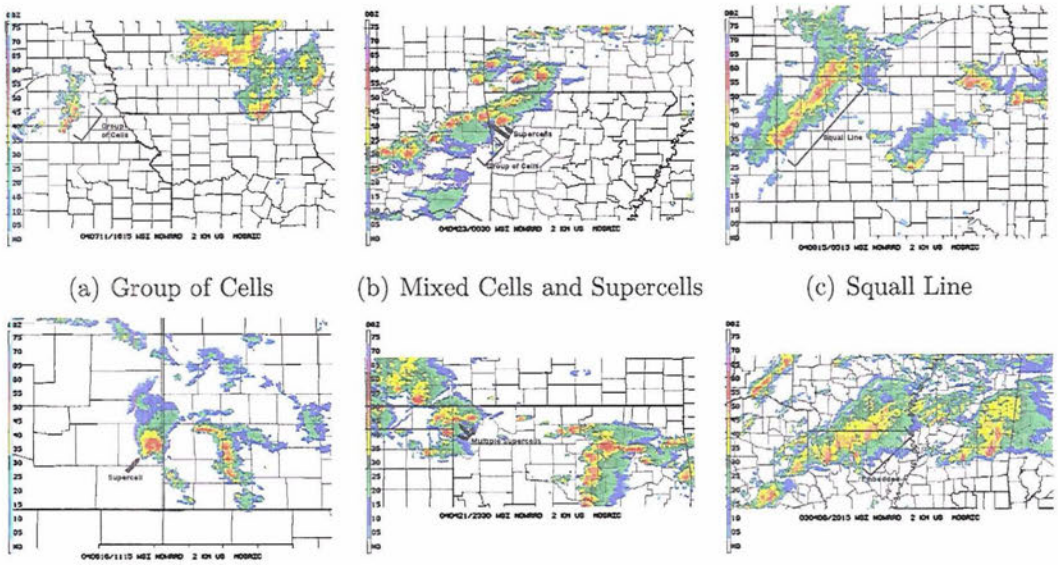

(a) Group of Cells (b) Mixed Cells and Supercells (c) Squall Line

(d) Supercell (e) Multiple Supercells (f) Embedded

Figure 4.1: Composite radar reflectivity examples of six initial modes of convection that formed bowing convective systems during this study.

ing acceleration originating from a squall line involves development of rear-inflow in the existing mesoscale convective system (Johns and Hirt 1987, KHB04). BCSs emerging from embedded precipitation exhibit a localized enhancement of convective cells that generate a BCS. The transition of a single, isolated supercell into a BCS involves a progression as discussed by Moller et al. (1994) and Finley et al. (2001). The complex interaction of one or a few rotating supercells with ordinary or multicellular convection characterizes the development of bowing convection from the mixed supercells and cells' initial mode, which could involve a wide range of vertical wind shear environments. Multiple supercells merging to form a BCS entails intricate exchanges between adjacent supercells usually occurring in a strong vertical wind shear environment. Each of these six categories suggests unique convective processes that could also be manifest in the local kinematic and thermodynamic environments.

The most common initiating mechanism of a BCS was a group of ordinary or multicells that interact, accounting for 48% of the cases (Fig. 4.2). The other

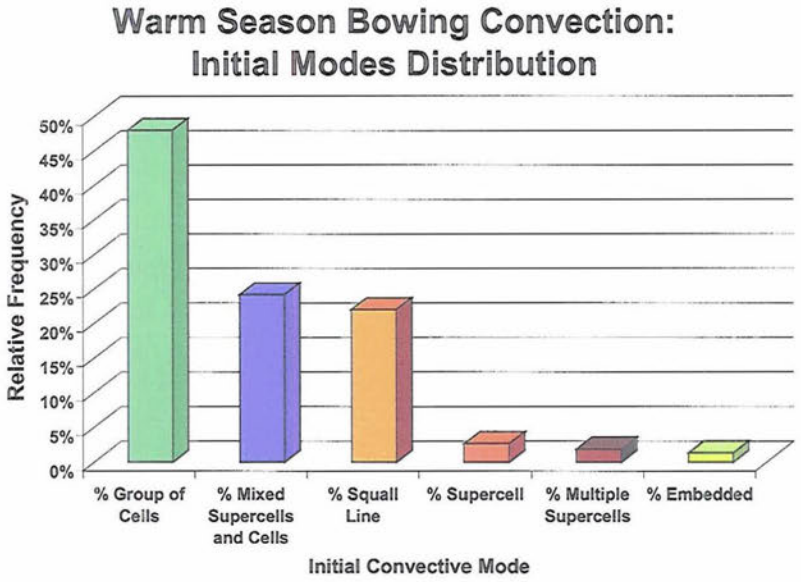

Figure 4.2: Relative frequency distribution of initial modes of convection that resulted in the formation of bowing convective systems from April through September 2003 and 2004 as identified in Fig. 4.1.

two primary initial convective modes that produced BCSs occurred when supercells interacted with ordinary or multicells (24%) and when a squall line experienced bowing accelerations (22%). The other three initial convective modes accounted for only about 6% of the total distribution.

To elaborate on the process observed by radar, reflectivity animations suggested that a group of cells that forms a BCS many times arranged in a small quasi-linear convective band before any bowing acceleration. However, this was not always found to be the case because ordinary or multicelluar clusters sometimes demonstrated bowing acceleration directly after cell initiation. Most BCSs that arose from the mixed supercells and cells mode usually had one or two dominant supercells which were usually classifiable in the classic or high-precipitation category. These rotating cells tended to merge with other nearby cells arranging in a quasi-linear fashion. The resulting BCSs that arose often exhibited strong mesoscale rotation. In order

to distinguish between the group of cells initial group and the squall line initial group, this study required a squall line to be at least 100 km in length and to last at least 30 minutes before exhibiting any bowing acceleration so that it was distinct from a group of cells merging to form a BCS. These MCSs were almost always of the Trailing Stratiform (TS) archetype (Parker and Johnson 2000). Embedded precipitation very rarely produced bow echoes. This is likely due to the slow moving nature of these systems along with limited potential for cold pool production that hinders the formation of strong convection along a common outflow.

4.1.2 Comparison to past studies

The present study observed that squall lines initiated BCSs less frequently than in KHB04 (22% vs. 40%). The fraction of BCSs initiated by groups of cells is very similar (48% vs. 45%).

In comparison to BS04, groups of cells are much more common in the present study (48% vs. 24%), squall lines are much less common (22% vs. 49%), while the supercell and embedded modes are somewhat comparable (2.6% vs. 6% and 1.3% vs. 6%, respectively). A possible explanation for the differences between these studies could be variations in BCSs that develop during the cold season versus the warm season. The differences could also be attributed to the nature of the forcing mechanisms. With regard to the overall fraction of deep moist convection in the cold season, squall lines are favored over groups of cells due to the more frequent occurrence of strong synoptic forcing causing the formation of large BCSs (Evans and Doswell 2001, see section 5.4.1).

4.2 Bowing convective modes

This section describes the spectrum of bowing convective modes discovered through the analysis of radar reflectivity observations. Bowing convective mode

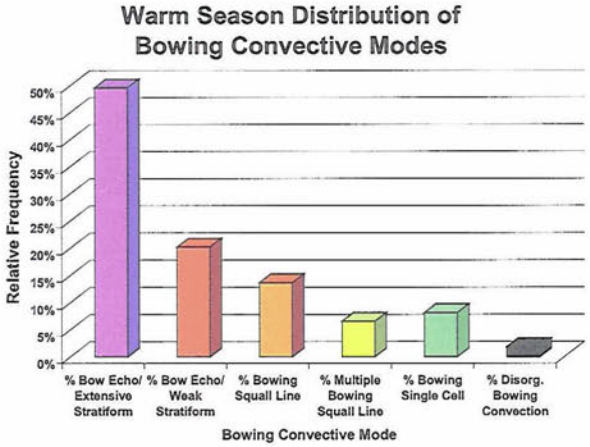

Figure 4.3: Relative frequency distribution of bowing convective modes observed throughout this study.

structures were chosen based on properties such as initial structure of convective cells, convective line length, stratiform precipitation, and convection evolution. In addition, modes were characterized by factors such as differences in line-end rotation, rate of bowing, and timing of stratiform precipitation production. In the following subsections, the timing of stratiform precipitation formation is discussed with regard to the initiation, bowing, mature, and dissipating stages of a BCS. In this study, the bowing stage is defined as a period of time when the bowing convective line exhibits nearly uniform acceleration along the leading edge. The mature stage is a period of time when the convective system's concavity is approximately unchanging.

Five bowing convective modes were assigned. They are termed **bow echo/extensive stratiform** (BE/ES), **bow echo/minimal stratiform** (BE/MS), **bowing squall line**, **multiple bowing squall line**, and **bowing single cell**. In these definitions, stratiform refers to convectively generated stratiform (Houze 1997). Fig. 4.3 displays the percentage distribution of each organizational mode as tabulated in the present study. Further study of the properties of the bowing convective modes reveals distinctions in the longevities, locations, reports of severe weather production, and kinematic/thermodynamic environments. The discussion that follows details the

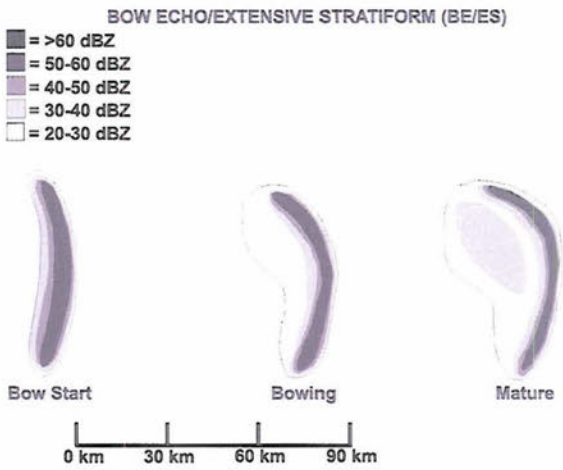

Figure 4.4: Schematic conceptual evolution of a bow echo/extensive stratiform (BE/ES) system observed in this study. The typical radar reflectivities correspond to the color scale given in the upper left of the figure. The length scale is given to show the average convective line length and track length.

factors that delineate properties among these modes.

4.2.1 Mode 1: Bow Echo/Extensive Stratiform

The most common bowing convective mode (49%) observed is the **bow echo/extensive stratiform** (BE/ES). The most distinguishing feature of this archetype is the development of moderate-to-heavy trailing stratiform precipitation (35-45 dBZ reflectivity precipitation) during the evolution of the precipitation structure. There is frequently a radar reflectivity trough and a secondary precipitation maximum as one proceeds rearward from the convective line (Smull and Houze 1985a). This mode is a bow echo consisting of a convective line in the 40-110 km length range. The conceptual evolution of this mode is displayed in Fig. 4.4 while a composite radar reflectivity example of the various stages of this mode is shown in Fig. 4.5.

Note that the conceptual model (Fig. 4.4) isolates the bowing convection; the possibility exists for a quasi-linear group of convective cells to be present on either

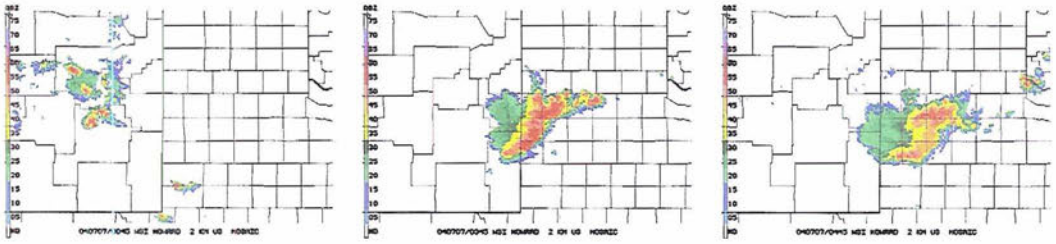

(a) First 40 dBZ Echoes, 0045 UTC (b) Initiation, 0345 UTC (c) Bowing Stage, 0445 UTC

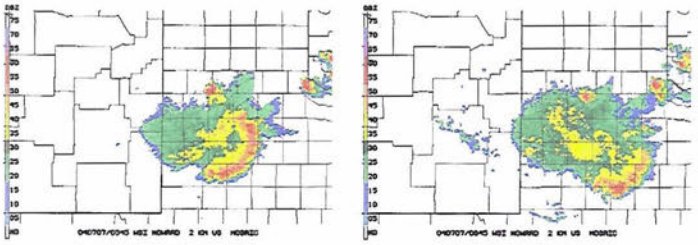

(d) Mature Stage, 0545 UTC (e) Dissipation, 0645 UTC

Figure 4.5: Composite radar reflectivity example of a bow echo/extensive stratiform (BE/ES) system from 7 July 2004 over western Texas.

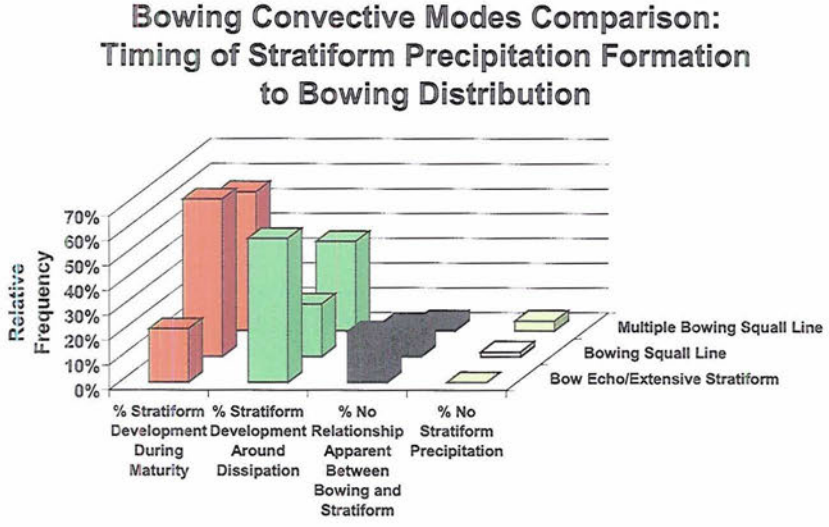

Figure 4.6: Relative frequency distribution comparison of trailing stratiform precipitation formation timing in relation to bowing stages for bow echo/extensive stratiform, bowing squall line, and multiple bowing squall line.

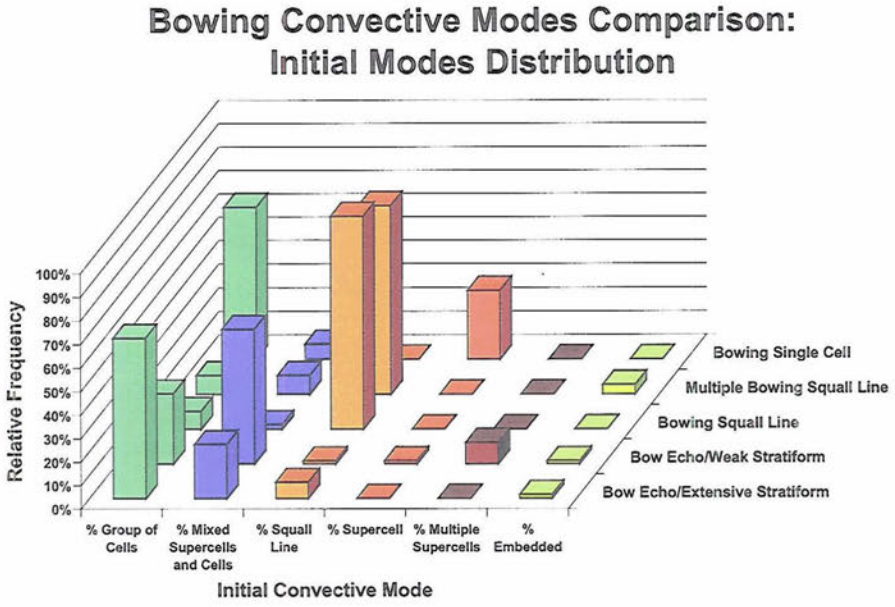

Figure 4.7: Relative frequency distribution comparison of initial convective modes to bowing convective modes for all cases observed in this study.

end of any of the models for any bowing convective mode. However, additional convection extending beyond the bow is less common than the depictions illustrated.

The trailing stratiform precipitation for this structure usually develops during the later-mature to dissipating stages of the bow echo evolution (Fig. 4.6). Comparison with two other bowing convective modes is also shown in Fig. 4.6. This mode typically displays a *noticeable lag* in the formation of stratiform precipitation after the bowing process has occurred. BE/ES convective lines often have a sharp reflectivity gradient on the convex leading edge with a weaker reflectivity gradient on the trailing edge of the convective line into the stratiform region.

Most often, bow echoes with extensive stratiform form from groups of ordinary or multicellular cells into a strong mesoscale cluster or quasi-linear convective band of cells and subsequently into a bow echo (Fig. 4.7). Supercells interacting with ordinary or multicells also initiate these structures at times. If this process occurs, usually *only one dominant supercell* influences the evolution of the convection into a

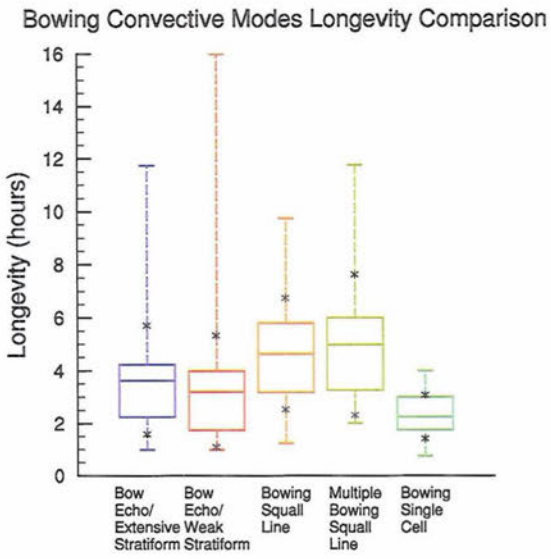

Figure 4.8: Comparison of bowing longevities for each bowing convective mode as defined in section 4.2. The middle line in each box represents the mean. The edges of the boxes represent the lower and upper quartiles of the distributions while the ends of the lines are the minima and maxima. The $\pm 1\ \sigma$ (standard deviation) locations of each distribution are shown as black "x"s on each distribution drawing.

BE/ES.

The average bowing longevity of a BE/ES is around 3.75 h with most cases lasting 2 to 6 h (Fig. 4.8). These storms are well distributed over most of the eastern two-thirds of the United States (Fig. 4.9). BE/ESs usually start bowing between 1200 and 2200 LST while dissipating between 1600 and 0300 LST (Fig. 4.10 and Fig. 4.11).

This mode of convection does not produce very much severe weather, usually producing 0-5 large hail reports, 0-15 severe surface wind reports, and rarely producing tornado reports (Figs. 4.12, 4.13, and 4.14). All bowing convective modes average about one severe wind report for every 10 km of convective line length for an entire convective evolution, but there is considerable variability from case to case.[1]

A representative sounding describing a BE/ES case on 29 April 2004 in South-

[1] The absolute number of severe weather reports does not necessarily reflect the proclivity of a bowing convective mode to produce severe weather. This is because systems are different sizes and normalization by storm size is needed but difficult to undertake for all BCSs.

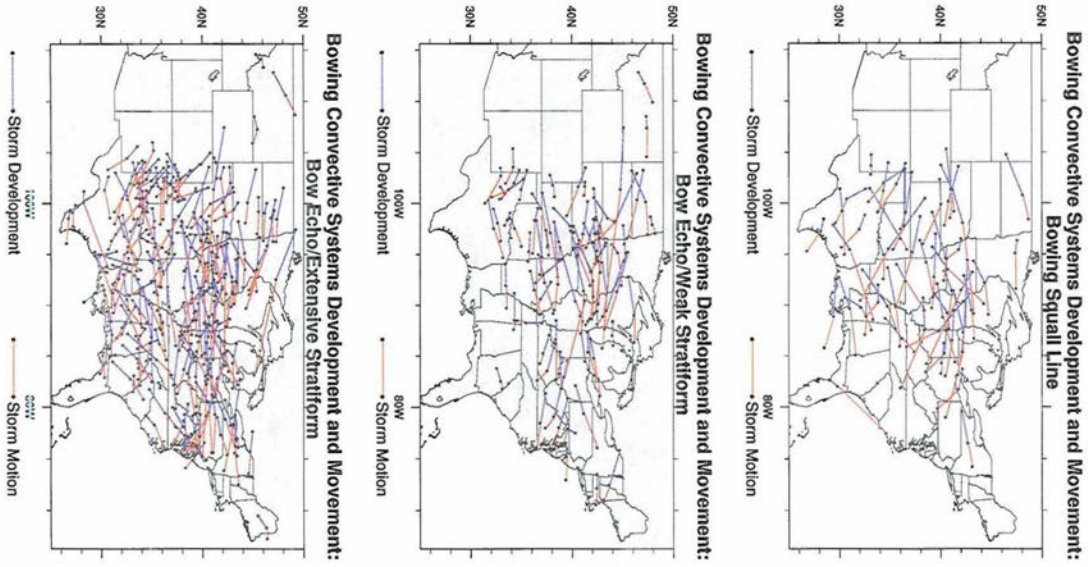

(a) Bow Echo/Extensive Stratiform

(b) Bow Echo/Minimal Stratiform

(c) Bowing Squall Line

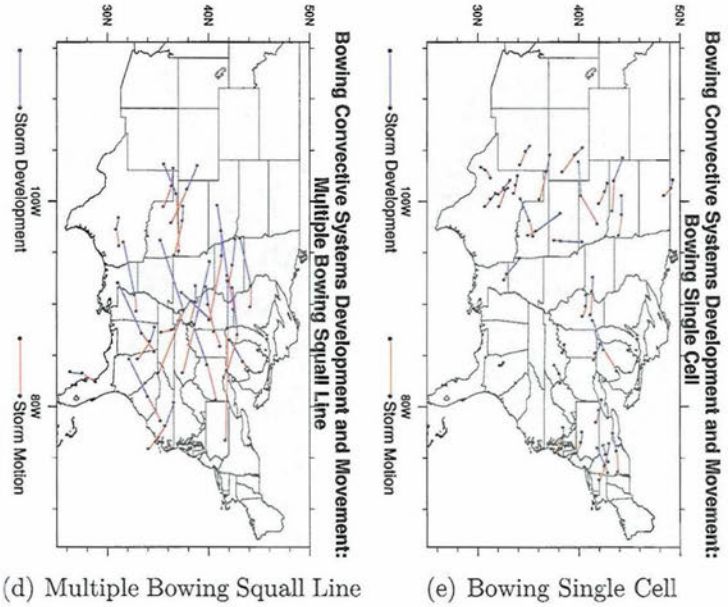

(d) Multiple Bowing Squall Line

(e) Bowing Single Cell

Figure 4.9: Bowing convective system development and movement locations divided up over bowing modes. Development and movement tracks are defined in section 2.2. Movements are taken to be approximately linear tracks between first echoes and bow start as well as between bow start and bow end.

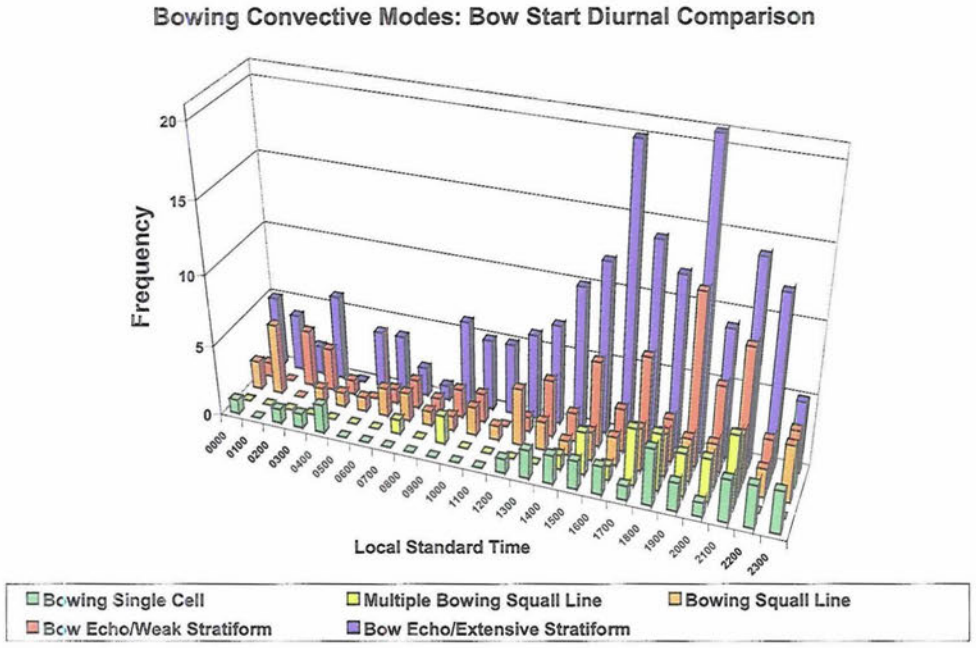

Figure 4.10: Comparison of bow start times in local standard time for each bowing convective mode as defined in section 4.2. Each bin is labeled with the leading time so that the 0500 bin includes times through 0500-0559 LST.

west Oklahoma is shown in Fig. 4.15.[2] According to SPC sounding estimates, the surface and Mixed Layer (ML) CAPE were 1746 J kg^{-1} and 2262 J kg^{-1}, the 0-3 km and 0-6 km vector wind difference magnitudes were 8.0 m s^{-1} and 10.3 m s^{-1}, with a 9.8 m s^{-1} storm-relative wind inflow in the 0-2 km layer. The ML CAPE for this sounding corresponds to a mid-range instability compared to past studies, while the vector wind difference magnitudes are on the lower end of magnitudes of vertical wind shear compared to past studies (see appendix A). These parameters will be compared with the next bowing convective mode in the next subsection.

[2] A close proximity sounding is shown instead of showing a composite sounding. As discussed in Brown (1993), averaging many cases causes smoothing which diminishes soundings used for comparison purposes.

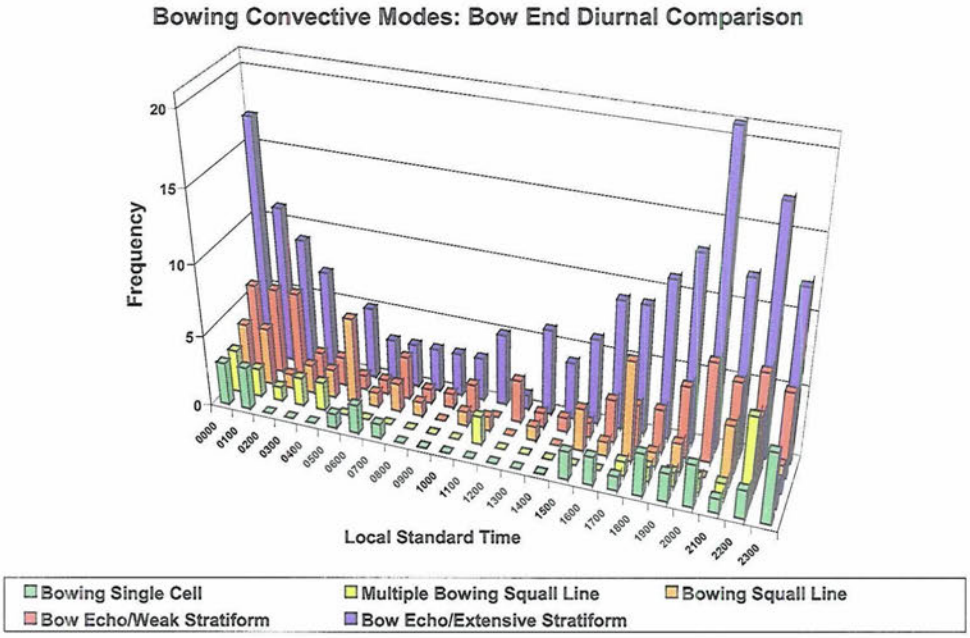

Figure 4.11: Same as Fig. 4.10, except for bow end time.

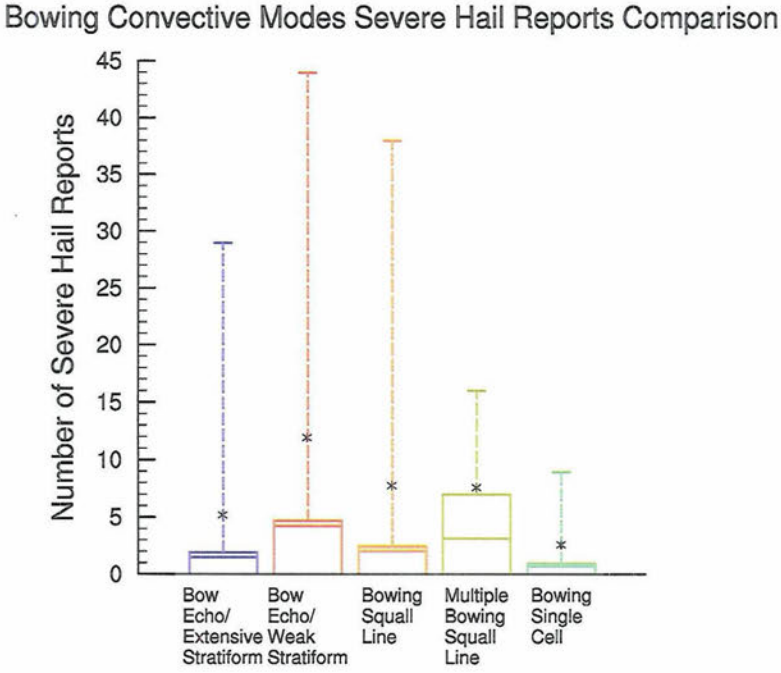

Figure 4.12: Same as Fig. 4.8, except for comparison of the number of severe hail reports.

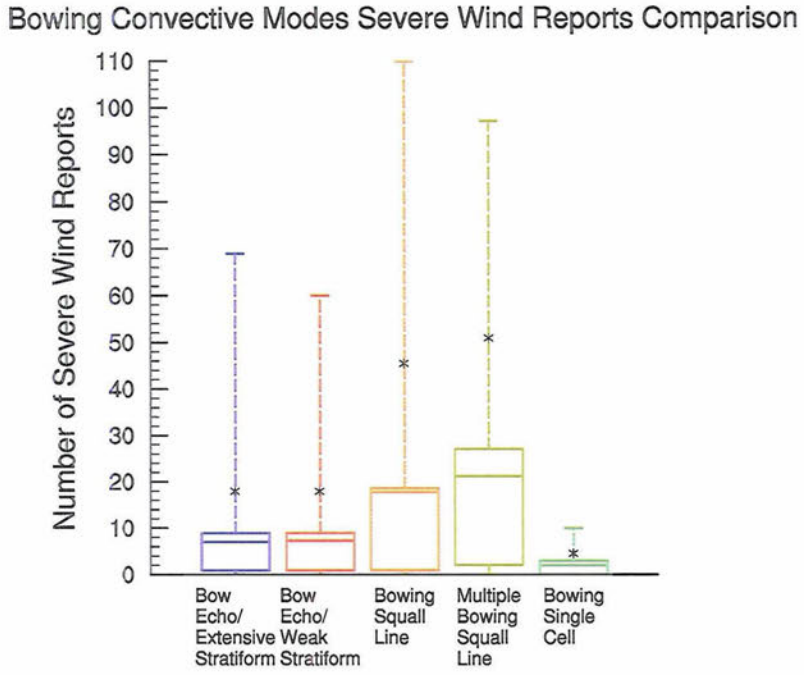

Figure 4.13: Same as Fig. 4.8, except for comparison of the number of severe wind reports.

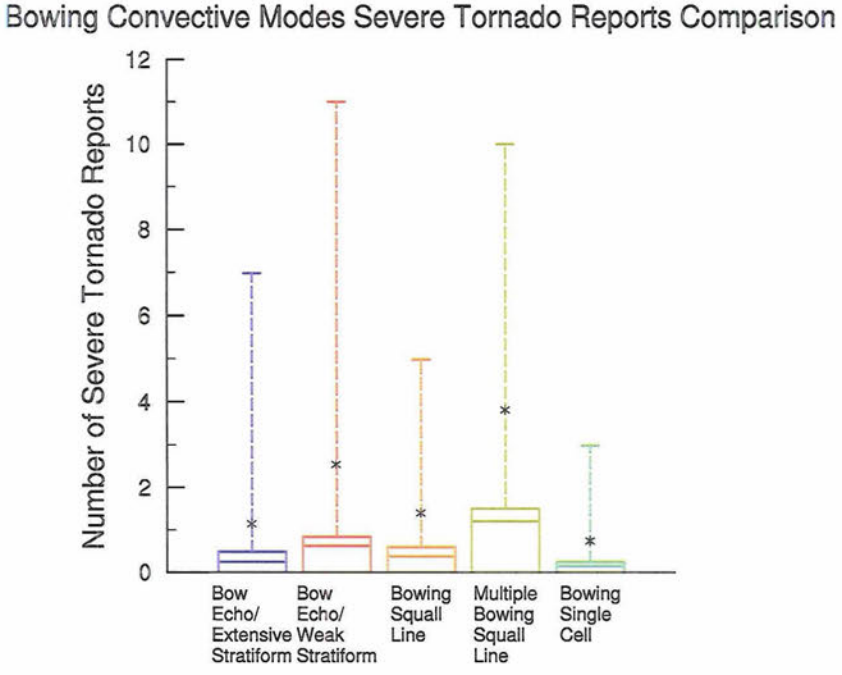

Figure 4.14: Same as Fig. 4.8, except for comparison of the number of severe tornado reports.

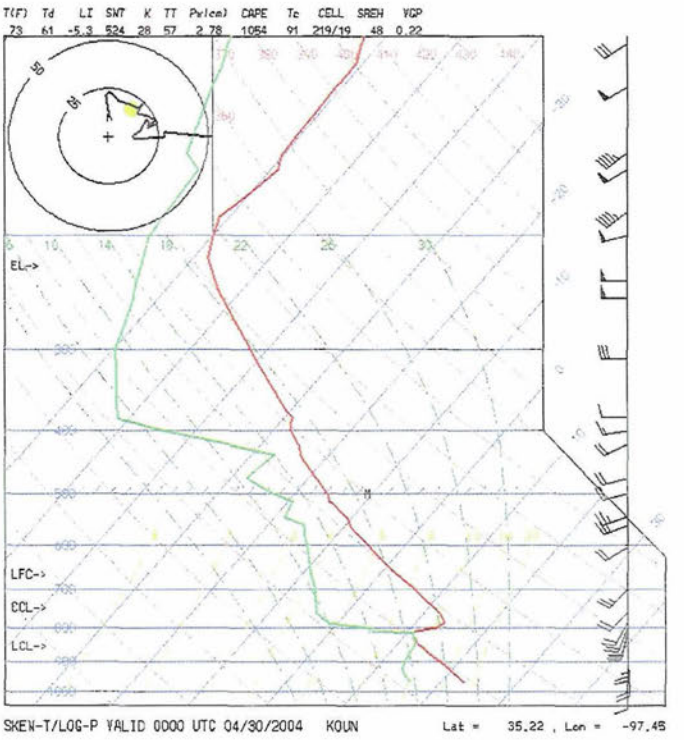

Figure 4.15: Skew T-log p plot of rawinsonde observation from Oklahoma City, OK (OUN), at 0000 UTC 30 April 2003.

4.2.2 Mode 2: Bow Echo/Minimal Stratiform

The second most common bowing convective mode (20%) is the **bow echo/minimal stratiform** (BE/MS). The most distinguishing characteristic of these bow echoes is *very little trailing stratiform precipitation* throughout their evolution (Figs. 4.16 and 4.17). This mode is a bow echo with a convective line in the 40-110 km length range. As depicted in the conceptual evolution, BE/MS systems tend to have a sharp radar reflectivity gradient immediately behind and in front of the reflectivity maximum, whereas the BE/ES systems have a sharp reflectivity gradient only on the leading edge.

The conceptual model of the BE/MS looks similar to the original bow echo model of Fujita (1978) (Fig. 1.1). The tall echo that Fujita referred to appears to resemble the convection that initiates this bowing convective mode (not shown). Su-

Figure 4.16: As in Fig. 4.4 but for a bow echo/minimal stratiform system.

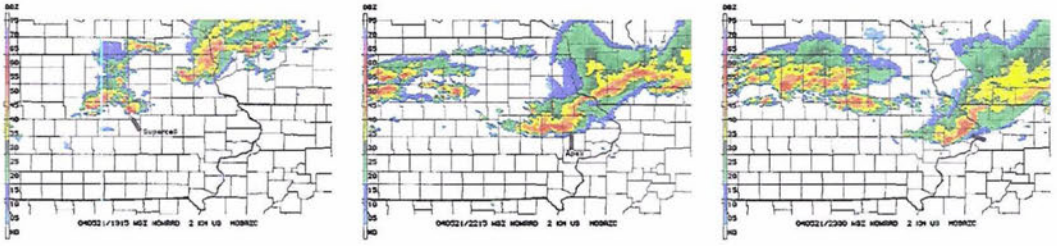

(a) First 40 dBZ Echoes, 1915 UTC (b) Initiation, 2215 UTC (c) Bowing Stage, 2330 UTC

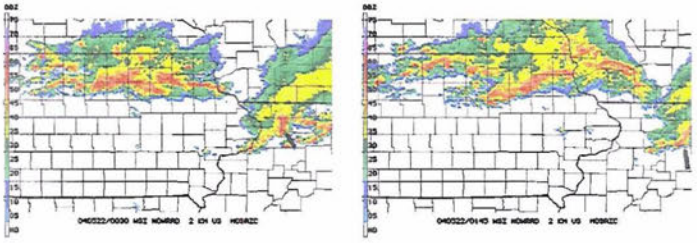

(d) Mature Stage, 0030 UTC (e) Dissipation, 0145 UTC

Figure 4.17: As in Fig. 4.5, but for a bow echo/minimal stratiform (BE/MS) system from 21-22 May 2004 over eastern Iowa and western Illinois.

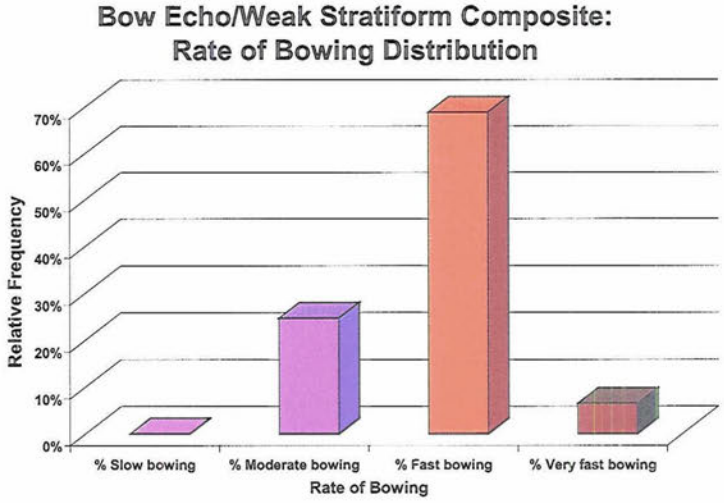

Figure 4.18: Relative frequency distribution of the rate of bowing for the bow echo/minimal stratiform composite.

percells and very strong, tall convective cells often initiate BE/MSs (Fig. 4.7); one can infer that this initiating convection remains *vertically erect* resulting in light trailing stratiform precipitation production. Radar reflectivity animations suggested that even when supercells or strong convective cells interacted with ordinary or multicellular convection to form these systems, the supercells or strong convective cells appeared to dominate the convective evolution into a bow echo. Moreover, when the mixed supercells and cells initial convective mode produced BE/MS systems, there were greater numbers of supercells and higher reflectivity supercells compared to the BE/ES systems.

BE/MSs at times inherit trailing stratiform precipitation from nearby convection, but these convective systems tend to diminish this influence or produce no significant stratiform rain throughout their evolution. Sometimes this mode is difficult to distinguish from a BE/ES if it develops in a very moist environment where pre-existing stratiform precipitation exists.

Strong rotation is often observed in the line-end vorticies for BE/MSs, with 46% of storms in this mode with an identifiable cyclonic vortex compared with only

32% for all other modes.[3] According to the distribution of the rate of bowing for this mode in Fig. 4.18, there is a very strong tendency for fast and very fast bowing in BE/MSs. In general, stronger damaging surface wind gusts are possible in faster-moving or faster-accelerating BCSs since the observed surface wind speeds are the sum of the storm motions and the storm relative winds (Wakimoto et al. 2006a). Interestingly, many examples of rear-inflow notches (RINs) from past studies are identified for cases with limited trailing stratiform precipitation like this convective mode (e.g. Fig. 2.13, Przybylinski 1995). The statistics from this study indicate that there exists a higher frequency of RINs for the BE/MS compared to the rest of the cases (44% vs. 27%).

BE/MSs are slightly shorter lived than the BE/ES systems, usually around 3.5 h in longevity with most cases lasting 1 to 5 h (Fig. 4.8). It seems reasonable that bowing convective modes that produce trailing stratiform precipitation while continually regenerating convection on the leading edge have a greater potential to be long-lived. Radar reflectivity animations suggest that BE/MSs appear somewhat unstable and not well suited for convection regeneration due to strong rotation, large bowing accelerations, and the maintenance of strong convective cells on the leading edge, although additional data would be needed to assess the dynamical linkages.

Notably, this mode tends to be preferentially located north of 32°N latitude (Fig. 4.9). These results could be indicative of large-scale conditions conducive to the formation of this bowing mode. It is possible that the climatologically moist environment of the southern U.S. states is more likely to produce bowing convection with trailing stratiform precipitation. However, vertical wind shear could also play a role. BE/MSs have a similar but narrower diurnal distribution than BE/ESs (Fig. 4.10 and Fig. 4.11). BE/WSs usually start bowing between 1500 and 2100 LST and dissipate between 1900 and 0200 LST.

[3] Unless otherwise noted, percentages listed as results are statistically significant on the 95% or 99% level taking into account the overall population size and the composite sample size.

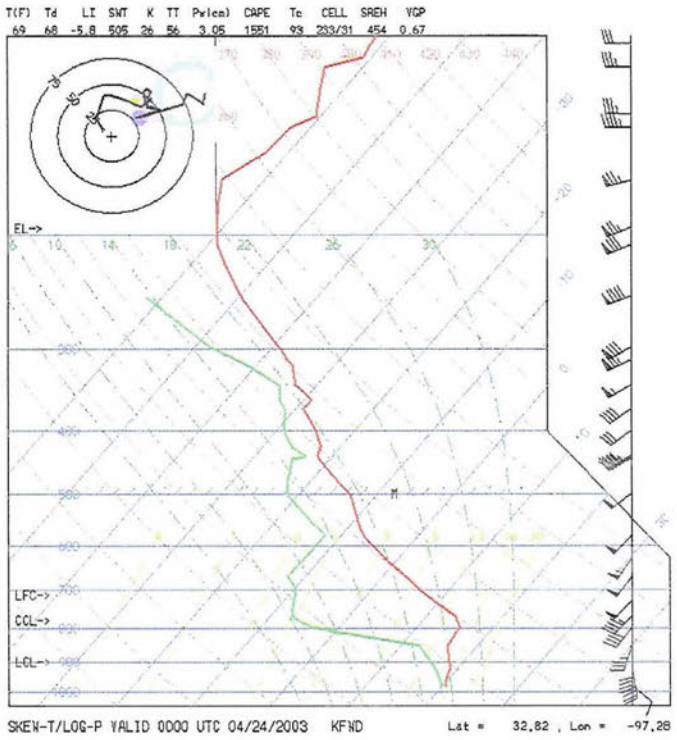

Figure 4.19: Skew T-log p plot of rawinsonde observation from Fort Worth, TX (FWD), at 0000 UTC 24 April 2003.

BE/MSs produce about twice as many hail and tornado reports as BE/ESs on average (Figs. 4.12, 4.13, and 4.14). This result could be related to the stronger reflectivity cells and their stronger influence on these systems as they form.

A representative sounding describing a BE/MS case on 24 April 2003 in Southwest Oklahoma is shown in Fig. 4.19. According to SPC sounding estimates, the surface and ML CAPE were 1979 J kg^{-1} and 2745 J kg^{-1}, the 0-3 km and 0-6 km vector wind difference magnitudes were 23.9 m s^{-1} and 28.8 m s^{-1}, with a 11.3 m s^{-1} storm-relative wind inflow in the 0-2 km layer. The ML CAPE for this sounding corresponds with a mid-range instability compared to past studies while the vector wind difference magnitudes are on the upper end of magnitudes of vertical wind shear compared to past studies (see appendix A).

In comparison to the BE/ES mode of convection, the convective instabilities,

drying of air above 2 km, and storm relative wind inflows are similar between the two case studies. However, the BE/MS sounding has much larger low-layer and deep-layer vector wind difference magnitudes compared to the BE/ES sounding. Note that these examples are chosen around a similar time of year with similar regional placements. Thus, these cases could provide some distinction between the BE/ES and BE/MS modes of convection. Furthermore, the greater vertical wind shear for the BE/MS mode may account for the higher frequency of severe weather compared to the BE/ES mode. It is also consistent with more upright convection and minimal trailing stratiform precipitation.

4.2.3 Mode 3: Bowing Squall Line

The third most common bowing convective mode (14%) is the **bowing squall line**. This mode is a bowing MCS with a convective line in the 110-225 km length range and includes the longest convective lines established for a BCS. It is noted that bowing squall lines are substantially smaller than many squall lines. Although in this study 225 km has been selected as the upper limit to bowing convection, additional work is needed to ascertain the dynamical basis for the upper limit to bowing convection. It is certainly possible that longer squall lines could exhibit bowing (e.g. Johnson and Hamilton 1988, Skamarock et al. 1994). The 225 km bowing convective line fits in between the upper limits of the recent studies of BS04 and Coniglio et al. (2004a) (see Table 2.1). This bowing convective mode is described as the bowing of an entire squall line that existed for at least 30 minutes as a linear MCS prior to the bowing process (Figs. 4.20 and 4.21). This mode almost always demonstrates extensive trailing stratiform precipitation (96% moderate-to-heavy stratiform precipitation).

According to the distribution of the timing of stratiform precipitation formation in relation to bowing for this mode (Fig. 4.6), bowing squall lines generate trailing

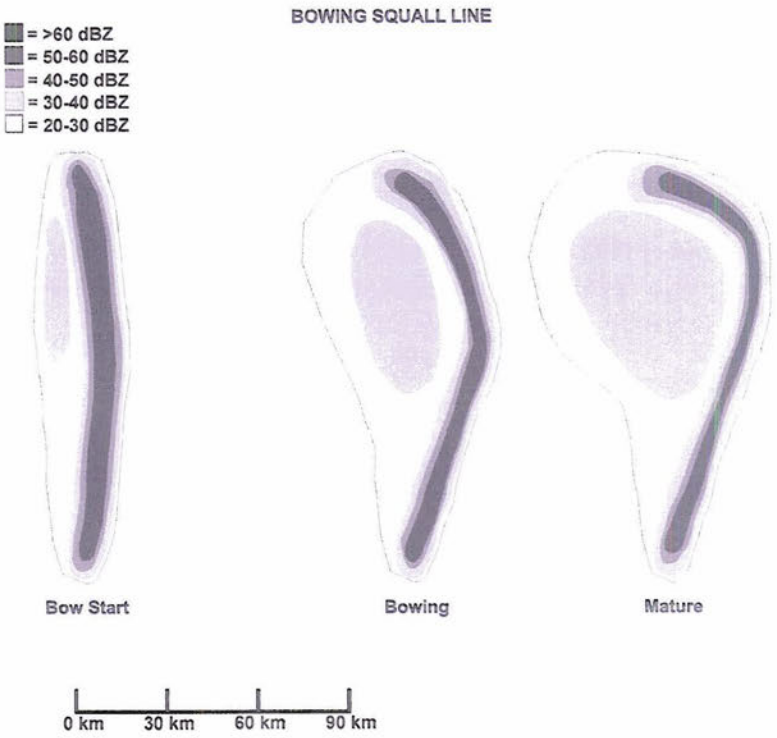

Figure 4.20: As in Fig. 4.4 but for a bowing squall line system.

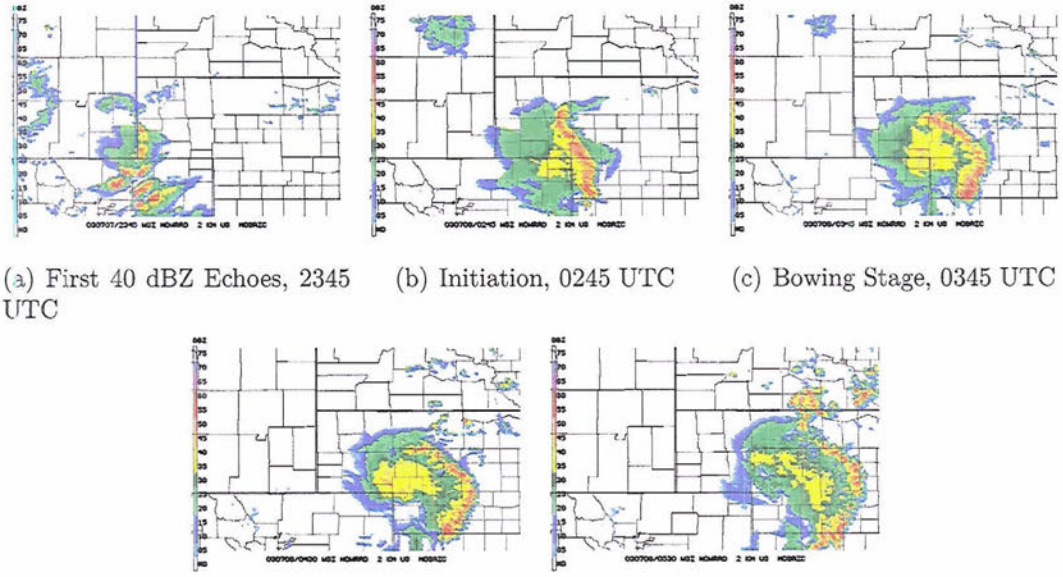

(a) First 40 dBZ Echoes, 2345 UTC (b) Initiation, 0245 UTC (c) Bowing Stage, 0345 UTC

(d) Mature Stage, 0430 UTC (e) Dissipation, 0530 UTC

Figure 4.21: As in Fig. 4.5, but for a bowing squall line system from 7-8 July 2003 over western Nebraska.

stratiform precipitation *much earlier* in the bowing process compared to BE/ESs. Usually, early in the mature stage, shortly after bowing acceleration begins, substantial trailing stratiform precipitation develops in a bowing squall line. That is, the formation of trailing stratiform precipitation in this mode occurs early in the evolution while maintaining a bowing convective line for several hours longer. Furthermore, 54% of all bowing squall lines have pre-existing trailing stratiform precipitation before any bowing occurs (as compared to 20% for all other modes).

The distribution of initial modes that form bowing squall lines demonstrates that a squall line produces this mode of convection 87% of the time (Fig. 4.7). The other initial modes rarely cause a bowing squall line. Also, the bowing squall lines forced from the other initial modes typically have a less-organized structure compared to those that arise from a longer lasting TS MCS.

This mode averages a longevity of 4.75 h, which is much greater than BE/ESs or BE/WSs, with many bowing squall line cases lasting 2.5 to 7 h (Fig. 4.8). These systems reveal a preference for formation over the central United States (Fig. 4.9). Presumably, this finding is connected to the climatological tendency of MCS formation over the central United States. Bowing squall lines have a unique diurnal distribution: the bow start and bow end times are well spread throughout the local day with very small peaks in the distributions (Fig. 4.10 and Fig. 4.11).

Bowing squall lines produce around the same number of severe hail and tornado reports as BE/ESs (Figs. 4.12 and 4.14). However, these convective systems tend to produce many more severe wind reports than the two previous bow echo modes (usually 0-45 reports, Fig. 4.13). The large-scale nature of the bowing squall lines with a potentially wide rear-inflow jet (RIJ) could contribute to a wide areal extent of severe surface wind damage.

Ten of all 31 derechos observed in this study are bowing squall lines. In addition, 19% of all bowing squall lines tabulated meet the derecho criteria of Johns and Hirt

(1987). These statistics imply that this mode of convection is commonly a large-scale MCS that continually regenerates convection on the leading edge.

4.2.4 Mode 4: Multiple Bowing Squall Line

The next bowing convective mode is the **multiple bowing squall line**, totaling 7% of all cases. The conceptual evolution of this mode is displayed in Fig. 4.22, while a radar example of this mode from this study is shown in Fig. 4.23. This mode is described as the bowing of an entire squall line into two or more bowing convective segments that are adjoined. Each individual bowing segment falls anywhere between 30 and 190 km (based on the observations) while the total line lengths (all bow lengths added) occur anywhere between 110 and 510 km. While 510 km is much greater than the 225 km maximum of the bowing squall line, *no individual segment* was any longer than 190 km (see the multiple bowing line segments distribution in Fig. 4.24). In fact, this distribution is very similar to the overall BCS line lengths distribution in Fig. 4.27. While the overall horizontal extent of the bowing convection is usually greatest for multiple bowing squall lines compared to all other modes, the individual bowing segments fall into the preferred ranges previously discussed. In the present study, out of the 25 cases that were multiple bowing squall lines, 16 cases contained two bowing segments, 6 cases contained three bowing segments, and 3 cases contained four bowing segments.

The bowing portions of the squall line in this mode are not required to bow at the same time. In fact, most often, the bowing segment located the farthest leftward (usually the farthest north) in the multiple bowing squall line is the first to accelerate, followed by one or more segments farther to the right along the convective line (usually farther south) which subsequently accelerate.

These convective systems usually demonstrate extensive trailing stratiform precipitation like bowing squall lines (96% moderate-to-heavy stratiform). However, the

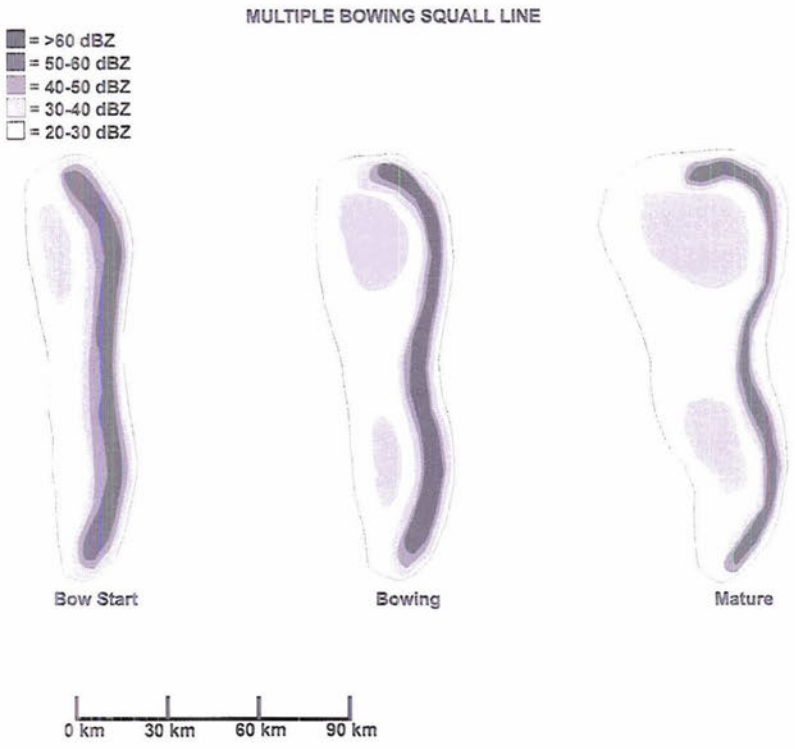

Figure 4.22: As in Fig. 4.4 but for a multiple bowing squall line system.

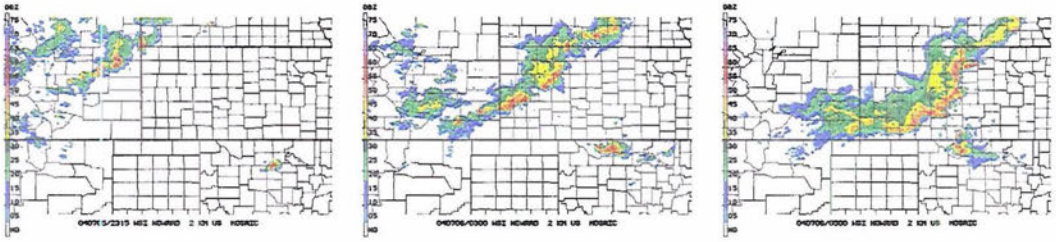

(a) First 40 dBZ Echoes, 2315 UTC (b) Initiation, 0300 UTC (c) Bowing Stage, 0500 UTC

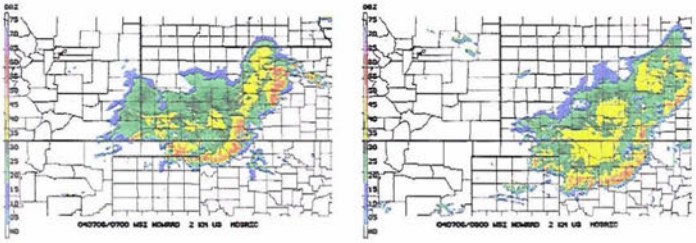

(d) Mature Stage, 0700 UTC (e) Dissipation, 0900 UTC

Figure 4.23: As in Fig. 4.5, but for a multiple bowing squall line system from 5-6 July 2004 over western Kansas and northern Oklahoma.

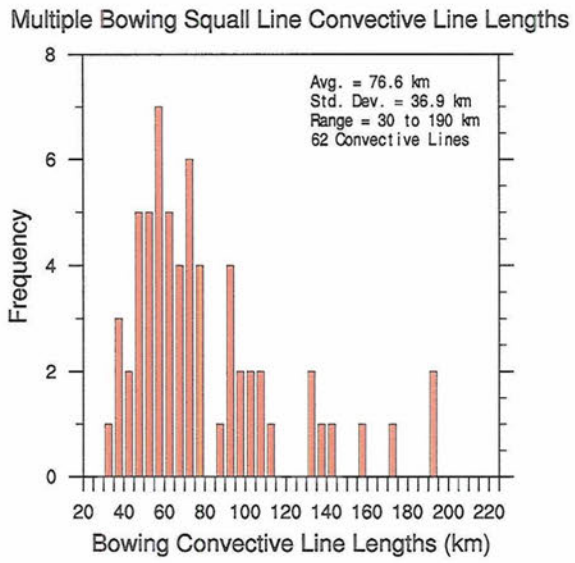

Figure 4.24: Histogram plot displaying the frequency distribution of each segment of the multiple bowing squall line convective mode. The average, standard deviation, range, and number of convective lines are shown in the upper right hand corner.

areal extent of the trailing stratiform precipitation for multiple bowing squall lines is generally less than that of the bowing squall lines. Multiple bowing squall lines usually generate trailing stratiform precipitation earlier in the bowing process compared to BE/ESs (Fig. 4.6), yet the difference is not as great when one compares stratiform formation timing of bowing squall lines to BE/ESs.

The distribution of the initial modes that form multiple bowing squall lines (Fig. 4.7) reveals that this mode arises 80% of the time from a squall line. Thus, bowing squall lines and multiple bowing squall lines usually form from initial squall lines that experience a bowing acceleration process.

The average longevity of a multiple bowing squall line is slightly greater than a bowing squall line; it tends to be 5 h with most cases lasting 2 to 8 h, making this the longest-lived bowing convective mode (Fig. 4.8). Like bowing squall lines, these storms display a formation preference toward the central United States (Fig. 4.9). Multiple bowing squall lines have a similar diurnal distribution to BE/WSs (Fig. 4.10 and Fig. 4.11). Multiple bowing squall lines tend to start bowing between 1500 and

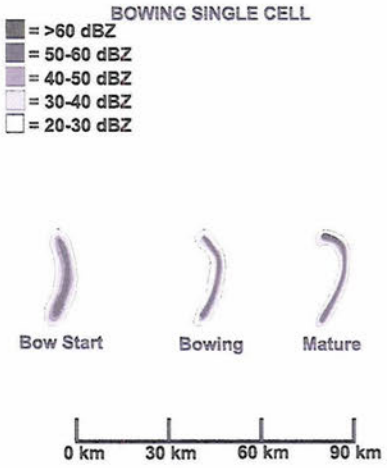

Figure 4.25: As in Fig. 4.4 but for a bowing single cell system.

2100 LST. They most often dissipate between 2200 and 0400 LST (slightly later than BE/WSs).

Multiple bowing squall lines are the most prolific producers of severe weather, usually producing 0-7 large hail reports, 0-50 severe surface wind reports, and 0-4 tornado reports per case (Figs. 4.12, 4.13, and 4.14). This result implies that many multiple bowing squall lines are extremely severe convective storms, and part of this is the large areal extent of these systems. Moreover, 6 of all 31 derechos observed in this study are multiple bowing squall lines. When considering all multiple bowing squall lines, 24% meet the derecho criteria of Johns and Hirt (1987).

4.2.5 Mode 5: Bowing Single Cell

The final organized bowing convective mode (8%) is the **bowing single cell**. This mode is a small bowing system with a convective line in the 20-40 km length range (Fig. 4.25 and 4.26). This mode generates very limited to no trailing stratiform precipitation (only 9% of these cases have trailing stratiform precipitation).

Groups of cells, manifest as small ordinary or multicell clusters, are favored to produce this bowing convective mode (65%), while single supercells commonly play

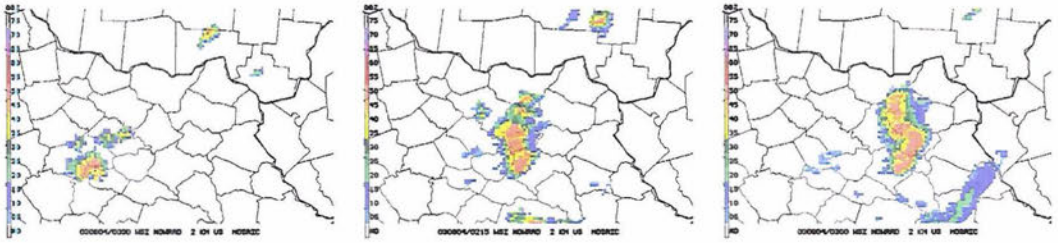

(a) First 40 dBZ Echoes, 0030 UTC (b) Initiation, 0215 UTC (c) Bowing Stage, 0300 UTC

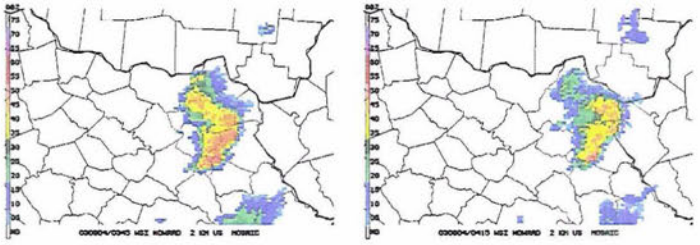

(d) Mature Stage, 0345 UTC (e) Dissipation, 0415 UTC

Figure 4.26: As in Fig. 4.5, but for a bowing single cell from 4 August 2003 over northeast Kentucky.

a role (29%, Fig. 4.7).

These are the shortest-lived of all the bowing modes, with an average lifespan of about 2.25 h with most cases lasting 1.5 to 3 h (Fig. 4.8). These storms usually develop over the central or northeast U.S. (Fig. 4.9). Bowing single cells have a similar diurnal distribution to BE/ESs but are much narrower (Fig. 4.10 and Fig. 4.11). Bowing single cells usually start bowing between 1800 and 2300 LST and dissipate between 1800 and 0100 LST.

Bowing single cells produce very little severe weather compared to other modes (Figs. 4.12, 4.13, and 4.14). Moreover, this mode did not produce any of the derechos in this study. Bowing single cells are generally non-severe and short-lived beyond their small size alone.

4.2.6 Disorganized bowing convection

The term disorganized bowing convection was given to a convective system selected in the original perusal, but not showing an organized bowing structure when viewed close up in the radar animations. According to Fig. 4.3, these were highly uncommon in the final sample, only comprising about 2% of the cases. Often, disorganized bowing convection exhibited bowing acceleration for only 15-30 minutes, while tending to be coincident arc shaped convection for a slightly longer time. These convective systems are generally very short-lived.

4.3 Formative line lengths of bowing convective systems

Convective line lengths of the BCSs that formed in this study were measured from radar images with a precision of approximately 5 km. The line lengths were taken to be the straight-line distance between the approximate centroids of the line-end vortices during the mature phase of each BCS. The results reveal that the length of the average bowing convective line in this study is about 75 km (Fig. 4.27). The distribution demonstrates that a *preferred range of sizes for bowing convective systems does exist.* Approximately 70% of all bowing convective lines fall between 40 and 110 km, about one standard deviation above and below the mean.

It is possible that the typical size range of sizes of BCSs is due to the contribution of line-end vortices which are important structural components of a strong bowing system. According to Weisman (1993), these vortices range between 20 and 50 km in diameter; evidence has been presented that they arise from tilting of boundary layer wind shear. There has been no explanation to date on how vortices of these sizes come to be. Little spacing could prevent vortex formation while large spacing could be detrimental to adding rear-inflow. Two average-sized line-end vortices of approximately 35 km would each contribute 17.5 km to the bowing convective line length as it was measured. Therefore, a distance of approximately 40 km between the

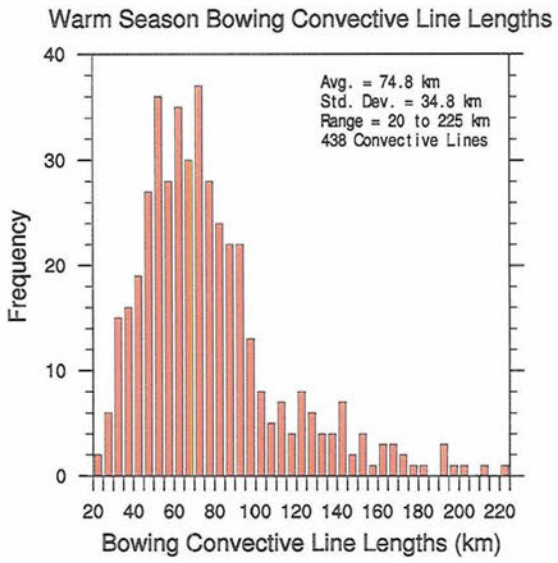

Figure 4.27: Frequency distribution displaying the frequency distribution of bowing convective line lengths observed in this study in 5 km bins. The average, standard deviation, range, and number of convective lines are shown in the upper right hand corner.

line-end vortices could indicate a preferred spacing for optimal addition of rear-inflow velocity fields induced by the vortices. If BCSs form from the tilting of boundary layer vorticity toward a vertical axis, BCSs less than 40 km would have little to no horizonal space for the formation of line-end vortices. Conversely, BCSs that form with lengths longer than 110 km would have large spacing between developing line-end vortices, lessening the potential for additive rear-inflow velocity fields induced by the vortices, even though bowing could still occur.

From the above observations of convective line lengths, the bowing convective systems which were termed "bow echoes" as part of their naming convention had convective line lengths between 40 and 110 km. BCSs below 40 km will be termed as "single cells". BCSs larger than 110 km contained "bowing squall line" as part of their name. The choice of ranges is consistent with past studies that have assigned small-scale bow echoes to events less than 40 km (e.g. Lee et al. 1992, KHB04); moreover, studies of MCSs have shown that convective systems greater than 100 km

can be strongly influenced by the Coriolis force (e.g. Parker and Johnson 2000).

4.4 Radar observed cell mergers

In this study, 58% of all BCSs were associated with convective storm mergers that aided in the evolution toward the bowing process, which is close to the fraction reported by other studies (see section 2.3.2). These cells aided the initiation of bowing convection between 15-45 minutes after the cell merger process. At times, multiple cell mergers were necessary to initiate bowing acceleration. Results were tabulated depending upon the flank of the greatest size and number of cells mergers occurring.

Results show that the merging process can occur on any flank with existing convection to aid in initiating the bowing process. Fig. 4.28 shows that the merging process is most favorable for producing a BCS when a convective cell or cells merge into the *central pre-existing convection* that soon becomes a BCS. The resulting bowing apex usually arises within 15-45 minutes near the location of the merging process. However, additional high-resolution research data or numerical simulations would be needed to document the production and evolution of vertical vorticity change resulting from this process in relation to studies like Finley et al. (2001).

Radar observations indicate that merging with strong supercells was favorable in the left (usually northern) flank to initiate bowing and enhance rotation in the line-end vortex. However, merging with large supercells near the central line was less conducive to greater longevity of the bowing convective lines. Southern flank convective mergers usually produced an increase in the size of the convective segment. Merging on this flank was infrequent and did not appear to aid the bowing process very strongly.

Not all convective cell mergers produced bowing convection. The merging of convective cells well before the initiation of bowing was observed at times. The data show cell mergers in systems several hours before the bowing process began that are

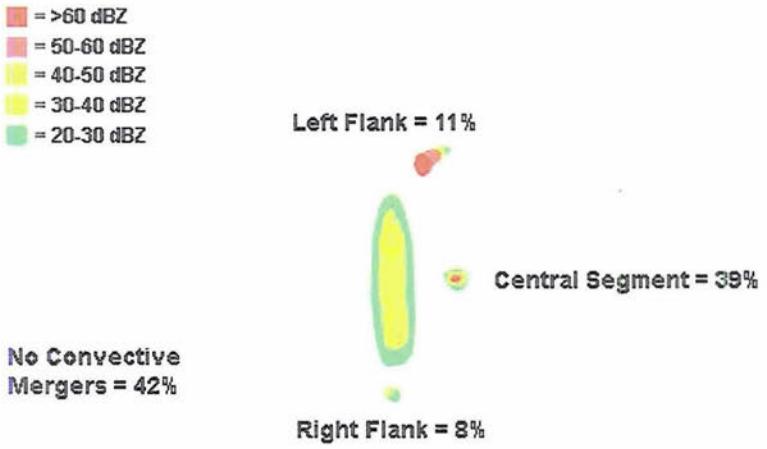

Figure 4.28: Schematic representation of radar observed convective merger percentages and locations observed in this study. The cells shown on each flank are closely representative of the cell types and sizes usually responsible for the initiation of bowing convection on the respective flank.

seemingly unrelated to the initiation of bowing convection. This occurrence of an earlier merger process was infrequent and not tabulated.

Interestingly, Fig. 2.2 from BS04 shows a mode of bow echo formation termed "Squall Line - Cell Merger". Note that the conceptual convection evolution shows the cell merger occurring *at the center of the existing convective line*, close to the subsequent bowing apex. Although this process for this mode is not discussed in BS04, this result is consistent with the tabulated observations from the current study: the central pre-existing convection is the preferred merging location for the initiation of BCSs.

4.5 Slabular and cellular bowing convective lines

Radar reflectivity examples of the convective regions of BCSs are shown in Fig. 4.29 (cellular, slabular, and hybrid bowing convective lines). The labeling system for the bowing convective regions closely follows the research of James et al. (2005). Statistical tabulation illustrates that bowing convective regions of BCSs are most

(a) Cellular Bowing Convective Line

(b) Slabular Bowing Convective Line

(c) Hybrid Bowing Convective Line

Figure 4.29: Composite radar reflectivity examples of the three convective region classifications of bowing convective lines observed in this study. The naming system closely follows that of James et al. (2005).

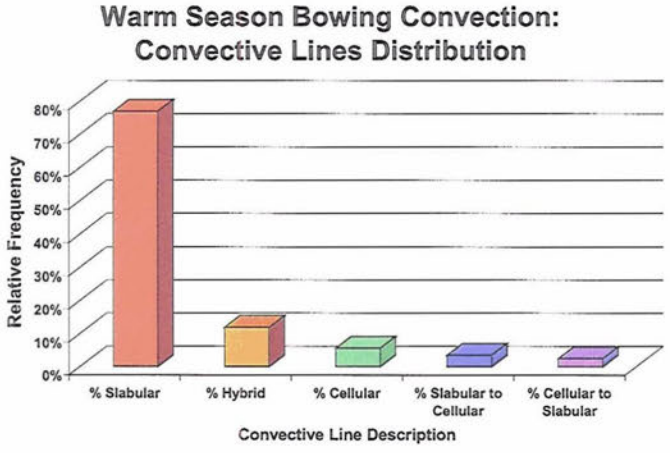

Figure 4.30: Relative frequency distribution of convective regions in bowing convective lines observed throughout this entire study.

often *slabular convective lines* comprising about 77% of the population (Fig. 4.30).

According to James et al. (2005), slabular lines typically experience much stronger low-level shear in the cross-line direction, as well as strong shear in the along-line direction compared to cellular lines. Low-level, line-perpendicular inflow of the slabular environments is much stronger than that for the cellular environments. Also, slabular convective lines have larger low-level relative humidities, and a lower vertical height than their lifting condensation level (LCL). Thus, further research beyond this study should reveal environmental differences between slabular and cellular BCSs and the differences between their surface-based cold pools.

Examining the evolutions of the convective regions suggests that the most organized bowing structures are strong, slabular convective lines. Composite analysis of slabular versus cellular convective lines illustrates statistically significant differences, with slabular lines possessing identifiable cyclonic and anticyclonic line-end vortices more frequently than cellular lines (37% vs. 5% and 15% vs. 5%). Further study is necessary for understanding significant environmental differences between slabular and cellular bowing convective lines. The rates of bowing acceleration are also increased for slabular bowing convective lines over cellular bowing convective lines (55% fast bowing in slabular vs. 29% fast bowing in cellular).

The findings show that bowing convection can evolve between the slabular and cellular modes before dissipation. This process could be indicative of a BCS moving into a different kinematic or thermodynamic environment. However, significant evolution in the bowing convective regions was only observed in about 6% of the cases. About 88% of all BCSs examined exhibited a sharp reflectivity gradient on the convex leading edge where reflectivities in the convective region progressed from 0 dBZ to at least 45 dBZ over a width of less than 20 km. This property was tested because of the bow echo definition used by KHB04. This research demonstrates that it is *not absolutely necessary*, as in the definitions of KHB04 and BS04 to have a

slabular convective line or a sharp reflectivity gradient on the convex leading edge for a convective system to produces bowing acceleration. However, this study does confirm that this property is usually present in bowing convective regions.

4.6 Observed stratiform variability of bowing convection

In the present study, 72% of all cases generated significant trailing stratiform precipitation. Not surprisingly, the distribution of bowing convective modes reveals that BE/ESs, bowing squall lines, and multiple bowing squall lines possess moderate-to-heavy stratiform precipitation. BE/WSs and bowing single cells infrequently possess extensive stratiform precipitation. If they do, it usually comes about 15 to 30 minutes before dissipation and usually is not significant in areal extent. In these cases that produce limited convectively generated trailing stratiform precipitation, evolutions suggest that the trailing precipitation regions had virtually no influence on the convective evolutions. These results are supported by the average bowing convective line lengths of BCSs possessing trailing stratiform precipitation verses those that do not (83 km vs. 59 km). Thus, convectively generated trailing stratiform precipitation is more common in BCSs of larger scales.

Trailing stratiform precipitation and pre-existing stratiform precipitation before bowing produce BCSs with greater longevity compared to the rest of the sample (Fig. 4.31). These observations could imply that a BCS configuration with convectively generated stratiform precipitation is more prone to regenerate convection with dynamics similar to a balanced squall line situation, where cold pool generated horizontal vorticity balances storm relative environmental wind shear (Weisman and Rotunno 2004).

Stratiform precipitation is important to note in understanding BCS longevity and severity because most discussions about the rear inflow jets (RIJs) in BCSs *assume the presence of a trailing stratiform precipitation region* with a midlevel mesolow

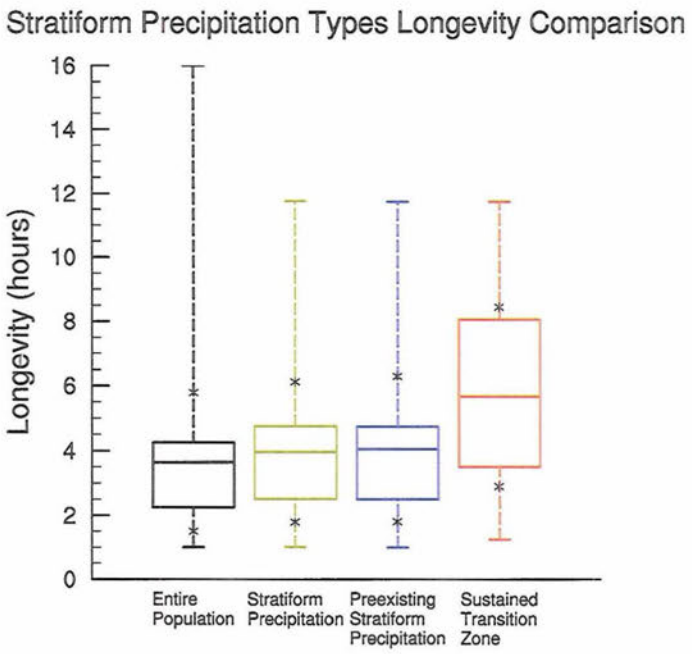

Figure 4.31: Same as Fig. 4.8, except for comparison of differing types of stratiform precipitation formation in bowing convective systems as defined in the text.

that accelerates the rear inflow toward the convective line (see Fig. 2.11). As discussed in Chapter 2, a counterexample of a trailing stratiform convective system appears to be Klimowski (1994), who observed a very strong squall line over North Dakota with no trailing precipitation but very strong rear inflow. Furthermore, 20% of all cases examined in this study are bow echoes with light trailing precipitation (BE/WSs). Thus, various questions remain unanswered such as, what are the implications of the stratiform precipitation on the development of RIJs in bowing convective systems? While examination of RIJs using radial velocity or research data is beyond the scope of this study, these observations should be taken into consideration when identifying or assessing the dynamics of a BCS.

4.6.1 Trailing stratiform precipitation shapes

Throughout the observation of trailing stratiform precipitation regions in this study, two extremes in orientation and shape of enhanced precipitation regions

(a) Line-parallel Elongation (b) Line-perpendicular Elongation (c) Perpendicular and Parallel Elongation

Figure 4.32: Composite radar reflectivity examples of three main trailing stratiform precipitation shapes observed in this study.

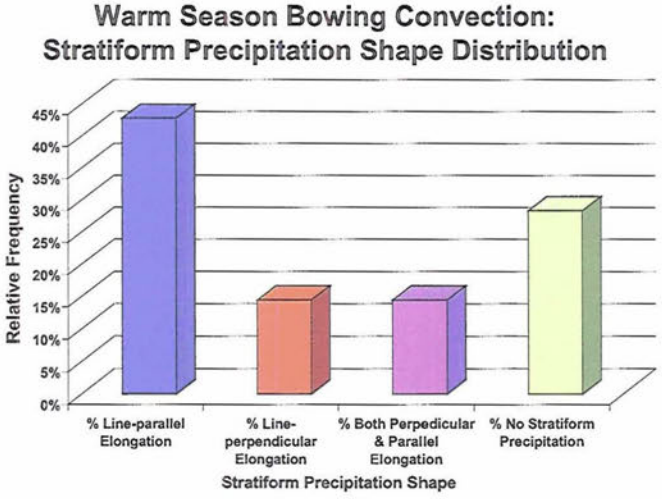

Figure 4.33: Relative frequency distribution of trailing stratiform precipitation shapes observed throughout this study. Examples of each of the stratiform shapes are noted in Fig. 4.32.

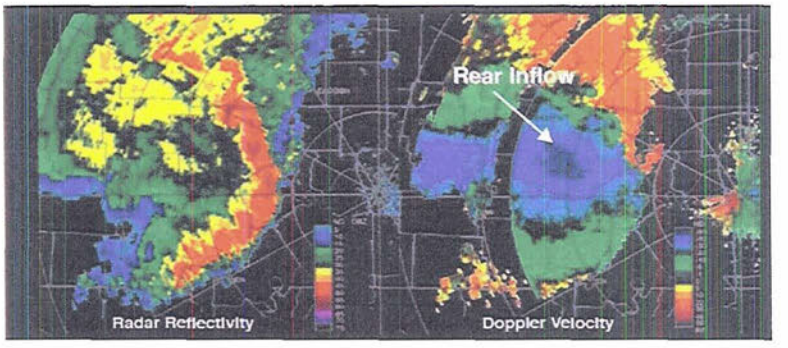

Figure 4.34: Radar reflectivity and doppler radial velocity comparison for 5 May 1996 derecho that affected Paducah, KY. The reflectivity and radial velocity scales are shown in the lower right hand sides of each panel. From Weisman (2001), adapted from a figure provided by R.W. Przybylinski (personal communication).

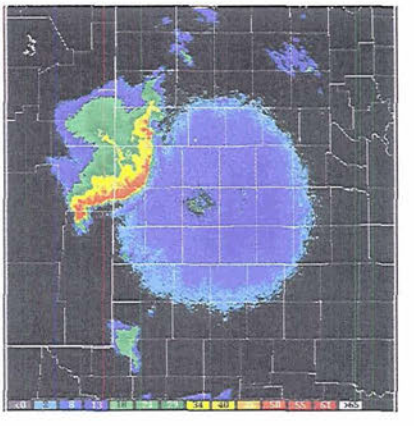

Figure 4.35: Radar reflectivity display at 0.5° azimuth from Lubbock, TX (KLBB) NEXRAD radar on 4 April 2000 at 0413 UTC. Reflectivity color scale is given on the bottom From the website (http://www.nssl.noaa.gov/mag/bowecho/) based on the study of Burke and Schultz (2004).

were noted. These shapes are labeled as **line-parallel elongation** and **line-perpendicular elongation**. The intermediate shape between these includes **both line-parallel and line-perpendicular elongation** (Fig. 4.32).

The frequency distribution of these shapes (Fig. 4.33) indicates that line-parallel stratiform precipitation is favored compared to either shape that contains a perpendicular component. Line-parallel trailing stratiform precipitation is similar in evolutionary properties to a typical TS MCS (Parker and Johnson 2000). However, a distinguishing component of BCSs appears to be very strongly developed rear-inflow compared to average squall lines.

Remarkably, line-perpendicular elongated trailing stratiform precipitation has been observed in past studies but has not been commented upon. Fig. 4.34 shows the famous Paducah, KY bow echo derecho from 5 May 1996 (http://www.crh.noaa.gov/pah/science/REWRITE2.php). The trailing stratiform precipitation region is elongated in the line-perpendicular direction and is collocated with a strong RIJ seen in the radial velocity data. Furthermore, Fig. 4.35 depicts a strong bow echo near Lubbock, TX on 4 April 2000 from BS04. The authors note in their writeup that this storm was very compact, severe, and produced a very concentrated RIJ (see http://www.nssl.noaa.gov/mag/bowecho/klbb-042800/case.html). It is possible that line-perpendicular elongated trailing stratiform precipitation could have implications for forecasting and warning for the onset of an RIJ in a BCS.

The frequency distribution of bowing convective modes exhibiting line-perpendicular elongated trailing stratiform precipitation demonstrate that the BE/ES systems most often exhibit enhanced trailing stratiform precipitation arranged in a perpendicular fashion behind the bowing convective line (Fig. 4.36). This result could indicate a convective line length preference that would concentrate RIJs, similar to the convective line arguments presented in section 4.3. Additional evidence for concentrated RIJs during this process includes cyclonic and anticyclonic

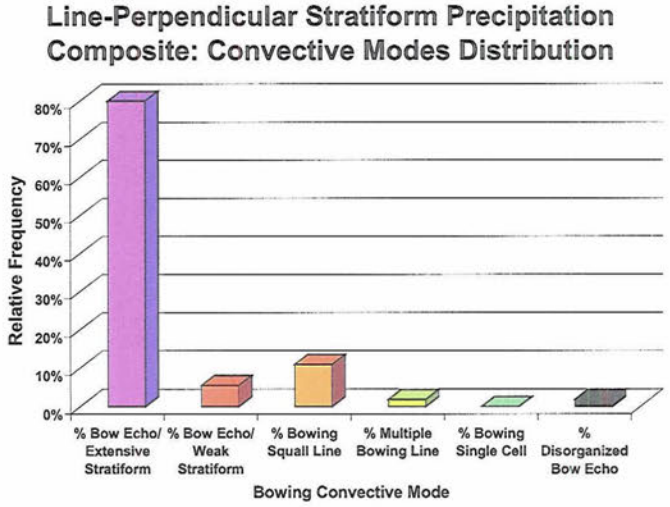

Figure 4.36: Relative frequency distribution of bowing convective modes for line-perpendicular shaped trailing stratiform precipitation composite.

vortices identified from radar reflectivity animations in 46% and 29% of these cases, respectively (compared to 29% and 10% for all other cases). Moreover, a perpendicular enhanced trailing stratiform precipitation region is related to a greater rate of bowing and thus acceleration in the bowing process compared to the rest of the sample.

The composite analysis of line-perpendicular elongated trailing stratiform precipitation shows greater severe surface wind speeds over other cases with only 90% statistical significance. Average severe surface wind speeds increase from 31 m s^{-1} to 33 m s^{-1} when comparing line-parallel to line-perpendicular stratiform precipitation; these speeds are highly sensitive to damage survey estimated speeds that could have reporting problems at times. Therefore, this radar signature may be indicative of a concentrated RIJ, but may not necessarily indicate strong severe surface winds.

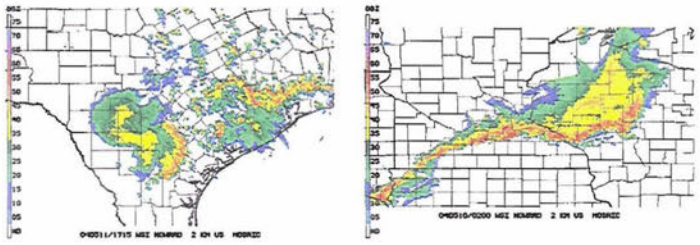

(a) Sustained Transition Zone (b) No Transition Zone

Figure 4.37: Radar reflectivity composite examples of a bowing convective system that has (a) sustained transition zone and (b) no transition zone at all.

4.6.2 Sustained Transition Zone

The observation of a **sustained transition zone** is defined as a bowing convective system generating trailing stratiform precipitation and maintaining a **transition zone** (e.g. Biggerstaff and Houze 1991) between the convective line and secondary enhanced precipitation that is at least the width of the convective region for at least half of the storm longevity. That is, there is a long duration of very light precipitation in the radar composite between the bowing convective line and moderate-to-heavy stratiform region. An example of this process and a counterexample are given in Fig. 4.37. The relative frequency distribution reveals that the sustained transition zone process is not very frequent, but radar reflectivity animations suggest that this process is significant to the evolution of the bowing convection when it occurs (Fig. 4.38). In general, the mean length of convective lines is greater when this process is realized (108 km vs. 79 km).

Composite analysis of BCSs that sustain a transition zone reveals differences in the bowing convective modes (Fig. 4.39). The results show that the number of bowing squall lines plus the number of multiple bowing squall lines that possess a sustained transition zone are about equal to the number of the BE/ES mode which exhibit this phenomenon. Composite analysis also shows that stratiform precipitation very frequently builds up during the mature stages of the bowing process for cases

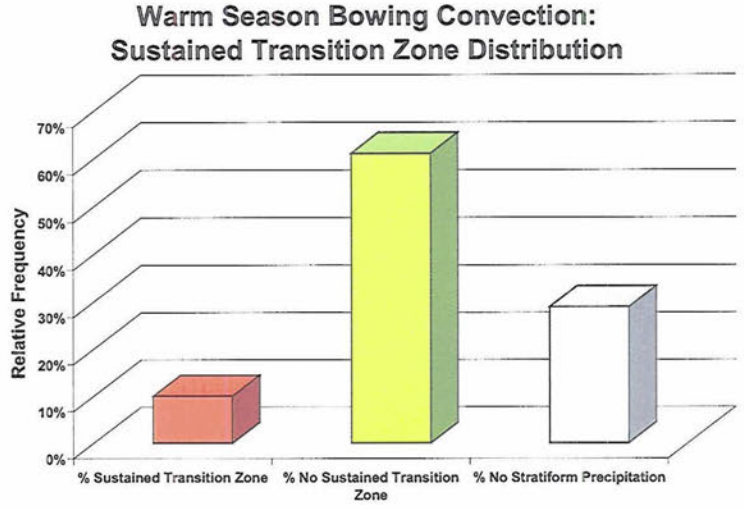

Figure 4.38: Relative frequency distribution of all bowing convective systems that demonstrate the sustained transition zone process.

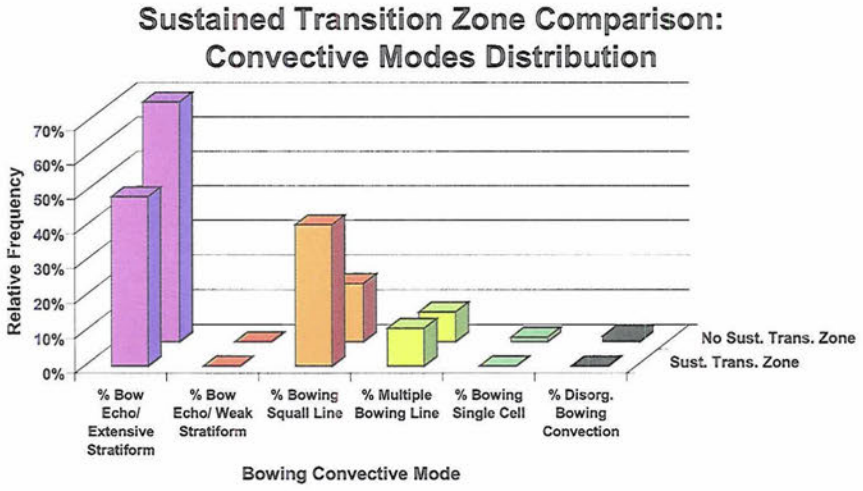

Figure 4.39: Relative frequency distribution comparison of bowing convective modes for bowing convective systems that sustain a large transition zone from strong stratiform precipitation and those that do not.

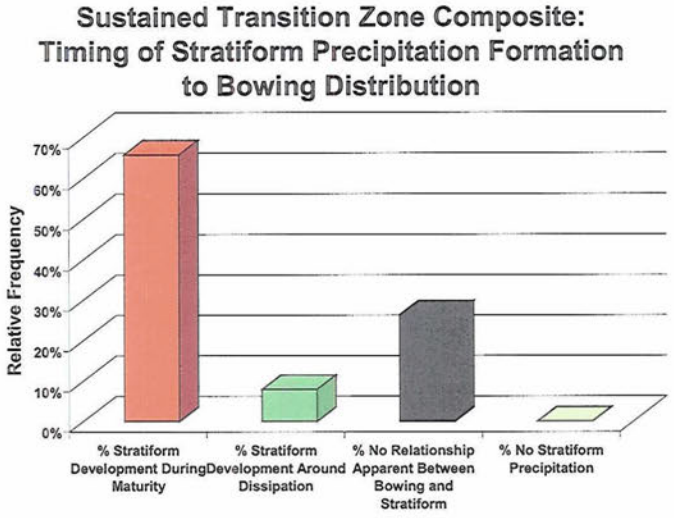

Figure 4.40: Distribution of trailing stratiform precipitation development timing in relation to bowing for the composite of bowing convective systems that sustain a large transition zone from their stratiform regions.

exhibiting a sustained transition zone (Fig. 4.40).

Eleven of all 31 derechos observed demonstrate a sustained transition zone for the majority of their evolution. Moreover, 29% of all the cases that sustain a large transition zone meet the criteria of a derecho. There is a strong indication in the composite analysis that a sustained transition zone enhances bowing longevity by an average of two hours over the whole sample (Fig. 4.31).

4.7 Bowing Series

The **bowing series** is a group of two or more BCSs which move along a similar track sequentially in a quasi-linear fashion. A radar reflectivity composite example of a series of four BCSs is displayed in Fig. 4.41.

Interestingly, subsequent BCSs in a bowing series *tend to form upstream*, in a relative sense. The resulting tracks of the BCSs are progressively displaced farther upstream in a quasi-linear sense. Composite analysis reveals that BCS track length and longevity are increased compared to the rest of the sample if BCSs arrange into a

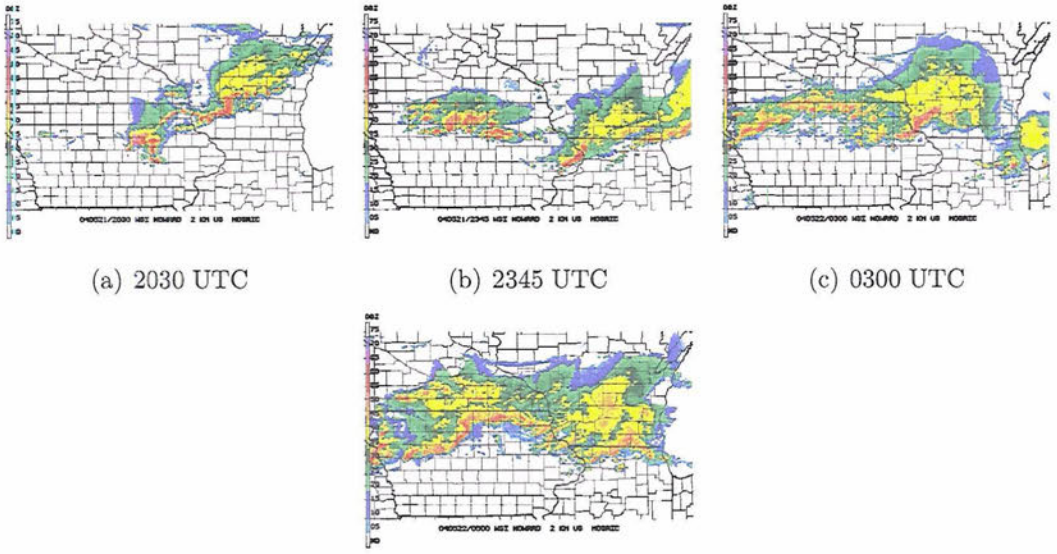

(a) 2030 UTC (b) 2345 UTC (c) 0300 UTC

(d) 0500 UTC

Figure 4.41: Composite radar reflectivity of bowing series for case on 21-22 May 2004 at (a) 2030 UTC, (b) 2345 UTC, (c) 0300 UTC, (d) 0500 UTC.

bowing series (44% track farther and 68% have larger longevities). There is a strong influence of stationary fronts and hybrid boundary forcing typically associated with a bowing series. Statistically, 43% of all BCSs in the bowing series move parallel to a synoptic boundary.

More research is needed to understand how the bowing series is related to the progressive derechos of Johns and Hirt (1987) as well as "cold pool events" of Kuchera and Parker (2004). The bowing series deserves some additional attention because it is not always linked with a synoptic scale boundary. Thus, progressive derechos and "cold pool events" are likely a subset of the bowing series.

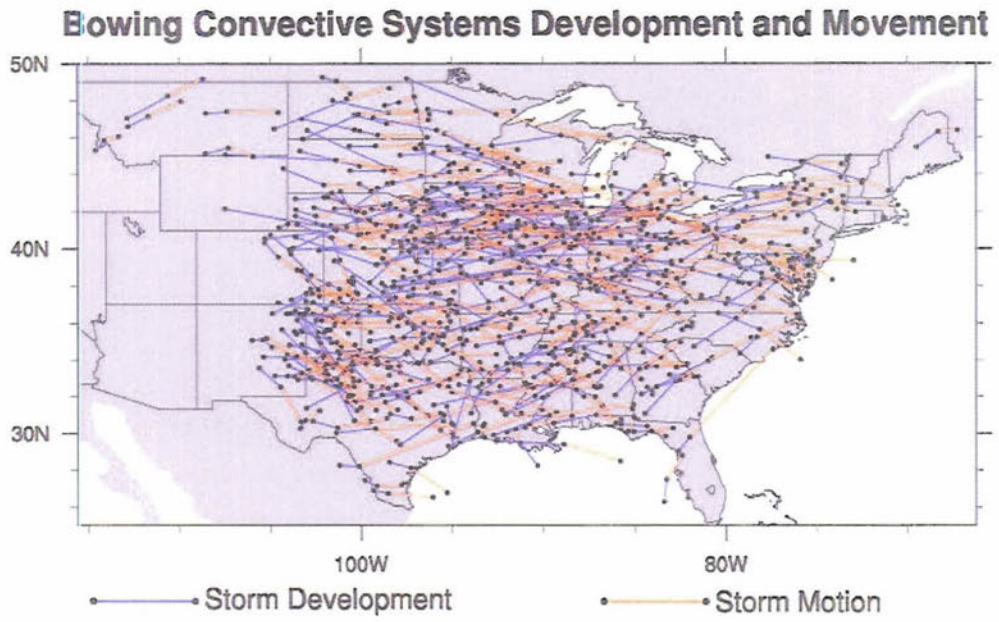

Figure 5.1: Bowing convective system development and movement locations for all warm season cases observed in this study. Development and movement tracks are defined in section 2.2. Movements are taken to be approximately linear tracks between first echoes and bow start as well as between bow start and bow end.

5.1.2 Distances traversed in the bowing lifecycle

As for other parameters, the distributions of development distance and track length are positively skewed (Fig. 5.3 and 5.4). Development distance shows that most 40 dBZ convective echoes that produce bowing convection develop over tracks of roughly 75 to 350 km. The resulting BCS track lengths are comparable, usually between 80 and 370 km. While the majority of BCSs move in this range, a few of these systems have the propensity for very long tracks with 5.7% of all BCSs possessing movement distances between 500 and 1015 km.

When compared on a case-by-case basis, BCS development and movement distributions are similar to one another. In fact, the comparison reveals a correlation coefficient of $r = 0.40$. While not all bowing convection has a strong relationship between the distance required to form a BCS and the distance traversed, an indication of a relationship between these distances is evident when graphed on a scatterplot (not

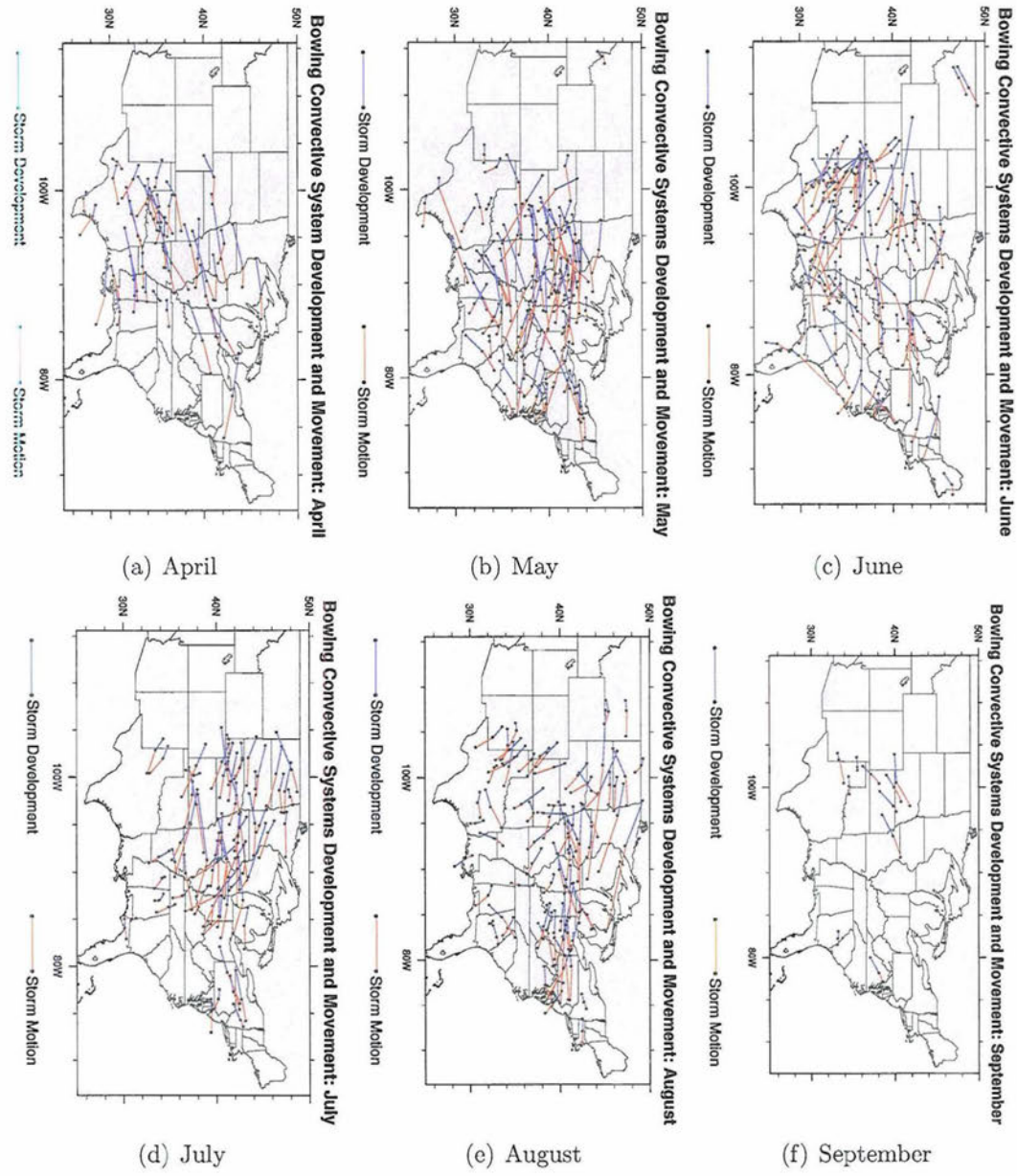

(a) April (b) May (c) June

(d) July (e) August (f) September

Figure 5.2: As in Fig. 5.1, but divided up over the warm season months examined.

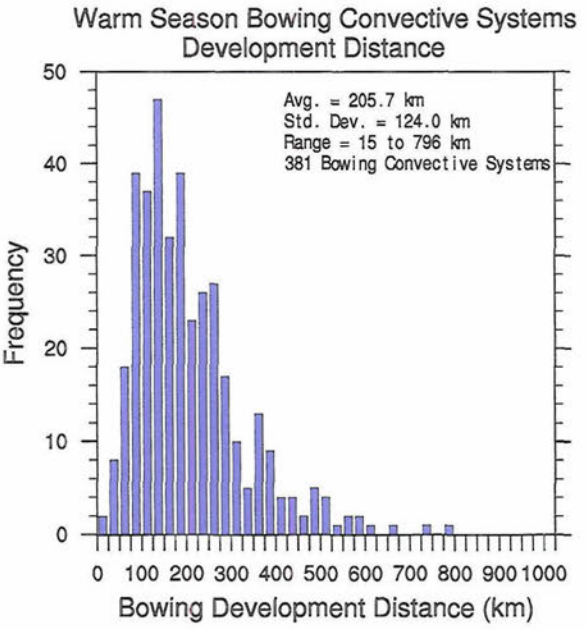

Figure 5.3: Frequency distribution of development distances (first echo to bow start, see section 2.2) for all warm season bowing convective systems observed in this study. The average, standard deviation, and range of development distances are shown in the upper right hand corner.

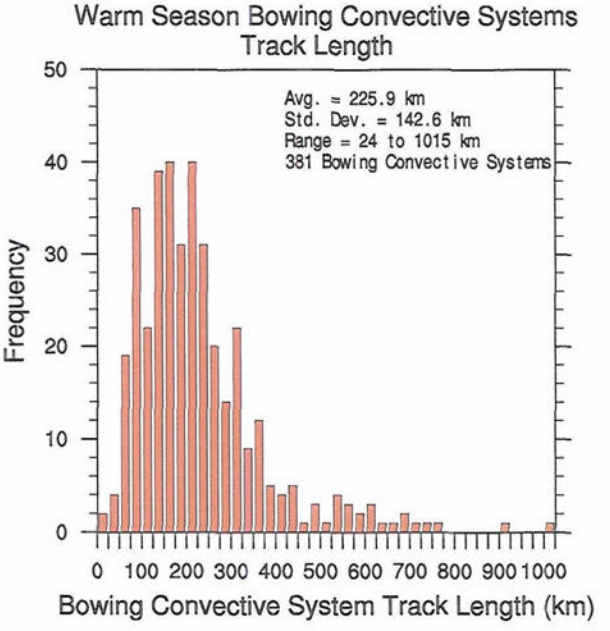

Figure 5.4: As in Fig. 5.3, but for track lengths (bow start to bow end, see section 2.2).

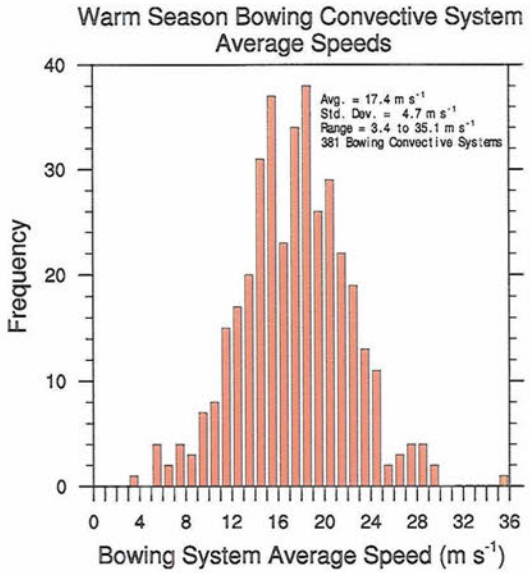

Figure 5.5: Distribution of average bowing convective system speeds (bow start to bow end, see section 2.2) for all warm season cases observed in this study. The average, standard deviation, and range of bowing convective system speeds are shown in the upper right hand corner.

shown). This connection between development and BCS track length (or longevity) will be explored further when bowing longevities are discussed in section 5.3.3.

5.2 Bowing speeds

Considering the relationship between BCS track length and longevity, the correlation coefficient is very large ($r = 0.87$). When the track lengths and longevities are examined together as the average movement speeds, the results display a nearly Gaussian distribution (Fig. 5.5). The findings reveal that *there is a preferred range of speeds of bowing convective system movement*, 10 to 24 m s^{-1}, the mean speed being 17.4 m s^{-1}. This speed may exceed the speed of a gravity current, indicating that the motion of these systems cannot be solely explained by gravity current dynamics for every case.

This range indicates that if a near-surface storm-relative wind moving in the same direction as an average BCS (moving 17.4 m s^{-1}) exceeds 8.3 m s^{-1}, then the

near-surface wind will qualify as an NWS severe wind gust (25.7 m s^{-1}) which is an F0 rating on the Fujita scale, usually indicating limited damage. This example demonstrates that BCSs can produce numerous severe surface winds because average movement speeds are very large. In fact, nearly 4% of all BCSs in this study moved with speeds which would exceed the criteria for a severe wind gust without any storm-relative wind.

5.3 Temporal distribution of bowing convective systems

5.3.1 Monthly distributions

The monthly distribution of warm season BCSs (Fig. 5.6) displays a shape like derechos studied by Coniglio et al. (2004a). The BCSs in this study show a ramping up of frequency from early to late April. The distribution shows May, June, July, and August as very active months. In contrast, Coniglio et al. (2004a) show a relative frequency decrease for August derechos. The large number of August BCSs in this study may not be statistically significant owing to the limited two-year period of study. The frequency of BCS decreases dramatically toward the cold season in September.

An asymmetry between the leading and trailing months on each side of the active warm season months is present in the monthly distributions (Fig. 5.6). This finding implies greater numbers of BCSs in the early warm season compared to the late warm season. The general large scale asymmetry of severe convection between the spring and fall seasons with large-scale static instability favoring the spring season could be related to this phenomenon.

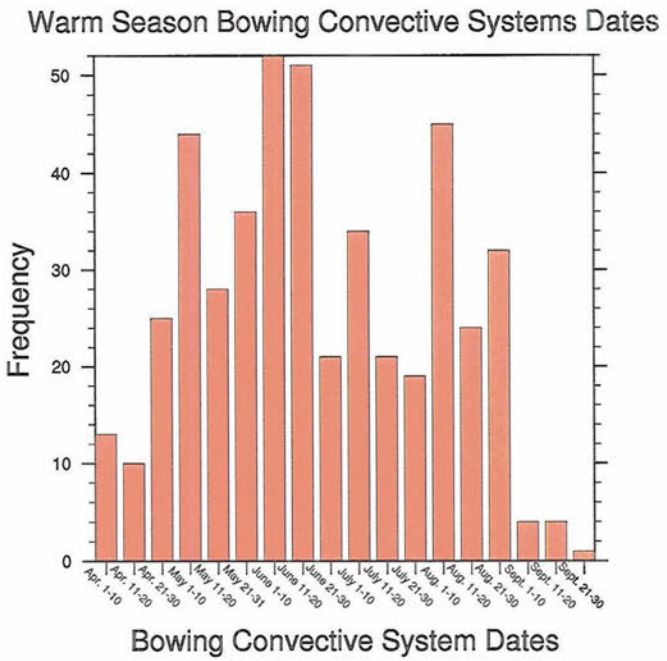

Figure 5.6: Frequency distribution of dates on which warm season bowing convective systems observed in this study. Bins are divided into 10 or 11 day increments depending upon the month in question.

5.3.2 Diurnal distributions

Diurnal distributions of the first 40 dBZ echo, bow start, and bow end times suggest that daily trends are generally similar in this study and BS04 (Figs. 5.7, 5.8, and 5.9). Observations from this study indicate that bowing convection initiates and dissipates during all hours of the day.

The diurnal distributions display that the first 40 dBZ convective echoes that initiate warm season BCSs usually start between 1100 and 1800 LST. These structures initially exhibit bowing between 1500 and 2300 LST for most cases. The majority of warm season bowing convection dissipates between 1700 and 0200 LST.

Two noteworthy features emerge from the diurnal distributions. First of all, first 40 dBZ echoes show a very sudden increase in frequency after 1130 LST. Secondly, the bow end time results indicate a change between about 0100 and 0300 LST. *The frequency of dissipating cases quickly drops off, especially around 0200 LST.*

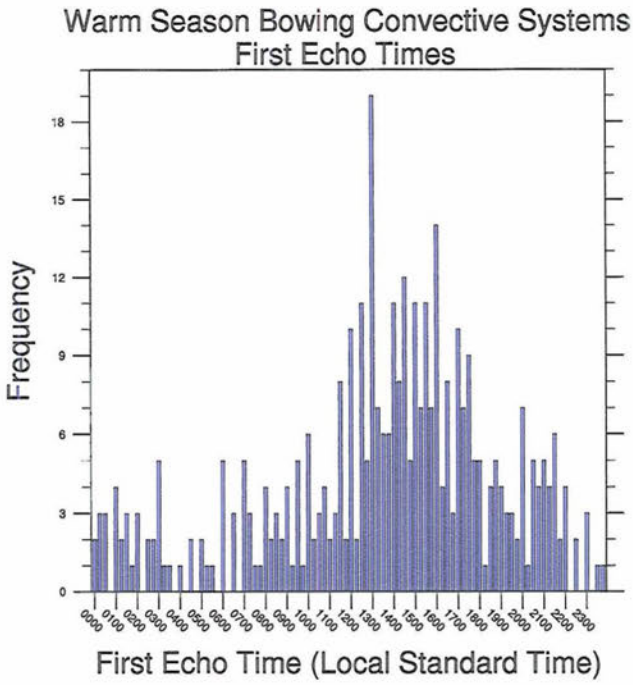

Figure 5.7: Frequency distribution of first echo times in Local Standard Time for all warm season bowing convective systems observed in this study. The bins are divided into 15 minute intervals.

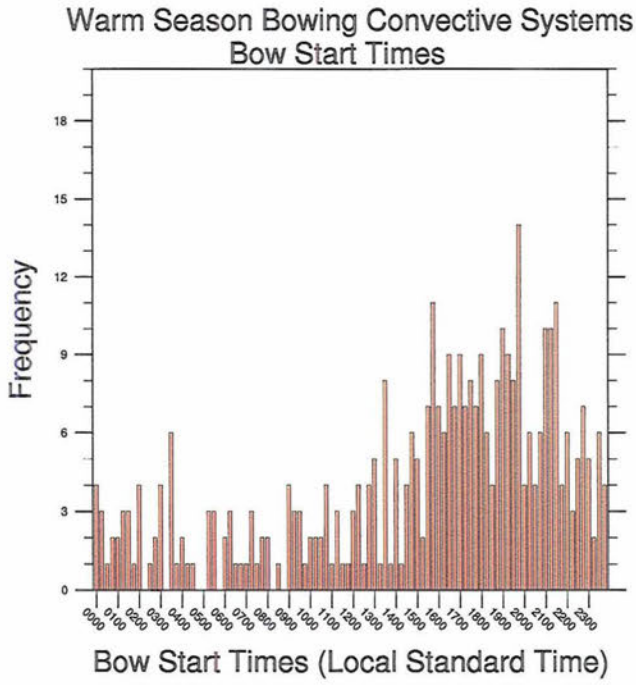

Figure 5.8: Same as Fig. 5.7, but for bow start time.

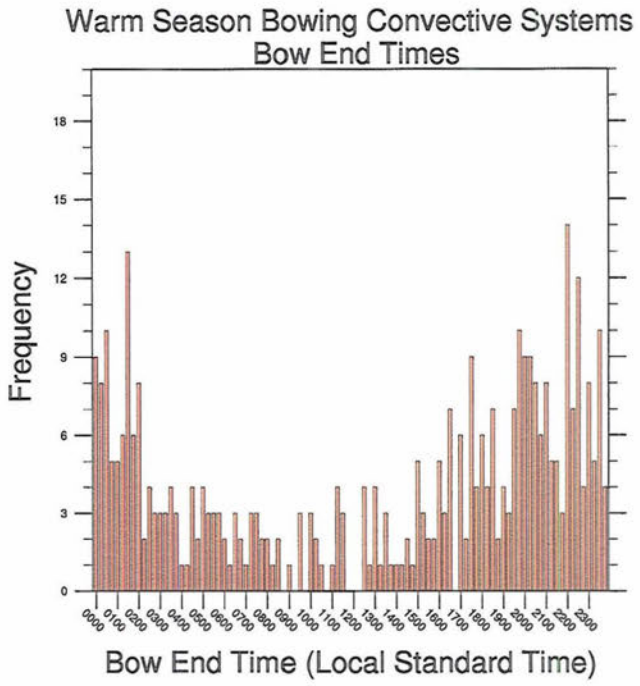

Figure 5.9: Same as Fig. 5.7, but for bow end time.

This observation could imply stabilization of nocturnal planetary boundary layers tending to hinder bowing convection survival so that most BCSs dissipate by 0300 LST, although events that continue after this time may be associated with elevated convection.

5.3.3 Bowing longevities

Similar to development distance and BCS track length, the distributions of development time and bowing longevity are positively skewed toward shorter times (Figs. 5.10 and 5.11). Development times show that most 40 dBZ convective echoes that produce bowing convection accomplish this process over periods of approximately 2 to 5.5 h. The bowing longevities extend slightly longer than the development times, usually between 2.5 to 6 h. A few BCSs possess the potential for very long lifespans, with 6.8% of all cases bowing 7 to 16 h.

In comparison to the longevities of cold season bow echoes examined in BS04,

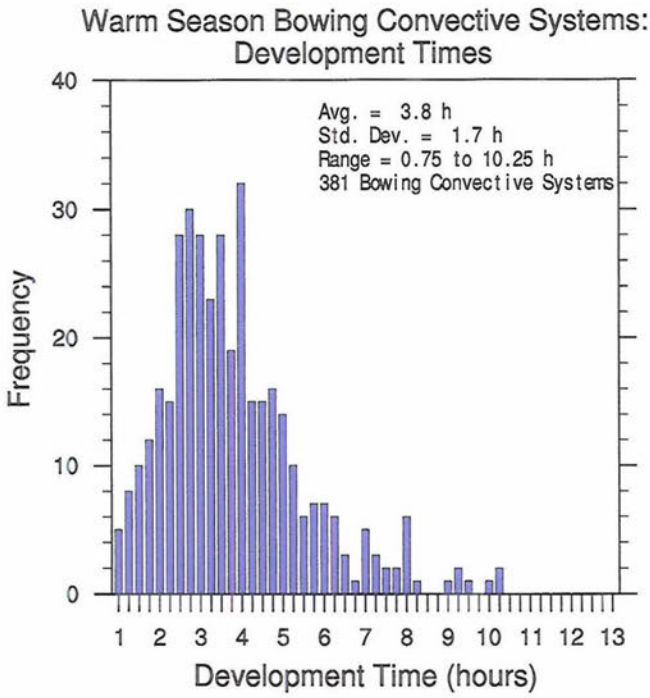

Figure 5.10: Frequency distribution of development times (first echo to bow start, see section 2.2) for all warm season cases observed in this study. The average, standard deviation, and range of longevity times are shown in the upper right hand corner.

the longevity distribution for warm season BCSs in the present study shows similar skewness and shape for cases lasting longer than 3 hours. However, the present study contains *many more bowing convective systems lasting 1 to 3 hours.* The longevity criterion for the study of BS04 was 2 hours compared to the 1 hour in this study. Also, the case selection process for the present study was performed using improved temporal and spatial resolution, allowing for the greater possibility of additional small, short-lived BCSs to be included. The differences in selection criteria cause the mean longevity of this study to be lower than BS04 (3.6 h vs. 5.3 h).

The development times and longevities are similar when compared on a case by case basis with a correlation coefficient of $r = 0.32$ (99% statistically significant). The scatterplot that compares these distributions is graphed in Fig. 5.12. While considerable scatter exists among cases that are outliers, the large majority of BCSs cluster around a linear relationship between development time and longevity that

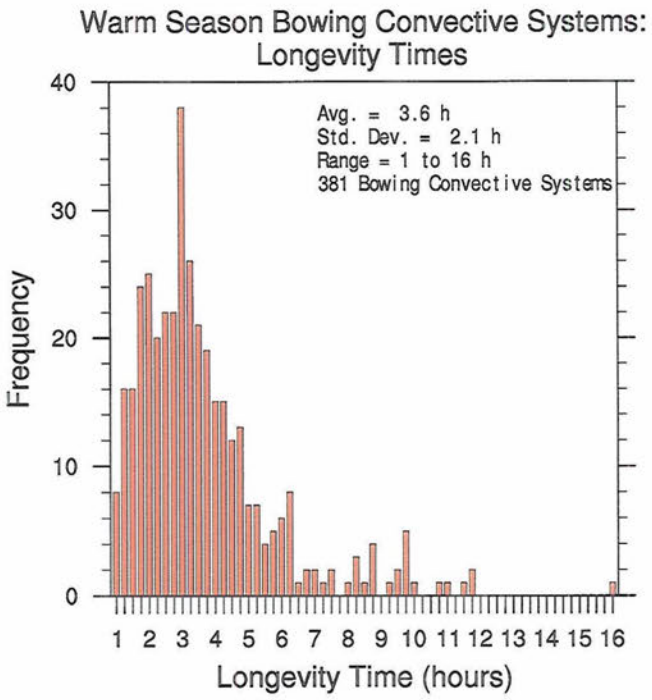

Figure 5.11: Same as Fig. 5.10, but for longevity times (bow start to bow end, see section 2.2).

has a slope of approximately $a_1 \approx 0.75$. As an example, a development time of 6 h would predict an expected longevity of approximately 4.5 h. However, there is too much scatter for a weather forecaster to base an entire forecast on this observation.

While some relationship between BCS development time and longevity exists (Fig. 5.12), there is considerable scatter. One reason for the scatter is the methodology in assigning first 40 dBZ echo times and bow end times. First echo times do not always represent the development of a BCS well since 40 dBZ convective cells can exist in a nearly stationary position for a long period of time before rapidly moving cells, supercells, or a squall line develops that forcibly causes the formation of a bowing system. Moreover, bowing longevity times are sometimes cut shorter than would be possible because of external factors (e.g. interaction with exterior convection, convective storm mergers during the bowing process, crossing synoptic boundaries, etc.). As a result, forecasters should examine on a case by case basis the

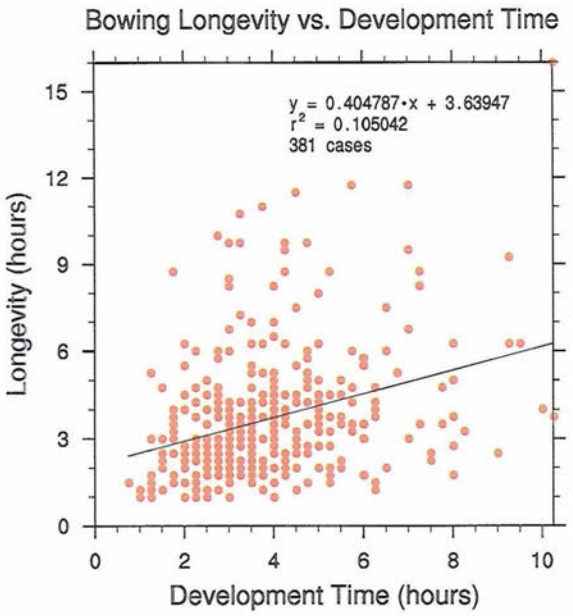

Figure 5.12: Scatterplot showing relationship between development time and longevity time for all warm season bowing convective systems observed in this study. A best fit linear relationship is shown on the chart as well as the equation of the line and the r^2 value.

development properties of BCSs which form, for the purpose of possible correlation with resulting longevity.

Dr. Morris Weisman has hypothesized an explanation for the connection between bowing convection development time and longevity (2004, personal communication). Convective cells that develop in a statically unstable environment with strong vertical wind shear tend to lean downshear and remain vertically erect for a longer period of time compared to an environment of interacting cells that quickly form larger convective systems. Generally, longer-lived BCSs (and derechos) have increased instability and vertical wind shear over shorter lived bowing convection (see appendix A). Therefore, the correlation between development time and longevity could be a manifestation of the thermodynamic and kinematic environments favorable for enhancing bowing longevity, although BCSs environments can change greatly over a long time period or a long BCS track.

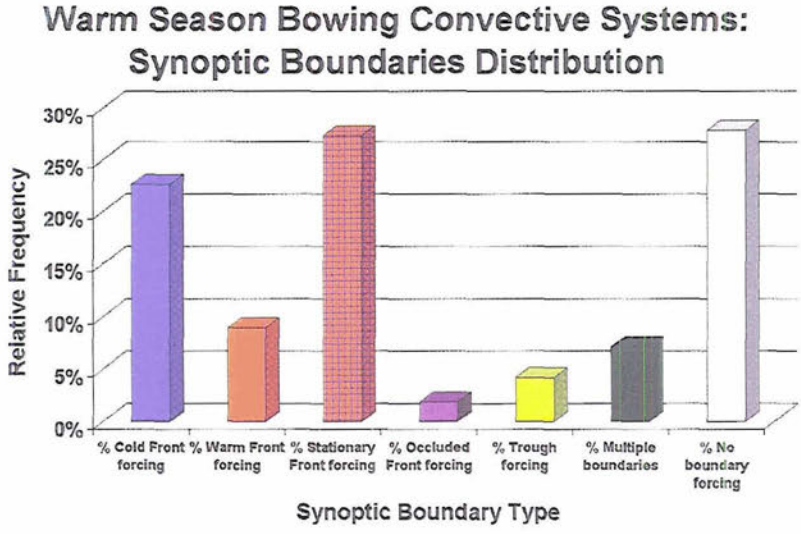

Figure 5.13: Relative frequency distribution of synoptic boundaries that initiated or significantly influenced bowing convective systems for all warm season cases observed in this study.

5.4 Observed surface boundaries

5.4.1 Synoptic scale boundaries

The distribution of synoptic scale boundaries that initiated or forced BCSs (Fig. 5.13) demonstrated that warm season bowing convection is most often forced by cold fronts, stationary fronts, and no synoptic boundaries, which comprise about 75% of the entire distribution. Warm fronts and multiple boundaries forced bowing convection less frequently, with about 9% and 7% frequency, respectively. Troughs and occluded fronts very infrequently forced BCSs, while drylines were never observed in this process directly. Since outflow boundaries were not reliably present on NCEP charts throughout the analysis, the effect of these small boundaries was not included.

5.4.2 Strong, weak, and hybrid forcing

The current study reveals various patterns of bowing convective system initiation and evolution in the vicinity of synoptic boundaries. Strong boundary forcing

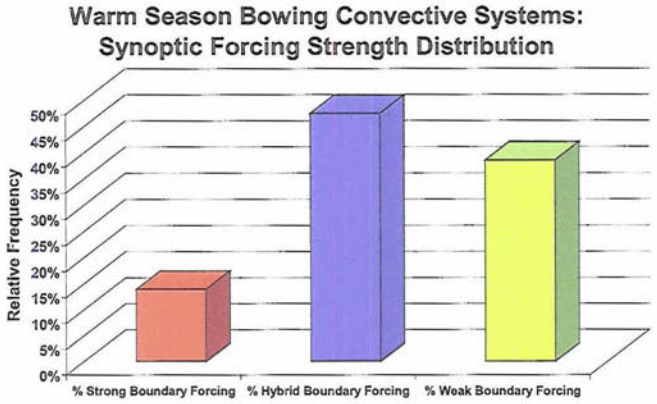

Figure 5.14: Relative frequency distribution of strength of synoptic scale forcing that initiated or significantly influenced bowing convection for all warm season cases observed in this study. The definitions closely follow those of Evans and Doswell (2001).

was caused when a synoptic scale boundary initiated and directly forced a BCS throughout its evolution. As expected, the source of this initiation was most frequently a cold front, but other types of boundaries were observed to strongly force bowing convection at times. One way that hybrid boundary forcing occurred was when a BCS was initiated by a synoptic boundary but moved faster than the boundary and hence away from it. The other scenario for hybrid boundary forcing was the initiation and movement of a BCS roughly parallel to a synoptic boundary. As expected, movement parallel to a synoptic boundary occurred most often along a stationary front or a slow moving warm front. Weak boundary forcing occurred when a bowing system was initiated at least 500 km from a synoptic boundary and was not forced by any boundary.

The statistics indicate that hybrid boundary forcing is the most common forcing mechanism for warm season BCSs while weak boundary forcing is of secondary importance (Fig. 5.14). This tendency of warm season bowing convection to develop away from strong synoptic boundary forcing is consistent with the findings for warm

season derechos (Evans and Doswell 2001, Coniglio et al. 2004a). Thus, the results suggest that BCSs can be forced with strong synoptic scale boundary forcing, but given that this forcing occurs infrequently during the warm season, it is not a common forcing mechanism for BCSs.

The composite analysis that shows the highest correlation between development time and longevities for BCSs is associated with the hybrid boundary forcing composite ($r = 0.45$, 99% significance). A possible reason for this strong correlation could be that the development and bowing stages of bowing convection moving along parallel boundaries pass through similar regions of CAPE and vertical wind shear. As a result, predictability between development time and longevity for BCSs is enhanced for hybrid forcing scenarios.

5.4.3 Placements in relation to midlatitude cyclones

Evans and Doswell (2001) noted that their strong forcing and weak forcing derecho cases roughly corresponded to the dynamic and warm season patterns of Johns (1993). The examination of warm season bowing convection in this study showed that the dynamic pattern is not favored for the warm season (~14% of the cases), while in contrast the warm season pattern is related to the development of many BCSs (~48%). Moreover, this study reveals that *bowing convection that develops near no synoptic boundary (weak synoptic forcing) is nearly as probable as hybrid forcing.* This discovery is noteworthy because forecasters must be aware that warm season BCSs frequently arise from convection not connected with synoptic boundaries or upper-level forcing, implying that the bowing process is linked directly to internal storm dynamics many times in the absence of large-scale forcing.

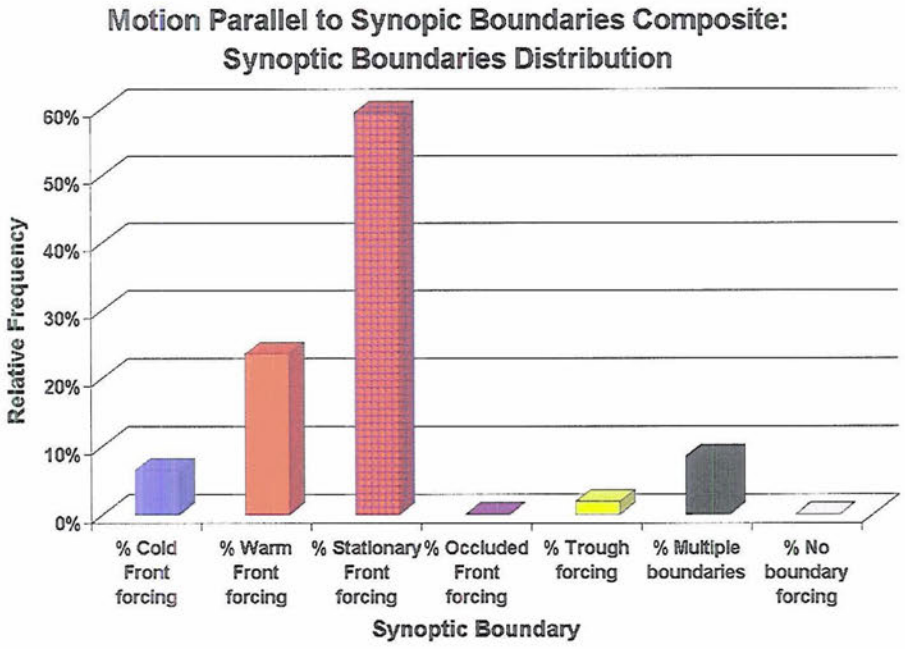

Figure 5.15: Relative frequency distribution of synoptic boundaries which bowing convective systems moved parallel to in this study.

5.4.4 Motion parallel to synoptic scale boundaries

Bowing convective systems moved parallel to synoptic scale boundaries in 28% of all cases. BCSs which moved parallel to synoptic boundaries primarily were identified near stationary fronts (59%) and warm fronts (24%) (Fig. 5.15). BCSs moved parallel to other types of synoptic boundaries less frequently.

The conceptual diagrams of Johns and Hirt (1987), Johns (1993), and Kuchera and Parker (2004) suggest that BCSs parallel synoptic boundaries on the cool side of a stationary front or slow moving warm front. However, similar to the hybrid forcing example of Evans and Doswell (2001), BCSs can move parallel to the warm side of a slow moving or stationary synoptic scale boundary. The present study found that bowing convection moved parallel to synoptic boundaries either on the cool side (41%), warm side (24%), or *with the apex roughly collocated along the synoptic scale boundary* (35%). Therefore, this observation provides evidence for three regimes of

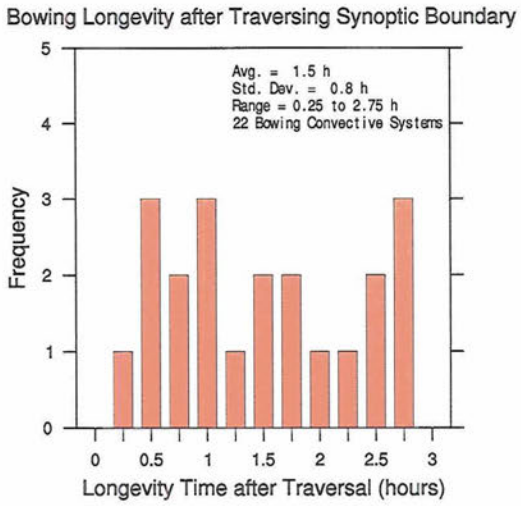

Figure 5.16: Frequency distribution of longevity times after a bowing convective system would traverse a synoptic scale boundary as observed in this study. Bins are shown in 15 minute intervals. The average, standard deviation, and range of longevities after traversing a synoptic scale boundary are shown in the upper right hand corner.

motion parallel to synoptic boundaries with BCSs.

5.4.5 Motion traversing synoptic scale boundaries

In the course of this study, a BCS traversed a synoptic scale boundary in 5.8% of all cases. Out of all the BCSs that traversed synoptic boundaries, 59% moved across stationary fronts, 23% moved across warm fronts, and 18% moved across cold fronts. This phenomenon might be explained by the rapid pace at which BCSs move (section 5.2).

Furthermore, the BCSs that traversed synoptic scale boundaries *tended to dissipate very quickly.* The results indicate that BCSs only lasted an average of 1.5 h after traversing a synoptic scale boundary (Fig. 5.16). Also, *no bowing convective system that traversed a synoptic boundary lasted longer than 3 hours after traversing the boundary.*

The overall longevity of the traversing BCSs remains comparable to the

longevity of the other cases (Fig. 5.17). However, this observation should be taken into account on an individual basis, as radar reflectivity composite animations showed weakening convection upon the traversal of synoptic boundaries.

The traversing motion could indicate the disruption of convection regeneration on the leading edge of a BCS that enters a distinctly different kinematic and thermodynamic environment. Indeed, these systems depend upon strong convective instability and vertical wind shear for maintenance of severe convection. The same level of convective instability might not always accompany the traversing motion of a synoptic scale boundary into a distinctly different airmass.

5.4.6 Boundary association with bowing convective system longevity

The longevity comparison of the entire population of BCSs with those cases that traverse synoptic boundaries, parallel synoptic boundaries, or arrange in a bowing series is summarized in Fig. 5.17. BCSs traversing synoptic boundaries display a narrow distribution so that the likelihood of a very long-lived bowing convective system is diminished. Not surprisingly, one can observe much similarity in the longevity distributions for bowing systems that parallel synoptic boundaries and those that arrange themselves in a bowing series (section 4.7). Compared to all cases, these two composites demonstrate increased bowing longevity averages of about 1 h.

5.5 Severe weather production patterns for bowing convection

Generally speaking, each severe weather survey showed variability, but clustered into recognizable patterns. Strong confidence exists in the severe weather damage shapes with 381 spatial distributions of severe weather examined. The main four shapes were: **narrow apex swath**, **widespread high winds**, **widening swath**, and **destructive rotation** (Fig. 5.18). Each of these will be explained in the subse-

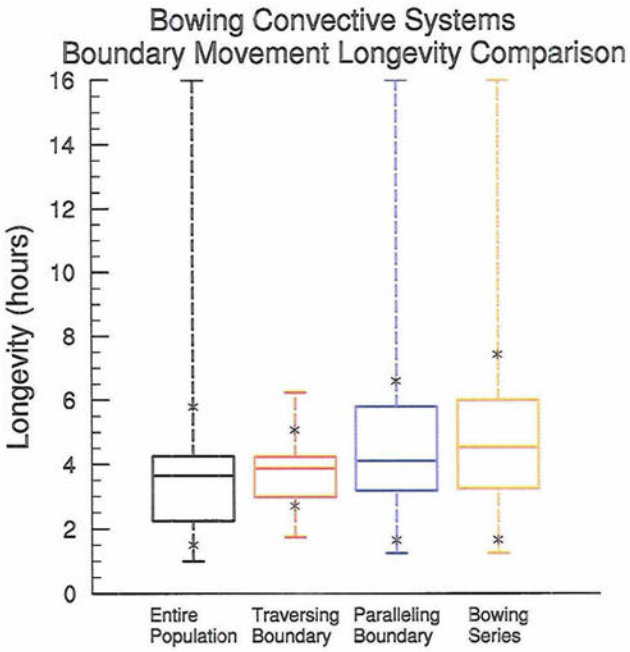

Figure 5.17: Comparison of bowing convective system longevities which move across or along synoptic boundaries as defined in the text. The middle line in each box represents the mean. The edges of the boxes represent the lower and upper quartiles of the distributions while the ends of the lines are the minima and maxima. The $\pm 1\sigma$ (standard deviation) locations of each distribution are shown as black "x"s on each distribution drawing.

quent subsections.

This study defined **little severe weather** as two or fewer severe weather reports for a single BCS or 3 reports that were separated by at least two hours each. A total of 65 cases (about 17% of all BCSs) were not associated with severe weather reports identifiable from SPC storm reports and were therefore termed **no severe weather**. This result is similar to BS04, who found about 14% of their cold season bow echo cases produced no severe weather. Composite analysis of cases producing zero severe wind reports indicated decreased bowing accelerations compared to the entire population. Over 66% of cases that produced no severe weather were classified as slow or moderately bowing. These definitions depend upon reliable reporting of severe weather data; otherwise, surveys revealing little or no severe weather could

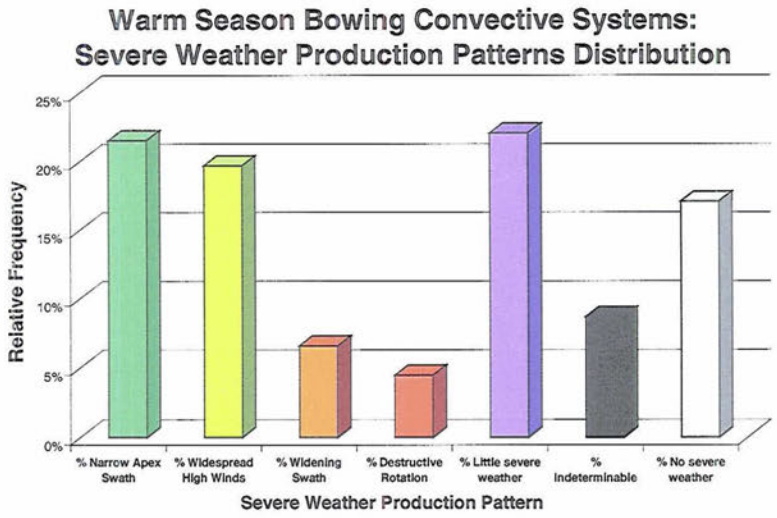

Figure 5.18: Relative frequency distribution of severe weather patterns produced by bowing convective systems for all warm season cases observed in this study.

have been another severe weather production pattern.

5.5.1 Severe weather pattern 1: Narrow apex swath

The most common severe weather production pattern of bowing convection (22%) is a **narrow apex swath**. An example of a severe weather survey that fits this pattern is given in Fig. 5.19. This pattern is described as a fairly narrow swath (usually only about 2 to 15 km in width) in the direction of BCS motion that arises from severe weather processes centered near a BCS apex. Small-scale BCSs usually produce this severe weather pattern. Bowing convection fitting this form tends to favor severe hail reports early in the evolution with the slight possibility of moderate F1 surface wind damage (33 m s^{-1} speeds or greater). The severity of the severe winds reports most often decreases in this mode as the BCS evolves. BCSs that produce this kind of damage usually have 15 or fewer severe wind reports, fewer than five severe hail reports, and rarely any tornadoes (see Figs. 5.20, 5.21, and 5.22).

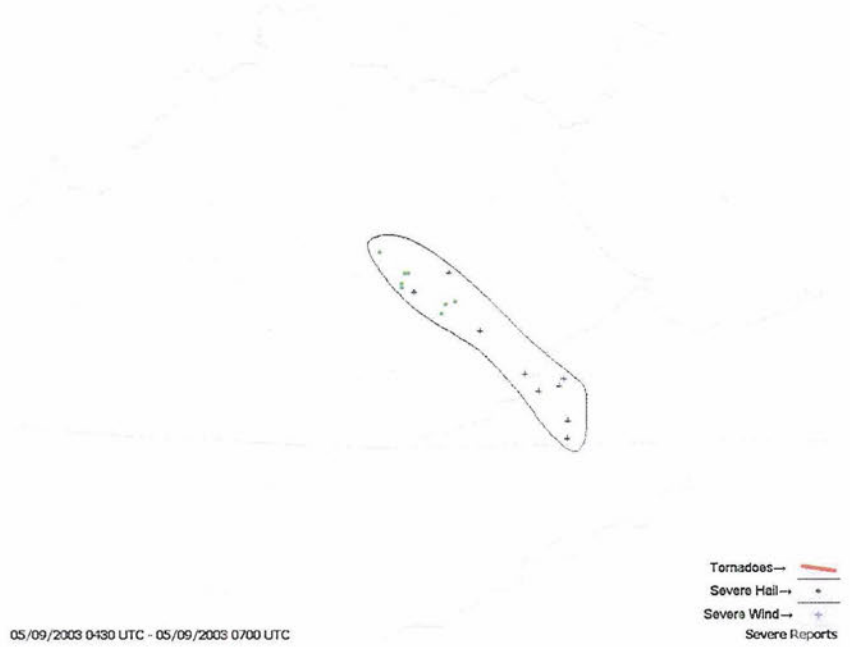

Figure 5.19: Example of severe weather reports constituting a narrow apex swath pattern. The bowing convective system moves from northwest to southeast in the image. A narrow black line demarcates the severe weather generated by the bowing convective system.

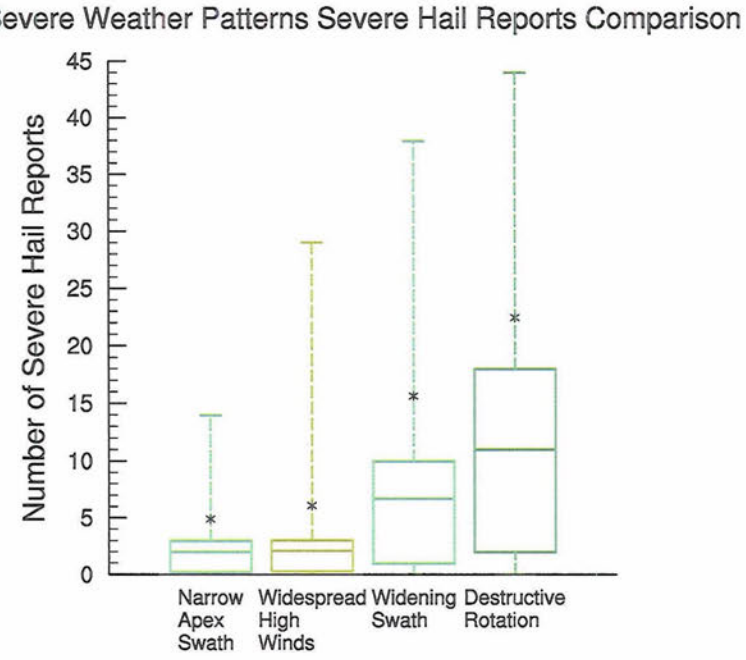

Figure 5.20: Same as Fig. 5.17, except for severe hail reports comparison between severe weather production patterns.

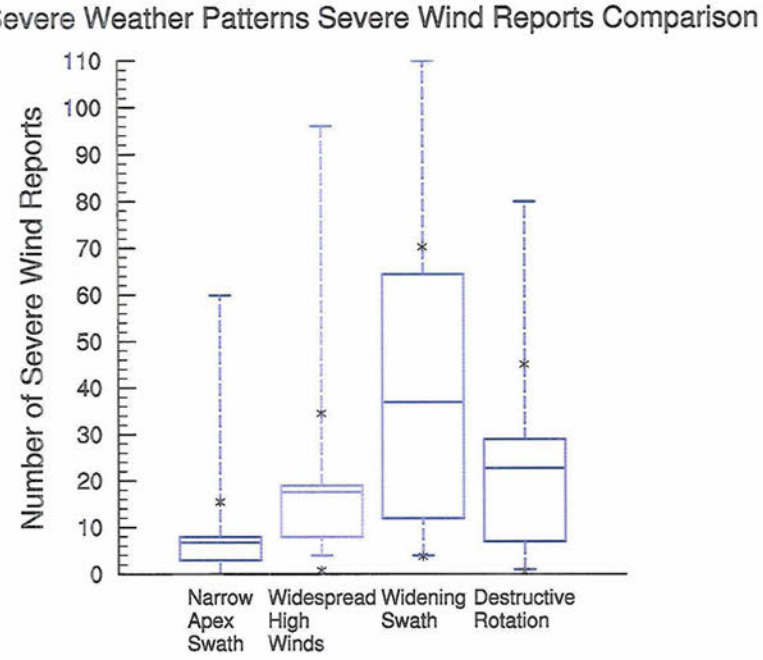

Figure 5.21: Same as Fig. 5.17, except for severe wind reports comparison between severe weather production patterns.

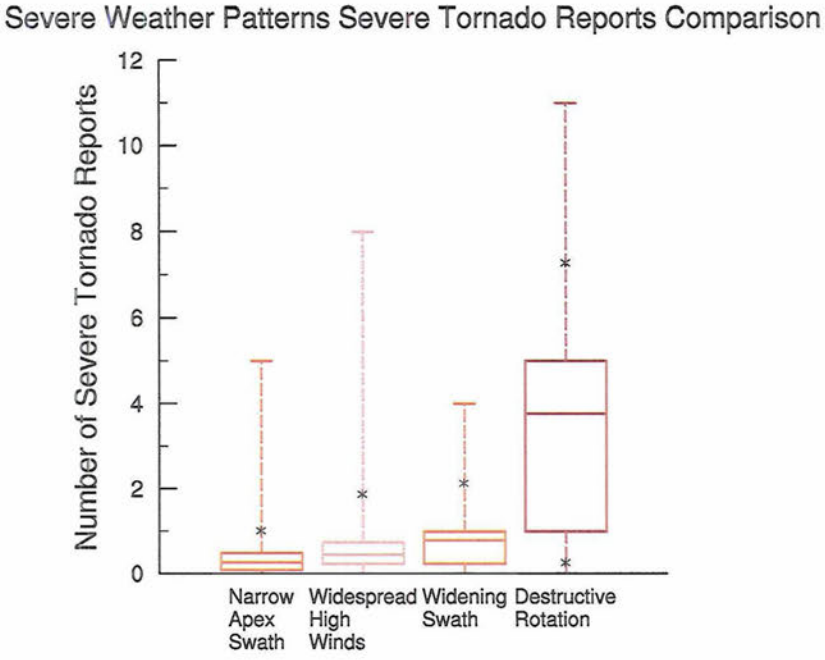

Figure 5.22: Same as Fig. 5.17, except for severe tornado reports comparison between severe weather production patterns.

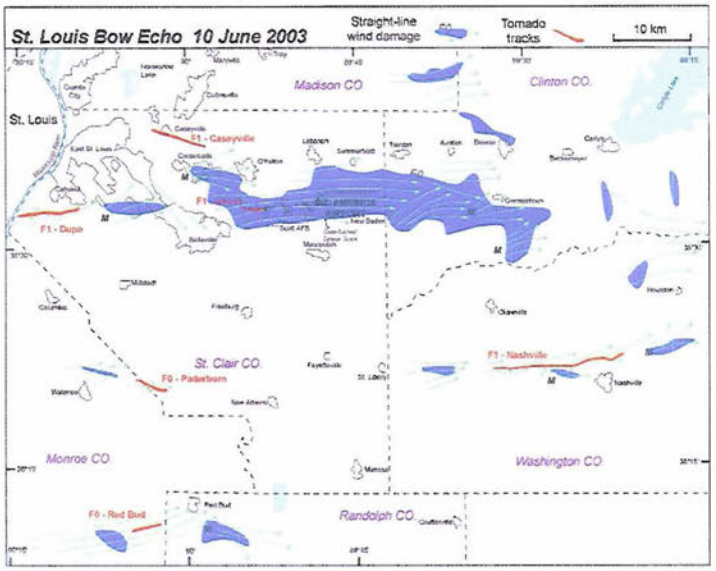

Figure 5.23: Damage survey from 10 Jun 2003 severe bow echo near Mid America St. Louis Airport. Blue shading denotes straight-line winds with damage equivalent to F0. Green arrows indicate wind direction inferred from debris orientation. Individual tornado tracks are denoted by heavy red lines. Time of damage ranged from about 2300 UTC 10 Jun to 0000 UTC 11 Jun. From Davis and Coauthors (2004).

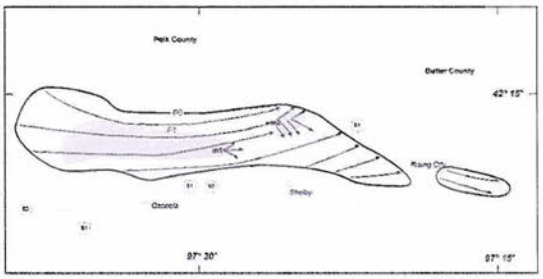

Figure 5.24: Damage analysis performed for the "Shelby" bow echo on 10 June 2003 over northeast Nebraska. F0 damage is outline with a solid line. The key at the top of the figure shows pieces contributing to damage assessment. Adapted from Wheatley et al. (2006).

Two cases examined with detailed damage surveys conducted during the BAMEX field campaign appear to fit this profile of severe weather production. The first is the famous 10 June 2003 St. Louis bow echo that moved over the BAMEX operations center, forcing an evacuation of experiment participants (Fig. 5.23, Davis and Coauthors 2004, Atkins et al. 2005). Despite significant tornadoes and mesovorticies observed for this case, the main F0 damage swath is noted with approximately width of 7 km with straight-line winds mainly from west to east with a length of about 35 km. A second example of this pattern is the "Shelby" Nebraska bow echo on 9-10 June 2003 (Fig. 5.24, Wheatley et al. 2006). The main F0 swath of straight-line winds has a width of approximately 7 km and a length of about 25 km. This case also demonstrates that the severity decreases from F1 damage to mainly F0 damage from the earlier to the later stages, as seen in many narrow apex swath bowing systems. Therefore, BCSs producing a narrow apex swath will likely exhibit straight line winds in the direction of motion.

5.5.2 Severe weather pattern 2: Widespread high winds

The second most common severe weather production pattern (20%) is called a **widespread high winds** swath. An example of a severe weather survey that demonstrates this arrangement is given in Fig. 5.25. This pattern is described as a fairly wide swath of severe surface winds that remains approximately the same width throughout the evolution. Usually the width is between 20 and 90 km, about half to two thirds of the length of the causative bowing convective line. Also, the severe surface wind reports in this mode are most often 26 to 31 m s^{-1}. This mode is predisposed toward severe winds with 5 to 35 severe wind reports, fewer than five severe hail reports, and rarely any tornadoes (Figs. 5.20, 5.21, and 5.22).

One study from BAMEX that comes across to validate this pattern is the 5-6 July 2003 bow echo studied by Wakimoto et al. (2006a,b). The damage survey for this

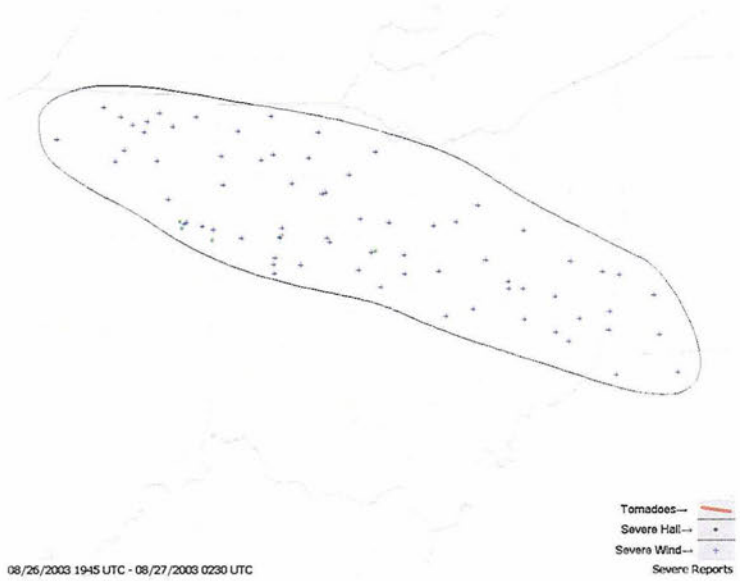

Figure 5.25: Example of severe weather reports constituting a winds spread throughout pattern. The bowing convective system moves from west-northwest to east-southeast in the image. A narrow black line demarcates the severe weather generated by the bowing convective system.

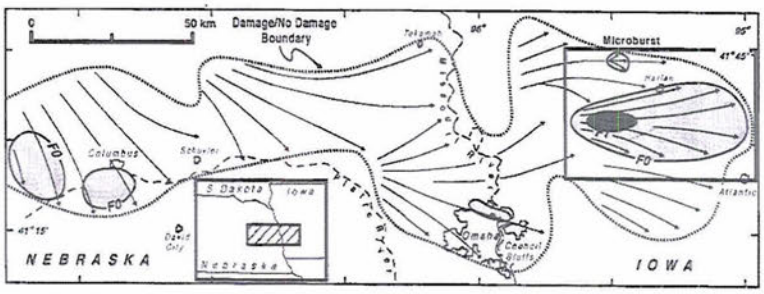

Figure 5.26: Map of the surface damage produced by the 5 July 2003 Omaha bow echo. The map was compiled based on several days of aerial and ground surveys throughout the region. The location of the rectangular map is indicated by the hatched box in the inset. The flow lines represent the direction of fallen trees or structural damage. The outer extent of the damage as well as the regions rated F0 and F1 in damage intensity are indicated in the figures. From Wakimoto et al. (2006a).

case is shown in Fig. 5.26. While the studies of Wakimoto et al. (2006a,b) focus on the F0 and F1 damage produced by a strong mesovortex, the overall damage boundary supports the widespread high winds depiction. Although there is some variability in the width of the damage swath, the damage retains a width of approximately 40 km. Notice also that the straight line wind damage is not unidirectional. In fact, the evolution of the convection as seen on radar shows that movement of the convective echoes shifted from southeastward to eastward movement as the BCS evolved.

Therefore, one can expect a much wider swath of light damage with this arrangement compared to the narrow apex swath with the potential for pockets of F0 or F1 damage associated with features like microbursts, mesovorticies, etc.

5.5.3 Severe weather pattern 3: Widening swath

The third severe weather production pattern (7%) is the **widening swath**. An example of a severe weather survey that fits this pattern is given in Fig. 5.27. This mode is described as an initially narrow swath of severe weather that progressively increases width as a BCS evolves. The swath may start off as narrow as 15 km, but can expand to widths of 400 km or greater. Many times, this severe weather pattern is caused by large-scale BE/ESs or bowing squall lines. BCSs producing a widening swath tend to have many more severe weather reports than either of the previous two patterns (Figs. 5.20, 5.21, and 5.22). Often, severe wind reports are observed between 5 and 70 times, severe hail reports are reported between 3 and 15 times, while tornadoes are rarely reported. Some cases that are labeled with this pattern experience convection regeneration on the BCS leading edge and reforming of the BCS. If this happens, usually there is a discontinuity in the width of the damage swath; radar observations usually confirm expanding convective lines with widening damage swaths during this severe weather pattern.

Composite analysis reveals that bowing squall lines and multiple bowing squall

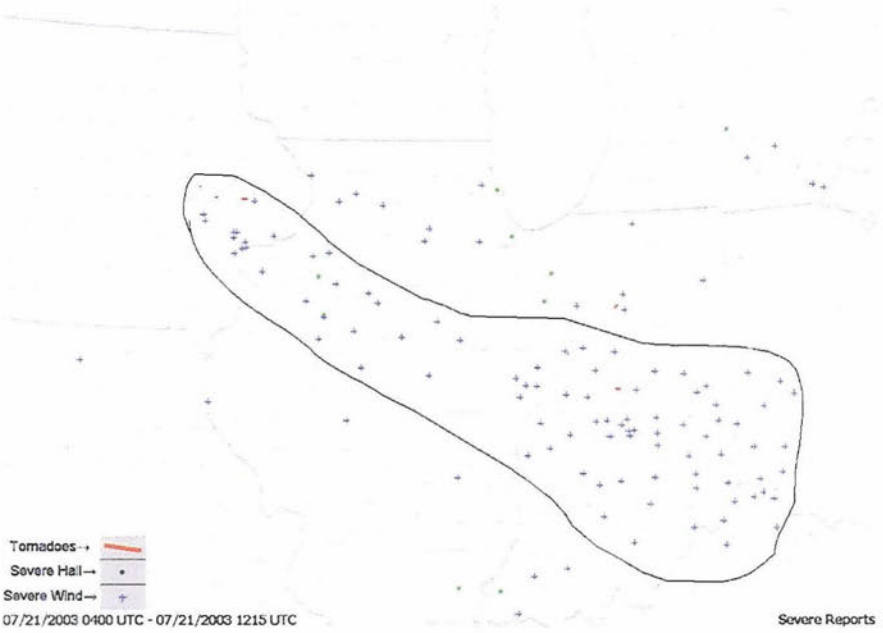

Figure 5.27: Example of severe weather reports constituting a widening swath pattern. The bowing convective system moves from northwest to southeast in the image. A narrow black line demarcates the severe weather generated by the bowing convective system and severe weather generated by other convection.

lines are nearly equally favored with the BE/ES and BE/MS modes for producing this severe weather pattern (see Fig. 5.28). Also, analysis of severe wind reports reveals that damaging surface wind magnitudes tend to decrease as the width of the swath increases.

A previous study appears to match this severe weather pattern. Miller et al. (2002) studied the famous 27-28 May 2001 derecho that caused enormous life and property damage throughout Oklahoma (Fig. 5.29). The radar reflectivity evolution displayed a very strong squall line that initiated over southern Kansas. The storm evolved into an expanding bowing squall line that caused widespread destruction over a large portion of southern Kansas and Oklahoma. The width of the damage swath expanded from approximately 40 km to 350 km throughout the evolution. Examination of SPC storm reports confirms that the magnitudes of the severe surface wind reports generally decreased in magnitude as the damage swath of the bowing

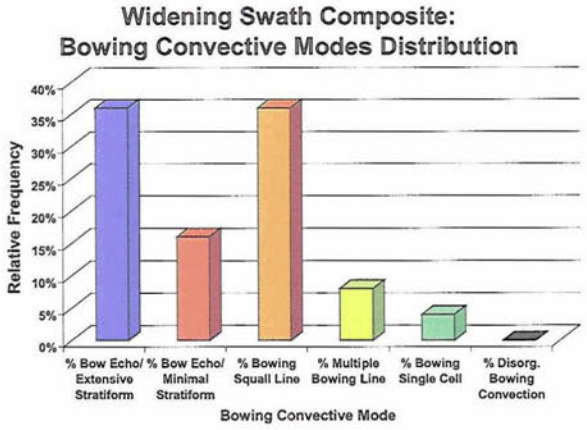

Figure 5.28: Relative frequency distribution of bowing convective modes for bowing convective systems producing the widening swath severe weather pattern.

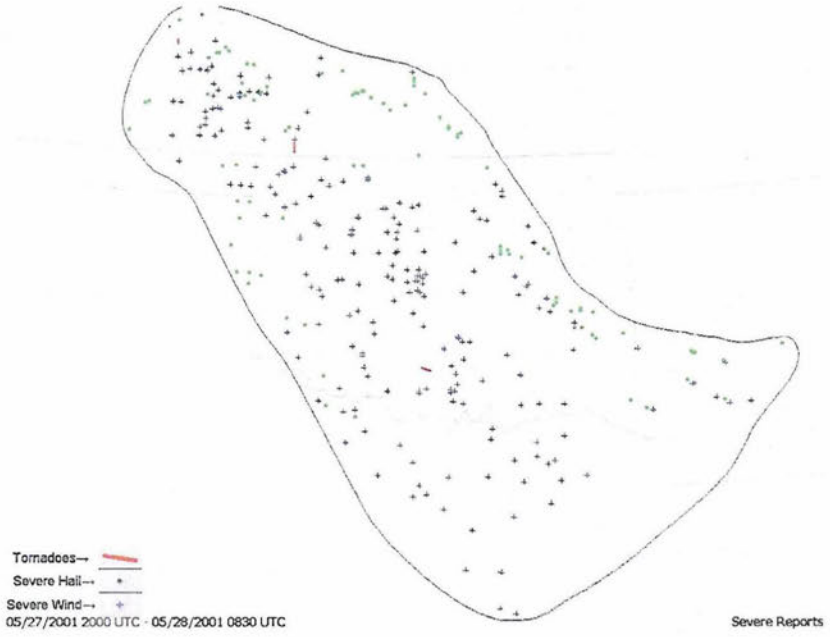

Figure 5.29: Severe weather reports associated with the 27-28 May 2001 derecho. The bowing squall line moves from northwest to southeast in the image. Severe weather reports are identifiable by the key given in the figure. A narrow black line demarcates the severe weather generated by the bowing convective system. Constructed from data in Miller et al. (2002).

squall line expanded. Thus, if the results from this bowing system can be applied to more cases, this severe weather pattern should be noted as a potentially destructive arrangement often associated with expanding bowing convection that can cause widening damage over large spatial regions.

5.5.4 Severe weather pattern 4: Destructive rotation

The final main severe weather production pattern (5%) is the **destructive rotation** swath due to the mesoscale rotation in the BCSs that produce this pattern and the rotation seen in the damage surveys. An example of a severe weather survey that fits this pattern is shown in Fig. 5.30 (although the rotation of the damage cannot be seen until detailed damage surveys are examined). This mode is described as a swath that has large variability in width, usually between 10 and 200 km. The damage swath tends to be fairly narrow, but not as narrow as the narrow apex swath pattern. Composite radar reflectivity animations disclose that BCSs exhibiting strong mesoscale rotation favor the production of a damaging rotation swath. In fact, composite analysis of this pattern confirms that 71% of the systems which produce this pattern are BE/MS systems.

BCSs producing a destructive rotation arrangement often have more severe wind reports than either of the first two patterns and *by far the most severe hail and tornado observations* (Figs. 5.20, 5.21, and 5.22). While severe wind reports are usually noted between 5 and 40 times, 3 to 20 severe hail reports and 1 to 5 tornado reports can be expected in this mode. The interesting property of this configuration is that severe hail, wind, and tornadoes are spread throughout the BCS evolution, likely to occur at any time. Severe hail diameters are also larger for this damage pattern. Severe wind magnitudes can be light or moderate throughout the bowing convection evolution with no decrease in magnitude apparent. Also, the frequency of bowing convective system-induced tornadoes increases along with the length of the

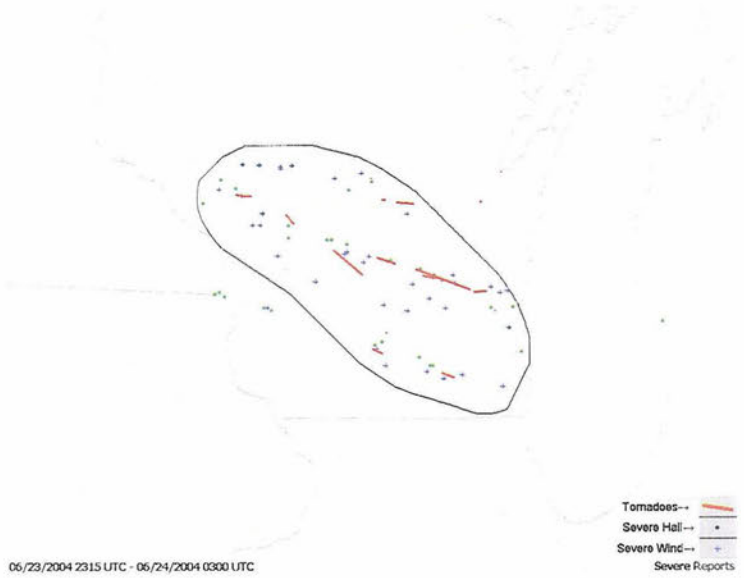

Figure 5.30: Example of severe weather reports constituting a destructive rotation pattern. The bowing convective system moves from northwest to southeast in the image. A narrow black line demarcates the severe weather reports generated by the bowing convective system and severe weather generated by other convection.

tornado tracks in this setup.

One detailed damage survey from the BAMEX campaign reveals a similar destructive rotation pattern. The "Emerson" Nebraska bow echo examined in Wheatley et al. (2006) demonstrated strong mesoscale rotation toward the comma head of the system. Fig. 5.31 illustrates the detailed damage survey for the early stages of the

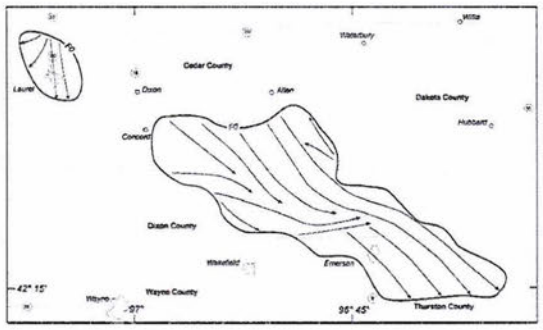

Figure 5.31: Damage analysis performed for the "Emerson" bow echo on 10 June 2003 over east-central Nebraska. The key at the top of the figure shows pieces contributing to damage assessment. Adapted from Wheatley et al. (2006).

bowing in northeast Nebraska. The detailed damage survey depicts wind damage parallel to the bowing system motion, perpendicular to the bowing convection motion, and anti-parallel to the bowing convection motion. Thus, the mesoscale rotation present in the "Emerson" bow echo is supported with swirling in the detailed damage survey debris.

Therefore, if the findings from this example apply more liberally, bowing convection exhibiting strong mesoscale rotation and usually little to no trailing stratiform precipitation are predisposed to producing severe wind patterns with rotating features, not necessarily straight line winds in a single direction. These systems should be noted for their production of severe hail and tornadoes.

5.5.5 Indeterminable severe weather pattern

This study assigns a severe weather production pattern as indeterminable (9%). An indeterminable severe weather pattern must have at least three severe weather reports or else it would be classified as a BCS with little severe weather. Generally speaking, this group of severe weather production has severe weather reports spread apart by several hours, excessive hail reports with no severe winds, severe weather concentrated in a very small cluster (perhaps indicative of a single microburst), or severe weather reports located near ends of bowing convective lines that are not clearly connected with an identifiable physical process. Some BCS cases in this severe weather category might have been classified in other categories if all the proper severe weather data was reported.

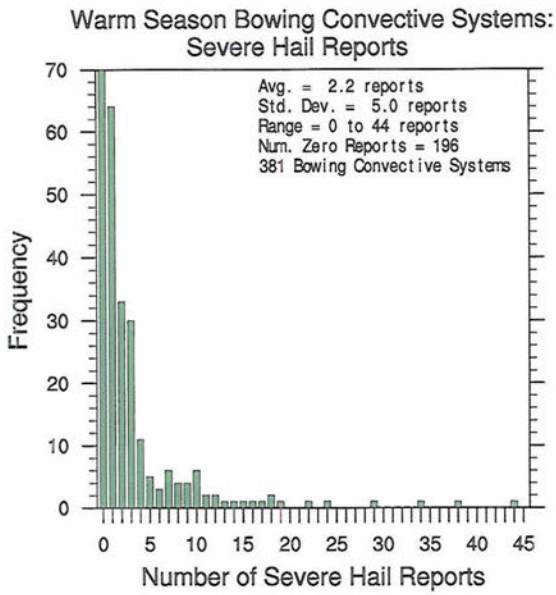

Figure 5.32: Frequency distribution of number of SPC hail reports per bowing convective system for all warm season cases observed in this study in bins of one severe report. The number of bowing convective systems with zero hail reports goes off the chart and is noted in the upper right hand corner, along with the average, standard deviation, and range of severe hail reports.

5.6 Bowing convective systems severe weather climatology

5.6.1 Distributions of number of severe weather reports

The frequency distribution of the number of SPC severe hail, wind, and tornado reports for each BCS is plotted in Figs. 5.32, 5.33, and 5.34, respectively. Considered as a whole, for all warm season BCSs, 49% produce severe hail, 77% produce severe wind, and 16% produce tornadoes. Warm season BCSs in this study averaged about nine severe wind reports. This is about four times the average number of severe hail reports while severe hail reports are about five times as likely as tornado reports in BCSs. As mentioned in chapter 4, the reports of severe wind per system are correlated to the size of the BCS with larger systems averaging more severe wind reports.

Each of the severe weather frequency distributions is strongly skewed toward

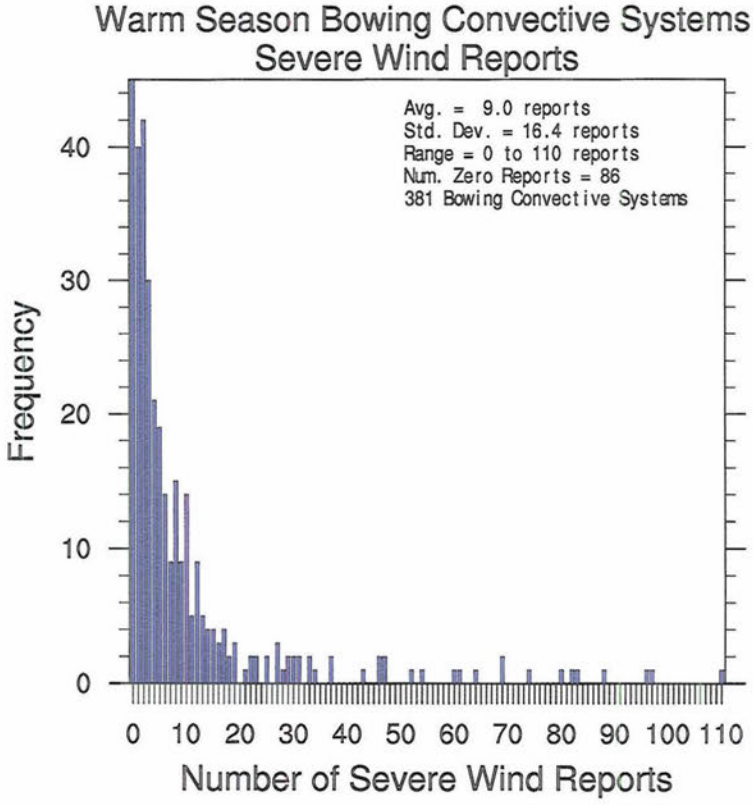

Figure 5.33: Same as Fig. 5.32, except for severe wind reports.

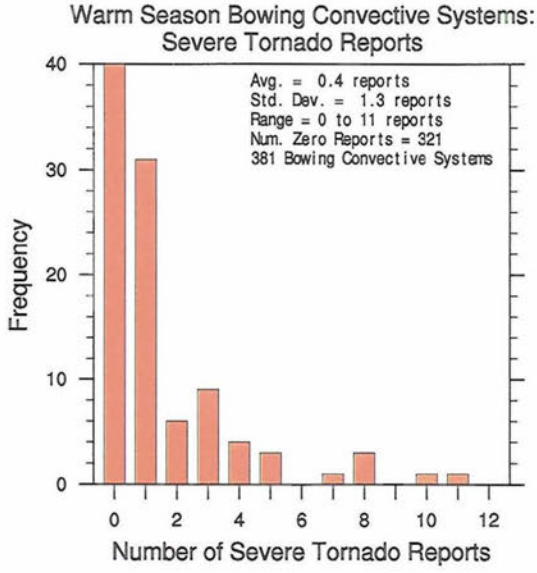

Figure 5.34: Same as Fig. 5.32, except for severe tornado reports.

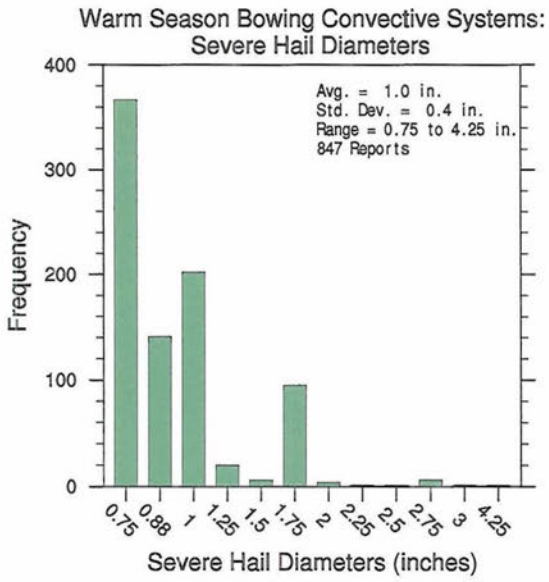

Figure 5.35: Frequency distribution of diameters of SPC hail reports for all warm season bowing convective systems observed in this study. Data include all reports from all cases. Bins are assigned based on NWS severe hail reporting diameters or measurements of hailstones retrieved. The average, standard deviation, and range of severe hail diameters is noted in the upper right hand corner.

zero. The greatest frequency occurs for zero reports with 17% of all BCS producing no severe weather of any kind. This is a considerable portion of the BCS population which has received no in-depth examination in any previous study; some studies even used severe wind reports to identify cases (e.g. BS04).

5.6.2 Distributions of severe weather magnitudes

The results of severe weather magnitudes show that most severe hailstones produced by BCSs are less than 2.00" in diameter (smaller than "golf ball sized" hail, Fig. 5.35). While severe hail between 0.75 and 1.00" ("dime to quarter sized hail") is most frequent, hailstones between 1.00 and 2.00" in diameter still occur with some regularity.

BCSs produce surface severe wind speeds between 26 and 31 m s^{-1} with great regularity (Fig. 5.36). These windspeeds qualify as NWS "severe wind gusts" and

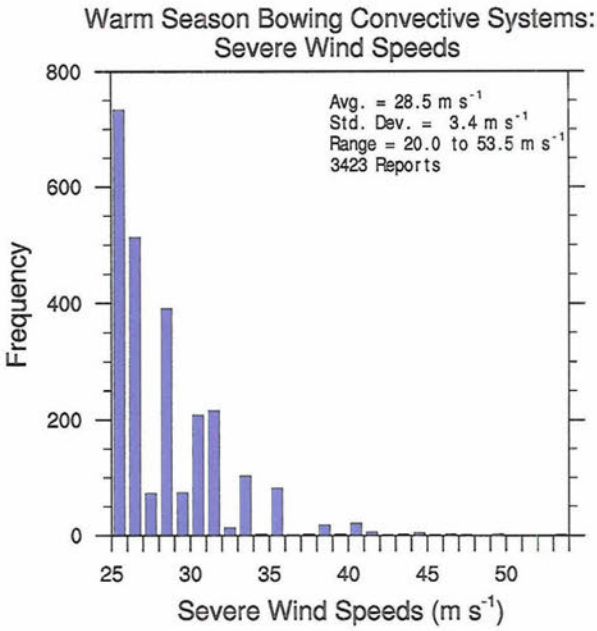

Figure 5.36: Frequency distribution of speeds of SPC wind reports for all warm season bowing convective systems observed in this study. Data include all reports from all cases. Bins are divided into 1 m s^{-1} intervals. Speeds are estimated from damage assessments from spotters near severe wind reports. The average, standard deviation, and range of severe wind speeds is noted in the upper right hand corner.

light F0 damage. However, about 7.4% of all severe wind reports produced by bowing convective systems were estimated at 34 m s^{-1} or greater, making them "moderate" F1 or greater surface winds. These windspeeds can damage the roofs of homes or blow moving automobiles off roads. The two most extreme severe wind reports that resulted from two different bowing systems were estimated at 53.5 m s^{-1}, which is on the low end of the F2 "considerable" damage scale, close to blowing roofs off of homes or even overturning automobiles.

The criteria for a derecho from Johns and Hirt (1987) includes a damage swath of at least 400 km long of F0 damage with at least three F1 severe wind reports. For the present study, 8% of BCSs met the necessary criteria for a derecho.

The most extreme severe wind magnitudes for each individual BCS reveal that 30% of all cases produce severe surface winds with speeds greater than 34 m s^{-1}

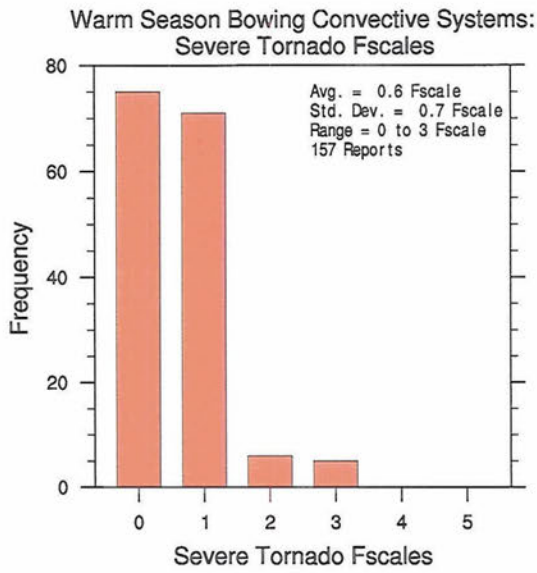

Figure 5.37: Frequency distribution of Fscales of SPC tornado reports for all warm season bowing convective systems observed in this study. Data include all reports from all cases. Bins are assigned bases on the NWS Fujita scale from F0 to F5 with increasing intensity. The average, standard deviation, and range of severe tornado Fscales is noted in the upper right hand corner.

(F1 damage or greater). This result implies that "pockets" of moderate severe wind damage are possible for all bowing convection, even if most severe wind reports are light in magnitude. This is also revealed in detailed damage surveys where small scale moderate to considerable damage is often observed (e.g. Fig. 5.24 and Fig. 5.26).

BCSs that produce tornadoes almost always produce F0 or F1 magnitude tornadoes (Fig. 5.37). Consequently, most BCS tornadoes produce damage that mimics the level of destruction of bowing convection severe winds. While the tornado track distances were not tabulated in this study, severe weather surveys suggest that most bowing convection tornadoes traverse only around 0.5 km. Rare exceptions do exist (e.g. destructive rotation pattern), but generally BCS tornadoes are short-lived.

5.6.3 *Diurnal distributions of severe weather*

The diurnal distributions of severe hail, wind, and tornado reports for all warm season BCSs observed in this study are shown in Figs. 5.38, 5.39, and 5.40, respectively. The diurnal distribution of bowing convection hail reports illustrates hail production mainly between 1000 LST and 0030 LST. The most active times for hailstones from BCSs occur between 1500 and 2200 LST.

The daily cycle of severe wind reports shows a distribution ascending in frequency from the late morning hours up until the peak around 1930 LST. Interestingly, *the results show a steady decrease in the frequency of severe wind reports from 0000 LST until 0830 LST.* A possible explanation is increasing static stability of nocturnal planetary boundary layers would tend to inhibit the production of severe surface winds. In comparison to the diurnal cycle of severe hail reports, the peak of severe wind reports tends to show about a two hour time lag compared to that of severe hail reports. Thus, the diurnal plots confirm the general finding of the severe weather surveys which reveals that severe hail reports are favored just after bowing convection initiation while severe wind reports are favored throughout the evolution of a BCS.

The diurnal tendencies of BCS-induced tornadoes have a more ragged distribution due to the smaller number of tornadoes reported compared to severe hail or severe winds, yet the general trend appears to show a peak around 1800 LST just after the peak of the severe hail reports during mature stages of BCS development. Very few tornadoes are observed after about 2300 LST. Thus, the stabilization of the nocturnal planetary boundary layer could also have a detrimental effect upon the formation of BCS-induced tornadoes, similar to the reduction of severe surface winds.

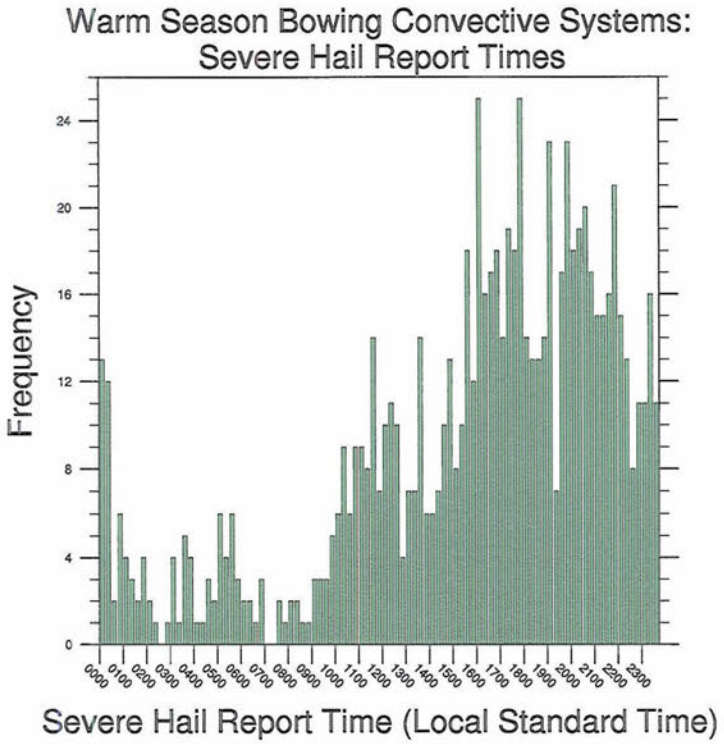

Figure 5.38: Frequency distribution of SPC severe hail reports produced by bowing convective systems in this study. Times are displayed in Local Standard Time. The bins are divided into 15 minute intervals.

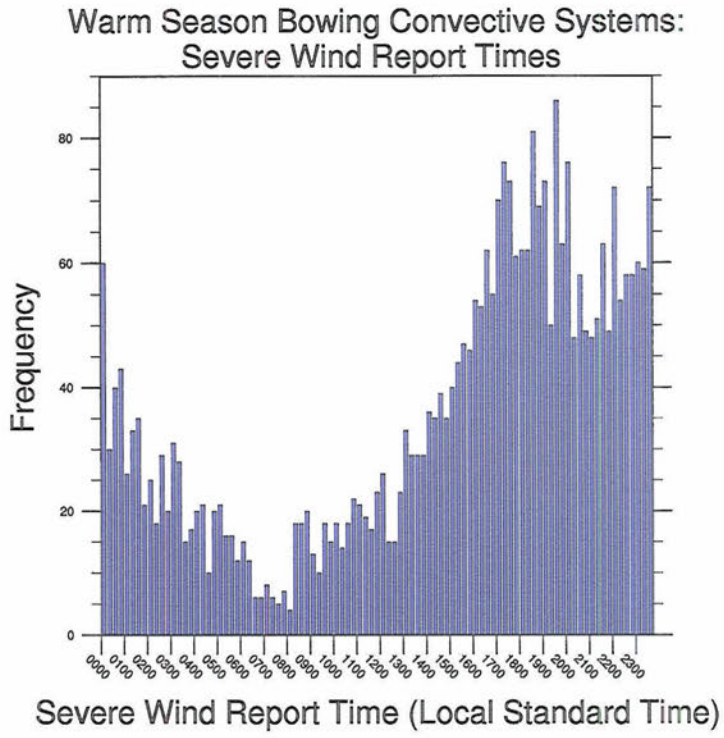

Figure 5.39: Same as Fig. 5.38, but for severe wind reports.

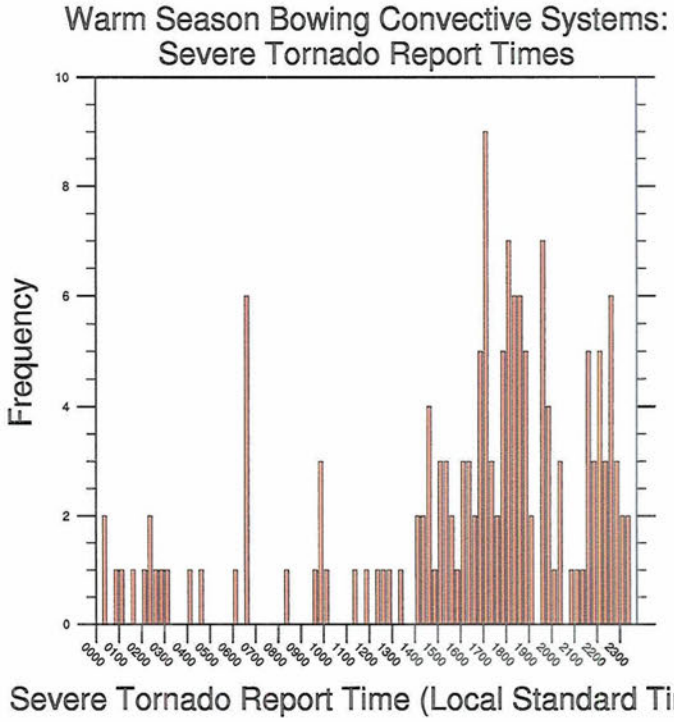

Figure 5.40: Same as Fig. 5.38, but for severe tornado reports.

Chapter 6

CONCLUSIONS AND FUTURE WORK

6.1 Summary of study and findings

Using a systematic method of perusing radar data for April through September of 2003 and 2004, 381 cases of bowing convective systems (BCSs) were selected to categorize observed convective structures related to the bowing process while examining an unbiased two-year climatology of warm season bowing convection. The motivation for this study included objectives such as clarifying the nature of bowing convection, understanding the convection evolution of BCSs, and recording useful climatological information about BCSs. This was accomplished by thorough investigation of radar reflectivity data, surface data, and severe weather data while tabulating observations like times, locations, and convective structures.

Several new findings emerged from this research:

- Five modes of bowing convective systems have been identified: bow echo/extensive stratiform (BE/ES), bow echo/minimal stratiform (BE/MS), bowing squall lines, multiple bowing squall lines, and bowing single cells. These modes were established after examination of initial convective cell structures, convection evolution, geographical location, local beginning and ending times, severe weather production, and kinematic/thermodynamic environments.

- Bow echoes/extensive stratiform (BE/ESs) exhibited trailing stratiform precipitation and most commonly evolved from groups of cells. Bow echoes/minimal stratiform (BE/MSs) showed very limited trailing precipitation evolving from the merging of supercells with ordinary or multicells. Single and multiple bowing squall lines most often evolved from trailing stratiform mesoscale convective systems (TS MCSs).

- Trailing stratiform precipitation was generated by 72% of all BCSs. This (or pre-existing) precipitation was associated with longer-lived BCSs.

- Bowing convection possessing an enhanced trailing stratiform precipitation region arranged perpendicular to the rear of a BCS was associated with a strengthening rear-inflow jet that was observed in past studies.

- BCSs that sustained a wide stratiform transition zone, a region of light precipitation separating the bowing convective line and the moderate-to-heavy trailing stratiform precipitation region, showed increased longevities.

- Supercells interacting with ordinary or multicells produced BCSs in 24% of all cases. This grouping of cells was overlooked in previous studies.

- Size criteria were established for bow echoes in this study; 70% of all BCS cases displayed convective line lengths between 40 and 110 km to be termed bow echoes. The average BCS convective line length was about 75 km.

- Radar observed convective mergers that initiated BCSs interacted with environmental convective cells near the resultant apex in 39% of all BCSs. This merging location was four times more likely than the left or right flank of the convection.

- Tabular bowing convective lines, strong convective lines that are nearly homogeneous along the bowing convective line, were strongly favored in BCSs

(77%) as opposed to cellular bowing convective lines, which are characterized by discrete convective cells along the line.

- BCSs developing in a quasi-linear series, defined as a bowing series, tended to form upstream from one another.

The second half of this study examined and compared the climatological characteristics of U.S. warm season BCSs against cold season bow echoes (Burke and Schultz 2004) as well as derechos (Coniglio et al. 2004a). Findings related to these previous two studies include:

- Warm season BCS locations showed a spatial distribution similar to warm season derechos with an Upper Great Plains maximum, with a secondary maximum toward the Central/Southern Great Plains.

- The frequency of bowing convection peaked between May and July, similar to the peak of derechos.

- Hybrid boundary forcing, a BCS moving parallel to or initiating along a synoptic boundary, was favored for warm season BCSs while weak boundary forcing with no synoptic boundary was of secondary importance.

The following results had not previously been identified for warm season BCSs:

- The monthly distributions of BCSs showed an asymmetry, with more storms favored for months leading into the warm season compared to months coming out of the warm season.

- BCSs showed very strong correlation between track length and longevity (r=0.87). When these properties are examined together as average movement speeds, a preferred range from 10 to 24 m s^{-1} emerged, with an average speed of 17.4 m s^{-1}.

- BCS development time and longevity were linearly related for many cases. This outcome facilitates the task of forecasting BCS longevities.

- BCSs that parallel synoptic boundaries (usually stationary or warm fronts) averaged one hour greater longevity compared to BCSs that did not. Any BCSs that traversed a synoptic boundary dissipated within three hours.

- Severe weather production from bowing convection usually arranged itself into one of four patterns: narrow apex swath, widespread high winds, widening swath, and destructive rotation.

- Severe hail production was favored early in the evolution of BCSs. Severe wind production occurred throughout BCS evolutions. BCS-induced tornadoes tended to be favored in the early-to-mature stages.

6.2 Suggestions for future work

One of the main goals of this work was to determine, for a large number of cases, how BCSs are organized. However, many of the internal dynamics of the storms and the processes that determine severe weather production occur on scales smaller than can be resolved by this dataset and require more thorough analysis. Future work could take several approaches.

First, radar data have the capability to provide more information than has been used here. Dual-Doppler analyses and studies using polarimetric radar would provide greater insights into the dynamical and microphysical properties of bowing convection. Radar observations could be used in conjunction with a high-density surface mesonetworks to better identify severe weather production, strength and shapes of surface cold pools, and surface pressure transients as they are related to known structures.

Secondly, a thorough examination of the kinematic and thermodynamic environments of bowing convection for many cases would prove useful in understanding the differences among the modes of bowing convection. These data would clarify the spectrum for which BCSs are expected.

Third, a study of BCSs in other parts of the world may increase the general understanding of such events as well. Some characteristics of bowing convection for the present study may apply only to the geography and climate of the United States. Such a study might provide insights into favored times and locations for such severe convection.

Finally, since many of the processes involving the production of severe weather in bowing convection are difficult to observe using conventional methods, additional numerical simulations could provide further insight. Sensitivity studies related to the modes of bowing convective systems and processes would provide additional insights into the nature and evolution of the resulting convection.

The aim of these suggestions for future research would be increased understanding and to more accurately forecast bowing convective systems. Since bowing convection tends to develop in environmental conditions that favor other modes of severe convection, additional work toward understanding their structures and evolutions would provide useful information. The ultimate goal should be longer lead times for severe weather watches and warnings for the mitigation of losses of life and property.

REFERENCES

Atkins, N. T., C. S. Bouchard, R. W. Przybylinski, R. J. Trapp, and G. Schmocker, 2005: Damaging surface wind mechanisms within the 10 June 2003 Saint Louis bow echo during BAMEX. *Mon. Wea. Rev.*, **133**, 2275–2296.

Baldwin, M. E., J. S. Kain, and S. Lakshmivarahan, 2005: Development of an automated classification procedure for rainfall systems. *Mon. Wea. Rev.*, **133**, 844–862.

Bentley, M. L., and T. L. Mote, 1998: A climatology of derecho producing mesoscale convective systems in the central and eastern United States, 1986-95. Part I: Temporal and spatial distribution. *Bull. Amer. Meteor. Soc.*, **79**, 2527–2540.

Bernardet, L. R., and W. R. Cotton, 1998: Multiscale evolution of a derecho-producing mesoscale convective system. *Mon. Wea. Rev.*, **126**, 2991–3015.

Biggerstaff, M. I., and R. A. Houze, 1991: Kinematic and precipitation structure of the 10-11 June 1985 squall line. *Mon. Wea. Rev.*, **119**, 3034–3065.

Brown, R. A., 1993: A compositing approach for preserving significant features in atmospheric profiles. *Mon. Wea. Rev.*, **121**, 874–880.

Burke, P. C., and D. M. Schultz, 2004: A 4-yr climatology of cold-season bow echoes over the continental United States. *Wea. Forecasting*, **19**, 1061–1074.

Coniglio, M. C., and D. J. Stensrud, 2001: Simulation of a progressive derecho using composite initial conditions. *Mon. Wea. Rev.*, **129**, 1593–1616.

Coniglio, M. C., and D. J. Stensrud, 2004: Interpreting the climatology of derechos. *Wea. Forecasting*, **19**, 595–605.

Coniglio, M. C., D. J. Stensrud, and M. B. Richman, 2004a: An observational study of derecho-producing convective systems. *Wea. Forecasting*, **19**, 320–337.

Coniglio, M. C., D. J. Stensrud, and L. J. Wicker, 2004b: How upper level shear can promote organized convective systems. Preprints, *22nd Conference on Severe Local Storms*, Hyannis, MA, Amer. Meteor. Soc., CD–ROM, 10.5.

Davis, C. A., and Coauthors, 2004: The bow echo and MCV experiment: Observations and opportunities. *Bull. Amer. Meteor. Soc.*, **85**, 1075–1093.

Doswell, C. A., and J. S. Evans, 2003: Proximity sounding analysis for derechos and supercells: An assessment of similarities and differences. *Atmos. Research*, **67–68**, 117–133.

Evans, J. S., and C. A. Doswell, 2001: Examination of derecho environments using proximity soundings. *Wea. Forecasting*, **16**, 329–342.

Finley, C. A., W. R. Cotton, and R. A. Pielke Sr., 2001: Numerical simulation of tornadogenesis in a high-precipitation supercell. Part I: Storm evolution and transition into a bow echo. *J. Atmos. Sci.*, **38**, 1597–1629.

Fovell, R. G., 2003: The role of the rear inflow current in organizing convective systems. Preprints, *11th Conference on Mesoscale Process*, Portland, OR, Amer. Meteor. Soc., P1.1.

Fujita, T. T., 1978: Manual of downburst identification for project Nimrod. Satellite and Mesometeorology Research Paper 156, Dept. of Geophysical Sciences, University of Chicago [NTIS PB-286048.], 104 pp.

Gilmore, M. S., and L. J. Wicker, 1998: The influence of midtropospheric dryness on supercell morphology and evolution. *Mon. Wea. Rev.*, **126**, 943–958.

Glickman, T. S., Ed., 2000: *Glossary of Meteorology.* Amer. Meteor. Soc., 855 pp.

Hamilton, R., 1970: Use of detailed intensity radar data in mesoscale surface analysis of the 4 July 1969 storm in Ohio. Preprints, *14th Conference on Radar Meteorology*, Tucson, AZ, Amer. Meteor. Soc., 339–342.

Hilgendorf, E. R., and R. J. Johnson, 1998: A study of the evolution of mesoscale convective systems using WSR-88D data. *Wea. Forecasting*, **13**, 437–452.

Hinrichs, G., 1888: Tornadoes and derechos. *Amer. Meteor. J.*, **5**, 341–349.

Hodges, K. I., and C. D. Thorncroft, 1997: Distribution and statistics of African mesoscale convective weather systems based on the ISCCP Meteosat imagery. *Mon. Wea. Rev.*, **125**, 2821–2837.

Houze, R. A., 1997: Stratiform precipitation in regions of convection: A meteorological paradox? *Bull. Amer. Meteor. Soc.*, **78**, 2179–2196.

Houze, R. A., M. I. Biggerstaff, S. A. Rutledge, and B. F. Smull, 1989: Interpretation of doppler weather radar displays of midlatitude mesoscale convective systems. *Bull. Amer. Meteor. Soc.*, **70**, 608–619.

James, R. P., J. M. Fritsch, and P. M. Markowski, 2005: Environmental distinctions between cellular and slabular convective lines. *Mon. Wea. Rev.*, **133**, 2669–2691.

James, R. P., P. M. Markowski, and J. M. Fritsch, 2006: Bow echo sensitivity to ambient moisture and cold pool strength. *Mon. Wea. Rev.*, **134**, 950–964.

Johns, R. H., 1993: Meteorological conditions associated with bow echo development in convective storms. *Wea. Forecasting*, **8**, 294–299.

Johns, R. H., and W. D. Hirt, 1987: Derechos: Widespread convectively induced wind-storms. *Wea. Forecasting*, **2**, 32–49.

Johnson, R. H., and P. J. Hamilton, 1988: The relationship of surface pressure features to the precipitation and airflow structure of an intense midlatitude squall line. *Mon. Wea. Rev.*, **116**, 1444–1473.

Jorgensen, D. P., H. V. Murphey, and R. M. Wakimoto, 2005: Rear-inflow structure in severe and non-severe bow-echoes observed by airborne doppler radar during BAMEX. Preprints, *11th Conference on Mesoscale Processes*, Albuquerque, NM, Amer. Meteor. Soc., CD–ROM, JJ.3.

Klimowski, B. A., 1994: Initiation and development of rear inflow within the 28-29 June 1989 North Dakota mesoconvective system. *Mon. Wea. Rev.*, **122**, 765–779.

Klimowski, B. A., M. J. Bunkers, J. N. Covert, and M. R. Hjelmfelt, 2003: Severe convective windstorms over the Northern High Plains of the United States. *Wea. Forecasting*, **18**, 502–519.

Klimowski, B. A., M. R. Hjelmfelt, and M. J. Bunkers, 2004: Radar observations of the early evolution of bow echoes. *Wea. Forecasting*, **19**, 727–734.

Kruk, M. C., R. M. Rauber, G. M. McFarquhar, B. F. Jewett, and R. J. Trapp, 2005: Bow echoes during BAMEX: Assessing transitions in surface wind damage using WSR-88D data. Preprints, *11th Conference on Mesoscale Processes*, Albuquerque, NM, Amer. Meteor. Soc., CD–ROM, JP5J.3.

Kuchera, E. L., and M. D. Parker, 2004: Using RUC-2 analysis parameters to identify severe convective wind environments. Preprints, *22nd Conference on Severe Local Storms*, Hyannis, MA, Amer. Meteor. Soc., CD–ROM, 7A.1.

Kuchera, E. L., and M. D. Parker, 2006: Severe convective wind environments. *Wea. Forecasting*, in press.

Lee, W. C., R. M. Wakimoto, and R. E. Carbone, 1992: The evolution and structure of a "bow-echo-microburst" event. Part II: The bow echo. *Mon. Wea. Rev.*, **120**, 2211–2225.

Loehrer, S. M., and R. H. Johnson, 1995: Surface pressure and precipitation life cycle characteristics of PRE-STORM mesoscale convective systems. *Mon. Wea. Rev.*, **123**, 600–621.

Machado, A. T., W. B. Rossow, R. L. Guedes, and A. W. Walker, 1998: Life cycle variations of mesoscale convective systems over the Americas. *Mon. Wea. Rev.*, **126**, 1630–1654.

Miller, D. J., D. L. Andra, J. S. Evans, and R. H. Johns, 2002: Observations of the 27 May 2001 high-end derecho event in Oklahoma. Preprints, *21th Conference on Severe Local Storms*, San Antonio, TX, Amer. Meteor. Soc., 13–16.

Moller, A. R., C. A. Doswell, M. P. Foster, and G. R. Wodall, 1994: The operational recognition of supercell thunderstorm environments and storm structures. *Wea. Forecasting*, **9**, 327–347.

Moller, A. R., C. A. Doswell, and R. W. Przybylinski, 1990: High-precipitation supercells: A conceptual model and documentation. Preprints, *16th Conference on Severe Local Storms*, Kananaskis Park, AB, Canada, Amer. Meteor. Soc., 52–57.

Nolan, R. H., 1959: A radar signature associated with tornadoes. *Bull. Amer. Meteor. Soc.*, **40**, 277–279.

Parker, M. D., and R. H. Johnson, 2000: Organizational modes of midlatitude mesoscale convective systems. *Mon. Wea. Rev.*, **128**, 3413–3436.

Parker, M. D., and R. H. Johnson, 2004a: Simulated convective lines with leading precipitation. Part I: Governing dynamics. *J. Atmos. Sci.*, **61**, 1637–1655.

Parker, M. D., and R. H. Johnson, 2004b: Simulated convective lines with leading precipitation. Part II: Evolution and maintenence. *J. Atmos. Sci.*, **61**, 1656–1673.

Parker, M. D., and R. H. Johnson, 2004c: Structures and dynamics of quasi-2d mesoscale convective systems. *J. Atmos. Sci.*, **61**, 545–567.

Przybylinski, R. W., 1995: The bow echo. Observations, numerical simulations, and severe weather detection methods. *Wea. Forecasting*, **10**, 203–218.

Przybylinski, R. W., and D. M. DeCaire, 1985: Radar signatures associated with the derecho, a type of mesoscale convective system. Preprints, *14th Conference on Severe Local Storms*, Indianapolis, IN, Amer. Meteor. Soc., 228–231.

Przybylinski, R. W., D. M. DeCaire, and Y.-J. Lin, 2000: A study of storm and vortex morphology during the 'intensifying stage' of severe wind mesoscale convective systems. Preprints, *20th Conference on Severe Local Storms*, Orlando, FL, Amer. Meteor. Soc., 173–176.

Reynolds, A. E., SOARS paper, cited 2003: Environments of bow echoes associated with localized vs. widespread straight-line wind damage. [Available from the National Center for Atmospheric Research, Boulder, CO 80307-3000].

Schmidt, J. M., and W. R. Cotton, 1989: A high plains squall line associated with severe surface winds. *J. Atmos. Sci.*, **46**, 281–302.

Schmocker, G. K., R. W. Przybylinski, and E. N. Rasmussen, 2000: The severe bow echo event of 14 June 1998 over the mid-Mississippi valley region: A case of vortex development near the intersection of a preexisting boundary and a convective line. Preprints, *20th Conference on Severe Local Storms*, Orlando, FL, Amer. Meteor. Soc., 169–172.

Sieveking, J. E., and R. W. Przybylinski, 2004: The interaction of a HP supercell thunderstorm and bow echo to produce a prolonged severe wind event in East

Central Missouri. Preprints, *22nd Conference on Severe Local Storms*, Hyannis, MA, Amer. Meteor. Soc., CD–ROM, 7A.5.

Skamarock, W. C., M. L. Weisman, and J. B. Klemp, 1994: Three dimensional evolution of simulated long-lived squall lines. *J. Atmos. Sci.*, **51**, 2563–2584.

Smull, B. F., and R. A. Houze, 1985a: Dual-Doppler radar analysis of a midlatitude squall line with a trailing region of stratiform rain. *J. Atmos. Sci.*, **44**, 2128–2149.

Smull, B. F., and R. A. Houze, 1985b: A midlatitude squall line with a trailing region of stratiform rain: Radar and satellite observations. *Mon. Wea. Rev.*, **113**, 117–133.

Snook, N., and W. Gallus, 2004: A climatology of severe weather reports as a function of convective system morphology. Preprints, *22nd Conference on Severe Local Storms*, Hyannis, MA, Amer. Meteor. Soc., CD–ROM, P4.5.

Steiner, M., R. A. Houze, and S. E. Yuter, 1995: Climatological characterization of three-dimensional storm structure from operational radar and rain gauge data. *J. Appl. Meteor.*, **34**, 1978–2007.

Trapp, R. J., and M. L. Weisman, 2003: Low-level mesovortices within squall lines and bow echoes. Part II: Their genesis and implications. *Mon. Wea. Rev.*, **131**, 2804–2823.

Trapp, R. J., D. M. Wheatley, N. T. Atkins, R. W. Przybylinski, and R. Wolf, 2006: Buyer beware: Some words of caution on the use of severe wind reports in postevent assessment and research. *Wea. Forecasting*, **21**, 408–415.

Wakimoto, R. M., H. V. Murphey, C. A. Davis, and N. T. Atkins, 2006a: High winds generated by bow echoes. part ii: The relationship between the mesovortices and damaging straight-line winds. *Mon. Wea. Rev.*, in press.

Wakimoto, R. M., H. V. Murphey, A. Nester, D. P. Jorgensen, and N. T. Atkins, 2006b: High winds generated by bow echoes. Part I: Overview of the Omaha bow bcho 5 July 2003 storm during BAMEX. *Mon. Wea. Rev.*, in press.

Weisman, M. L., 1992: The role of convectively generated rear inflow jets in the evolution of long-lived mesoconvective systems. *J. Atmos. Sci.*, **49**, 1826–1847.

Weisman, M. L., 1993: The genesis of severe, long-lived bow-echoes. *J. Atmos. Sci.*, **50**, 645–670.

Weisman, M. L., 2001: Bow echoes: A tribute to T. T. Fujita. *Bull. Amer. Meteor. Soc.*, **82**, 97–116.

Weisman, M. L., and C. A. Davis, 1998: Mechanisms for the generation of mesoscale vortices within quasi-linear convective systems. *J. Atmos. Sci.*, **55**, 2603–2622.

Weisman, M. L., and R. Rotunno, 2004: "a theory for long lived squall lines" revisited. *J. Atmos. Sci.*, **61**, 361–382.

Weisman, M. L., and R. J. Trapp, 2003: Low-level mesovortices within squall lines and bow echoes: Part I: Overview and dependence on environmental shear. *Mon. Wea. Rev.*, **131**, 2779–2803.

Weiss, S., J. A. Hart, and P. R. Janish, 2002: An examination of severe thunderstorm wind report climatology: 1970-1999. Preprints, *21st Conference on Severe Local Storms*, San Antonio, TX, Amer. Meteor. Soc., 446–449.

Wheatley, D. M., and R. J. Trapp, 2004: Radar and damage analysis of bow echoes observed during BAMEX. Preprints, *22nd Conference on Severe Local Storms*, Hyannis, MA, Amer. Meteor. Soc., CD–ROM, 4.3.

Wheatley, D. M., R. J. Trapp, and N. T. Atkins, 2006: Radar and damage analysis of severe bow echoes observed during BAMEX. *Mon. Wea. Rev.*, **134**, 791–806.

Appendix A

BOW ECHO KINEMATIC AND THERMODYNAMIC ENVIRONMENTS

Numerous studies have documented the thermodynamic and kinematic environments conducive to the formation of bow echoes (e.g. Weisman 1993, Weisman 2001, Klimowski et al. 2003, Reynolds 2003, and BS04). In addition, similar studies have documented the thermodynamic and kinematic environments conducive for the formation of derechos (e.g. Evans and Doswell 2001, Doswell and Evans 2003, and Coniglio et al. 2004a). The author of the present study constructed figures that intercompare CAPE, vertical wind shear, moisture, and storm-relative wind (SRW) environments for bow echoes and derechos. While a thorough examination of the kinematic and thermodynamic environments was not performed for the 381 warm season cases for the present study, the information presented in the appendix is useful for summarizing the body of knowledge known in this area and can be referred to a few times throughout the body of the main text.

A.1 Bow echo and derecho CAPE environments

The parameter space of CAPE values observed in various bow echo and derecho studies is summarized in Fig. A.1[1] (see figure caption for abbreviations used for various studies). Early studies have established that bow echoes must develop in

[1] Values estimated are as follows: Weisman (1993)–Used range of 2000 to 4000 J kg^{-1} as a box, Evans and Doswell (2001)–Calculated mean of known quartiles, Coniglio et al. (2004a)–Estimated quartiles, maximum, and minimum CAPE from cumulative distribution figure.

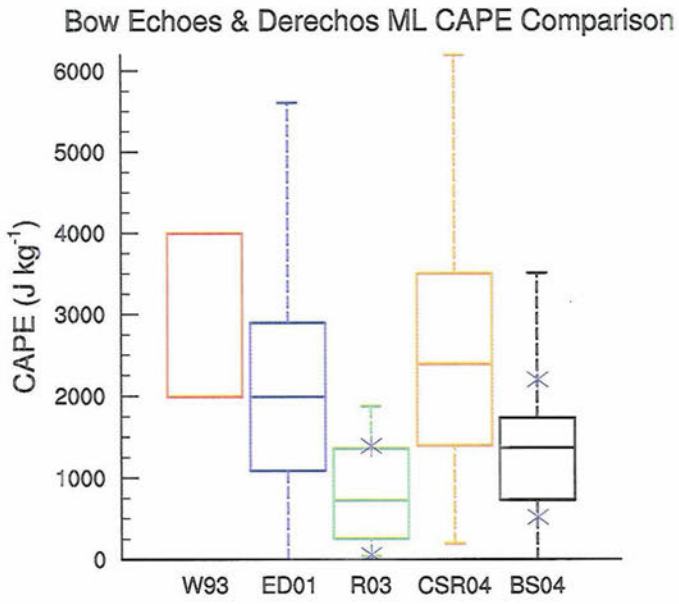

Figure A.1: Box and whisker plots of mixed layer CAPE values from various bow echo and derecho studies. The purple "x"s show the +/- 1 standard deviations from the mean where data is available. Figure based on data from data presented by Weisman (1993) (W93), Evans and Doswell (2001) (ED01), Reynolds (2003) (R03), Coniglio et al. (2004a) (CSR04), and Burke and Schultz (2004) (BS04).

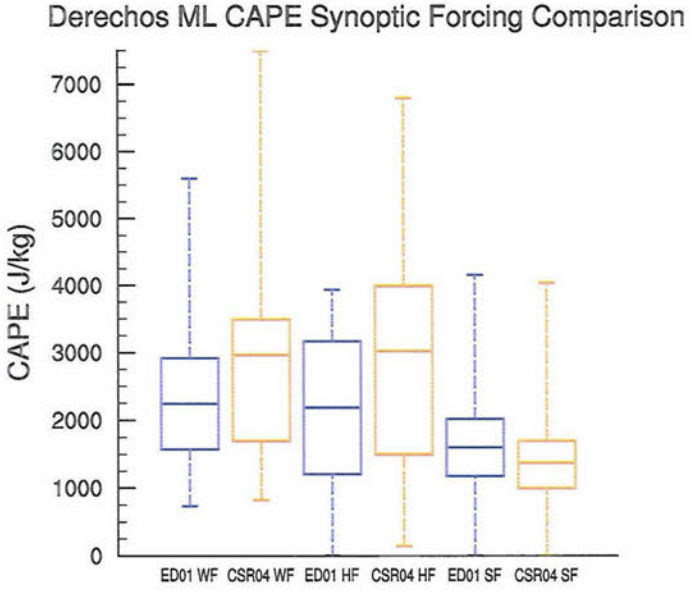

Figure A.2: Box and whisker plots of mixed layer CAPE values depending upon the strength of synoptic scale forcing. Weak Forcing (WF), Hybrid Forcing (HF), and Strong Forcing (SF) are all abbreviated in the figure. Figure based on data presented by Evans and Doswell (2001) (ED01) and Coniglio et al. (2004a) (CSR04).

high CAPE environments (e.g. Weisman 1993, Przybylinski 1995, Weisman 2001); however, Burke and Schultz (2004) and Evans and Doswell (2001) argue for a much larger parameter space of CAPE for long-lived bow echoes (LBEs) and derechos compared to the simulations of Weisman (1993). The occurrence of bow echoes and derechos over a broader range of CAPEs was argued in the more recent studies to be related to the strength of synoptic forcing. Cases of strong forcing (SF)—often convection induced from a cold front or a strong upper level trough—are capable of producing LBEs or derechos with *limited* CAPE. Evans and Doswell (2001) and Coniglio et al. (2004a) suggest that the simulated storms of Weisman (1993) represent the development of weak forcing (WF) LBEs that would be favored primarily during the warm season. Note the CAPE values of Reynolds (2003) and BS04 are relatively low compared to the other studies. Reynolds (2003) studied six BAMEX bow echoes with very close proximity soundings while BS04 studied bow echoes in the cold season.

The parameter space of CAPE values observed for derechos of various synoptic forcing strengths is summarized in Fig. A.2[2] based on data from Evans and Doswell (2001) and Coniglio et al. (2004a). These studies show a much smaller range and much smaller CAPE magnitude for SF compared to WF derechos. As mentioned by the authors, SF derechos are favored in the cold season (yet can occur year around) while WF derechos are primarily confined to the warm season. These tendencies are consistent with the CAPE values shown (Fig. A.2).

A.2 Bow echo and derecho vertical wind shear environments

Evans and Doswell (2001), Reynolds (2003), Coniglio et al. (2004a) and Burke and Schultz (2004) all show that bow echoes and derechos can be initiated with *much less* low-level (0-2.5/0-3 km) vertical wind shear compared to that in the simulations

[2] Values estimated are as follows: Evans and Doswell (2001)–Calculated mean of known quartiles, Coniglio et al. (2004a)–Estimated quartiles, maximum, and minimum CAPE from cumulative distribution figure.

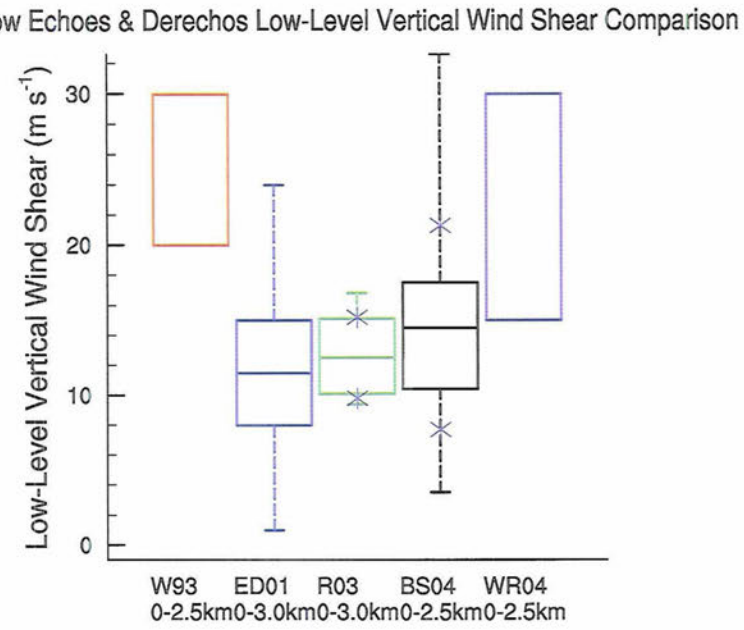

Figure A.3: Box and whisker plot of low-level vertical wind shear values from various bow echo and derecho studies. The depth that the shear was calculated over is shown in the figure labels. The purple "x"s are the +/- 1 standard deviations from the mean where the data are available. Figure based on data from data presented by Weisman (1993) (W93), Evans and Doswell (2001) (ED01), Reynolds (2003) (R03), Burke and Schultz (2004) (BS04), and Weisman and Rotunno (2004) (WR04).

of Weisman (1993) (Fig. A.3[3]). This is particularly true for cold season bow echoes (BS04) and SF derechos (Evans and Doswell 2001, Coniglio et al. 2004a). However, the range of low-level vertical wind shears from the more recent study of Weisman and Rotunno (2004) has better parameter space agreement with the other studies.

The studies of Evans and Doswell (2001), Coniglio et al. (2004a), and BS04 show some good agreement with Weisman (1993) and Weisman and Rotunno (2004) on the parameter space for the deep layer vertical wind shear (0-5/0-6 km) for LBEs and derechos (Fig. A.4[4]). Previous research suggested that bow echoes have very strong

[3] Values estimated are as follows: Weisman (1993)–Used range of 20 to 30 m s^{-1} as a box, Evans and Doswell (2001)–Calculated mean as mean of known quartiles, Weisman and Rotunno (2004)–Used range of 15 to 30 m s^{-1} as a box.

[4] Values estimated are as follows: Weisman (1993)–Used range of 25 to 35 m s^{-1} in equal spacing, Evans and Doswell (2001)–Calculated mean as mean of known quartiles, Weisman and Rotunno (2004)–Used range of 20 to 40 m s^{-1} as a box.

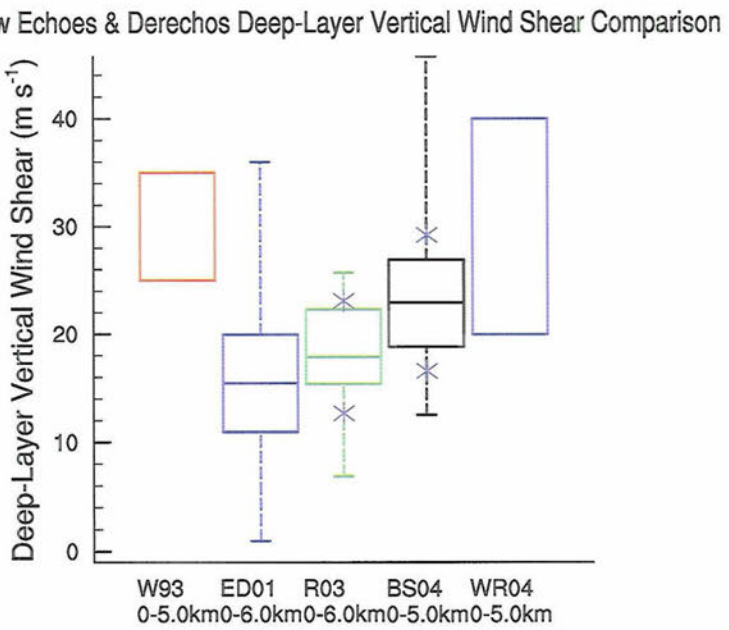

Figure A.4: Box and whisker plot of deep layer vertical wind shear values from various bow echo and derecho studies. The depth that the shear was calculated over is shown in the figure labels. The purple "x"s are the +/- 1 standard deviations from the mean where the data are available. Figure based on data from data presented by Weisman (1993) (W93), Evans and Doswell (2001) (ED01), Reynolds (2003) (R03), Burke and Schultz (2004) (BS04), and Weisman and Rotunno (2004) (WR04).

low-level wind shear (e.g. Weisman 1993) while supercells have very strong deep layer vertical wind shear (e.g. Doswell and Evans 2003). As an extention of Weisman (1993), the studies of Evans and Doswell (2001) and BS04 show that derechos and LBEs, respectively, can develop in strong deep layer shear environments.

A possible reason for the discrepancies in vertical shear parameter spaces between numerical modeling studies and observations has been proposed by James et al. (2006):

> A possible explanation for at least some of the discrepancy between the modeling and observational results was suggested by James et al. (2005), who noted that idealized models usually employ a free-slip lower boundary condition [see also Weisman (1993) for a brief discussion of the influence of the free-slip condition]. In observational studies, the wind magnitude at the bottom of the low-level shear layer is taken as the 10-m wind speed, which is reduced by friction

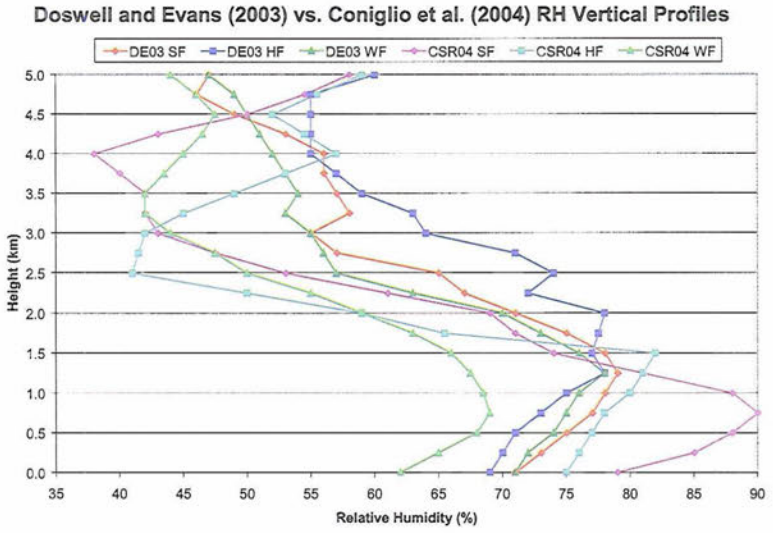

Figure A.5: Vertical profile of average tropospheric relative humidity for derechos. The caption colors correspond to the profiles from Doswell and Evans (2003) (DE03) and Coniglio et al. (2004a) (CSR04). The profiles are separated into their respective synoptic scale forcing strengths Weak, Hybrid, and Strong Forcing (WF, HF, SF). Figure based on combined profiles from Doswell and Evans (2003) and Coniglio et al. (2004a).

> from the wind speed a few hundred meters above the ground. Consequently, the measured low-level shear is reduced from the value that it would assume above a free-slip boundary. The results of James et al. (2005) show that the difference between the surface wind speed and the wind speed above the surface-based friction layer is as great as 5 m s^{-1} in the preconvective environments of strong slab-like squall lines. It is possible, therefore, that the rather high shear requirements of simulated bow echoes may not be grossly inconsistent with the less extreme observed values, because of the physically differing frameworks.

Finally, note that the upper-level shear as calculated for cold season bow echoes by BS04 usually falls between 10 and 30 m s^{-1}. In addition, Coniglio and Stensrud (2001) and Coniglio et al. (2004b) have shown the importance of upper-level shear on maintenance of an MCS.

A.3 Bow echo and derecho vertical moisture profiles

Burke and Schultz (2004) show that *all* LBEs have a low-level mixing ratio of at least 9 g/kg and an average of 11 g/kg in the lowest 100 hPa. The study of Coniglio et al. (2004a) show that for derechos there is substantial drying around 3 km (700 hPa), usually to 50% or lower. This is similar to Doswell and Evans (2003), who found dry midlevels for derechos. The results of these past two studies are summarized in Fig. A.5. These results suggest a possible mid-level (3 km or 700 hPa) dry layer necessary for strong evaporation (e.g. Gilmore and Wicker 1998) while moist low levels seem to be important to initiate strong convection. Moreover, as mentioned previously, James et al. (2006) show that varying the low-level mixing ratio lapse rate while retaining ambient CAPE values can provide some ways to distinguish between bowing convective lines, cellular lines, and slabular lines.

A.4 Bow echo and derecho storm relative winds

Doswell and Evans (2003) and BS04 suggest that derechos and LBEs should have strong **storm-relative wind** (SRW) inflow at low levels (0-2 km), especially compared to supercells or other storms (Doswell and Evans 2003). Evans and Doswell (2001) showed that derechos had smaller SRW at 4-6 km in comparison to low-level inflow (0-3 km). The derecho study of Coniglio et al. (2004a) agree that weak SRW at midlevels is important for the generation of strong cold pool outflow. Recently, studies of a large database of convective parameters by Kuchera and Parker (2004) and Kuchera and Parker (2006) showed that strong 2 km inflow wind was the best kinematic indicator for severe wind convective systems.

A.5 Unresolved environmental conditions

Evans and Doswell (2001) and Coniglio et al. (2004a) show significant differences in kinematic and thermodynamic conditions depending upon synoptic scale

forcing: weak forcing (WF), strong forcing (SF), or hybrid forcing (HF) for derechos.

There exists much documented environmental understanding for LBEs and derechos. However, there is little environmental information for non-severe bow echoes. These also deserve attention because a bowing radar signature does not always require a warning of severe winds for the weather forecaster.